CANADIAN THESES ON MICROFICHE

THÈSES CANADIENNES SUR MICROFICHE

NOTICE

The quality of this microfiche is heavily dependent upon the quality of the original thesis submitted for microfilming. Every effort has been made to ensure the highest quality of reproduction possible.

If pages are missing, contact the university which granted the degree.

Some pages may have indistinct print especially if the original pages were typed with a poor typewriter ribbon or if the university sent us an inferior photocopy.

Previously copyrighted materials (journal articles, published tests, etc.) are not filmed.

AVIS

La qualité de cette microfiche dépend grandement de la qualité de la thèse soumise au microfilmage. Nous avons tout fait pour assurer une qualité supérieure de reproduction.

S'il manque des pages, veuillez communiquer avec l'université qui a conféré le grade.

La qualité d'impression de certaines pages peut laisser à désirer, surtout si les pages originales ont été dactylographiées à l'aide d'un ruban usé ou si l'université nous a fait parvenir une photocopie de qualité inférieure.

Les documents qui font déjà l'objet d'un droit d'auteur (articles de revue, examens publiés, etc.) ne sont pas microfilmés.

THIS DISSERTATION HAS BEEN MICROFILMED EXACTLY AS RECEIVED

LA THÈSE A ÉTÉ MICROFILMÉE TELLE QUE NOUS L'AVONS REÇUE

Canada

CANADIAN THESES ON MICROFICHE SERVICE – SERVICE DES THÈSES CANADIENNES SUR MICROFICHE

PERMISION TO MICROFILM – AUTORISATION DE MICROFILMER

• Please print or type – Écrire en lettres moulées ou dactylographier

AUTHOR – AUTEUR

Full Name of Author – Nom complet de l'auteur

Faye Ellen Hicks

Date of Birth – Date de naissance

December 4, 1957

Canadian Citizen – Citoyen canadien

☑ Yes Oui   ☐ No Non

Country of Birth – Lieu de naissance

Canada

Permanent Address – Résidence fixe

5951 - 40 Avenue
Edmonton Alberta
T6L 3P6

THESIS – THÈSE

Title of Thesis – Titre de la thèse

SHEAR AND VELOCITY NEAR A SLOPED BANK IN A CURVED CHANNEL

Degree for which thesis was presented
Grade pour lequel cette thèse fut présentée   M.Sc.

Year this degree conferred
Année d'obtention de ce grade   1985

University – Université

University of Alberta

Name of Supervisor – Nom du directeur de these

Steffler, Dr. Peter M.

AUTHORIZATION – AUTORISATION

ATTACH FORM TO THESIS – VEUILLEZ JOINDRE CE FORMULAIRE À LA THÈSE

Signature   Faye E. Hicks

Date   March 20/85

NL-91 (r 84/03)

Canada

THE UNIVERSITY OF ALBERTA

SHEAR AND VELOCITY NEAR A SLOPED BANK IN A CURVED CHANNEL

BY

© FAYE E. HICKS

A THESIS

SUBMITTED TO THE FACULTY OF GRADUATE STUDIES AND RESEARCH

IN PARTIAL FULFILLMENT OF THE REQUIREMENTS FOR THE DEGREE

OF MASTER OF SCIENCE

DEPARTMENT OF CIVIL ENGINEERING

EDMONTON, ALBERTA

SPRING 1985

THE UNIVERSITY OF ALBERTA

RELEASE FORM

NAME OF AUTHOR   FAYE E. HICKS

TITLE OF THESIS   SHEAR AND VELOCITY NEAR A SLOPED BANK IN
                           A CURVED CHANNEL

DEGREE FOR WHICH THESIS WAS PRESENTED   MASTER OF SCIENCE

YEAR THIS DEGREE GRANTED   SPRING 1985

Permission is hereby granted to the UNIVERSITY OF ALBERTA

LIBRARY to reproduce single copies of this thesis and to lend or

sell such copies for private, scholarly or scientific research

purposes only.

The author reserves other publication rights, and neither the

thesis nor extensive extracts from it may be printed or otherwise

reproduced without the author's written permission.

(SIGNED) ....*Faye E. Hicks*......

PERMANENT ADDRESS: ·

.....5951 - 40 Avenue.............

.....Edmonton, Alberta...........

.....T6L 3P6.....................

DATED .....December 7, 1984.....

THE UNIVERSITY OF ALBERTA

FACULTY OF GRADUATE STUDIES AND RESEARCH

The undersigned certify that they have read, and recommend to the Faculty of Graduate Studies and Research, for acceptance, a thesis entitled SHEAR AND VELOCITY NEAR A SLOPED BANK IN A CURVED CHANNEL submitted by FAYE E. HICKS in partial fulfillment of the requirements for the degree of MASTER OF SCIENCE.

....

....

....
Supervisors

....
External Examiner

Date .....December 7, 1984.........

ABSTRACT

Understanding the effects of curvature on the flow in rivers is important to the practicing engineer. Consideration of the resulting redistribution of boundary shear stress and velocity are especially important in the design of bank erosion protection for river bends.

The purpose of this study was to examine the developing flow near a sloped bank in a bend. The intention was to determine if there is a potential for economizing on construction costs when using riprap, by zoning the sizes up the bank and around the bend. Zoning would involve using larger rocks in areas of severe attack and smaller rocks in areas of less severe attack.

The first part of this study reviews the results of previous investigations into the characteristics of shear and velocity distributions in channel bends. The second part presents a contribution to the existing body of data, with analysis directed toward an increased understanding of the development of the flow along the sloped bank as the flow progresses through the bend. The final section of this study compares these findings to previous laboratory and field investigations, and describes possible practical applications of these results.

The experimental investigation involved a laboratory flume study of a 270° bend in which six runs, comprised of three flow depths and two side slopes were made. Longitudinal and lateral velocities and

turbulent fluctuations, were measured with a Laser Doppler Anaemometer. Boundary shear stresses and boundary stress angles were computed from the measurements.

As a result of this investigation it was found that zoning riprap sizes up a bank is likely not feasible. However, the potential does exist for zoning around the bend. There was also some evidence that higher aspect ratios were associated with quicker developement of the secondary circulation.

ACKNOWLEDGEMENTS

TABLE OF CONTENTS

LIST OF TABLES

LIST OF FIGURES

LIST OF SYMBOLS

B	Channel mean width (at half depth)
C	Chezy coefficient
D	Hydraulic mean depth (area/topwidth)
F_R	Froude number
g	Acceleration due to gravity
L_s	Development length for the spiral flow
n	Refractive index of water
R	Hydraulic radius of channel section
R_0	Radius of curvature of channel centreline
R_e	Reynolds number
S_0	Longitudinal bed slope
u	Longitudinal velocity
u'	Deviation of longitudinal velocity from mean
$\bar{u}$	Depth averaged longitudinal velocity
u_*	Longitudinal shear velocity
U_*	Cross sectionally averaged longitudinal shear velocity in straight reach or shear velocity scale
V	Cross sectionally averaged longitudinal velocity or velocity scale
v	Lateral velocity
v'	Deviation of lateral velocity from mean
$\bar{v}$	Depth averaged lateral velocity
x	Longitudinal co-ordinate
y	Lateral co-ordinate
z	Vertical co-ordinate

zmax   Perpendicular distance from boundary to water surface at a given profile

Z_{max} Perpendicular distance from bed to water surface at a given section or depth scale

β Aspect ratio (width/depth)

θ Beam intersection angle

ν Kinematic viscosity

τ_0 Total boundary shear stress

δ Thickness of turbulent boundary layer

ρ Mass density of water

$\tan \phi$ Tangent of angle of total bed stress from longitudinal at a given profile

$\tan \Phi$ Tangent of angle of total bed stress from longitudinal at the centre of a given section

INTRODUCTION

Understanding the mechanics of flow around a bend in an open channel is essential to the practicing river engineer. Curvature effects are important in the consideration of the processes of flow resistance, superelevation of the flow, distribution of flow and especially channel stability and sediment transport.

In Canada, bank stabilization works involve the expenditure of millions of dollars every year, much of which is spent on riprap armouring of these eroded banks. Yet the three dimensional nature of the curved channel flow phenomenon is inadequately understood, and design techniques are for the most part empirical. Unfortunately, we are at present a long way from being able to adopt a purely analytical approach to erosion protection design. This is especially true considering the complexity of the problem for even simple channel shapes, and the lack of detailed flow information at most design sites.

The present study confined itself to a situation resembling a riprap armoured bank, allowing the examination of a limited range of practical side slopes and a rigid bank. However, for simplicity; a rigid bed, a prismatic channel shape and a smooth boundary were used. These simplifications limited the practical applicability of the results, however, it was the purpose of this study to gain information about the distribution of velocity and boundary shear stress on a sloped bank in an open channel bend, and to apply this knowledge to the considerations of riprap design in a general manner. It was the intent that the information gained from this

1

study would indicate what potential exists for zoning riprap sizes up a bank, and around a bend, in an effort to economize on construction costs.

The first part of this study reviews the results of previous investigations into the characteristics of shear and velocity distributions in channel bends. The second part presents a contribution to the existing body of data, with analysis of data directed toward an increased understanding of the redistribution of the flow around a bend as it pertains to the sloped bank. The final section of this study compares these results to previous laboratory and field investigations, and describes possible practical applications of these results.

1. PART ONE - LITERATURE REVIEW

1.1 INTRODUCTION

Characteristics of the flow in a bend are quite different from those in a straight reach. Centrifugal acceleration produces a number of effects such as superelevation of the water surface and helicoidal flow, which in turn lead to a redistribution of the velocity and boundary shear stress distributions. These flow characteristics have a pronounced effect on erosion, deposition and sediment transport in a natural channel.

In the past, numerous laboratory investigations have been conducted in an effort to better understand the complexities of flow around a bend, however, field investigations are rather scarce. This section discusses some of these investigations as they pertain to the current study.

1.2 VELOCITY DISTRIBUTION IN OPEN CHANNEL BENDS

1.2.1 Causes and Development of Secondary Circulation

The most signif   aspect of the flow in curved channels is the secondary ci ula   or helicoidal flow, which is set up by the transverse surfa   nt (superelevation) which itself occurs as a direct result of   gal acceleration. This spiral flow essentially originates becau   e ntrifugal force has a different effect at different depth   due to the decreasing longitudinal velocity of the flow in the vicinity of the bed. The lower fluid,

slowed by the bed resistance, has less inertia than the faster moving fluid above and is therefore less able to resist the effects of the transverse pressure gradient caused by the superelevation of the flow. Consequently, the slower moving fluid is accelerated toward the inside of the bend, until it is balanced by friction. The faster moving fluid near the surface experiences the opposite effect and is accelerated outward. Because the fluid possesses inertia, there is a distance over which this spiral flow becomes fully developed. Rosovskii (1961) and Nouh and Townsend (1979) estimate the development length as the distance to reach 90 percent of its 'developed' value. They presented,

$$L_s = (1.8 \text{ to } 2.3) \; D \; C/\sqrt{g} \tag{1}$$

where:

   L_s = development length for the spiral flow;

   C   = Chezy coefficient;

   D   = flow depth; and

   g   = acceleration due to gravity.

This assumes that the water surface changes abruptly from flat to superelevated. As the relationship indicates, development of the secondary circulation occurs relatively quickly. At the downstream end of the bend the decay occurs in the same way, although in reverse, therefore the decay length is the same as the development length. Steffler (1984), in his laboratory investigation using a rectangular channel, found this decay to begin soon after the spiral flow was observed to be fully developed.

The distribution of lateral velocities at a vertical profile can be said to be comprised of two parts. First is that portion which represents the spiral flow and exhibits a net value of zero transverse flow. Superimposed on this distribution is a net inward or outward flow, associated with the overcoming of inertial effects in the redistribution of the longitudinal velocities. That portion which represents the spiral flow increases in magnitude (strength) as the spiral flow develops, and decreases as it decays, over a distance such as estimated by Equation 1. That portion which reflects the longitudinal velocity redistribution is discussed further in Section 1.2.3.

In their field study of the flow around several actual river bends, Bathurst et.al. (1979) found that small cells of reverse circulation, commonly known as relic cells, seemed to be carried over from upstream bends to the outside of downstream bends. However, they also observed similar cells in isolated bends where the outside bank was steep, although not where the outside bank was sloped gently. They report that the effect of these cells seldom extend for more than one or two flow depths into the channel, however, the cells are significant in all cases concerning the problem of bank erosion. Steffler (1984) also observed evidence of a counter rotating cell on the outside of his rectangular channel section, once the secondary circulation was fully developed.

1.2.2 Strength of Secondary Circulation in Natural Channels

Bathurst et.al. (1979), in their field investigation, observed that the strength of the secondary circulation appeared to depend upon a number of factors including Reynolds number, aspect ratio (width to depth ratio), arc angle of the bend and the ratio of radius of curvature to channel width. As Steffler (1984) shows, the strength of the secondary circulation is most dependant upon the magnitude of the longitudinal velocity and the flow depth. This means that the strength of the spiral flow cannot only vary from bend to bend, but varies with discharge (as expected). Field measurements by Bathurst et.al. (1979) seemed to suggest that secondary circulation is weakest during very low flows, when primary velocities are low and the centrifugal force is therefore small; and during very high flows when, although primary velocities are high, point bars are submerged thereby increasing the effective radius of the curve and therefore reducing the centrifugal force. Conversely at medium flows when point bars are only partially submerged, the curvature remains relatively high, and primary velocities are high as well, consequently secondary circulation is strong.

1.2.3 Longitudinal Flow Distribution

Ippen et.al. (1962), in their laboratory investigations using trapezoidal channels, found that in cases of reduced curvature the helicoidal motion was the dominant factor in the development of high velocities along the outside of the bend. They also observed, however, that as curvature increased the separation zone commonly

observed on the inside of the bend effectively constricted the stream, thus further increasing velocities and deflecting the flow toward the outside bank.

Velocity distributions, presented by section in that study, indicated an initial shift in longitudinal maximum velocity toward the inside of the bend upstream of this separation zone. McCrea (1983) and Steffler (1984) also observed this shifting of the longitudinal maximum velocity first toward the inside of the bank, followed by the outward shift of the maximum longitudinal velocity. In fact, this is a well known characteristic of the longitudinal velocity redistribution, Chow (1959) states that where bank protection is required it is needed on the outside bank near its downstream end, and to a lesser extent, on the inside of the bend near its upstream end.

Initially the longitudinal velocity redistribution occurs independent of friction. This results in a 'free vortex' velocity distribution, exhibiting an increase in velocities towards the inside of the bend. There is a corresponding net inward transverse flow. As the secondary circulation develops (due to friction), there is a strong skewing of the flow outward, and the maximum longitudinal velocity moves to the outside bank. This is accompanied by a net outward transverse flow. In a sufficiently long bend, the longitudinal velocity may become fully developed as the net transverse flow approaches zero. At the bend exit, a redistribution of the longitudinal velocity to the outside again occurs, equal yet opposite to that which occurred at the entrance to

the bend. This is again accompanied by a net outward transverse flow.

Although development of the longitudinal velocity redistribution follows the development of the spiral flow, it occurs at a much slower rate. Steffler (1984) did not observe the longitudinal velocity redistribution to be fully developed even in his 270° bend. Considering the irregular shape of natural channels, and the fact that they seldom sustain a constant radius of curvature, it is unlikely that the longitudinal velocity redistribution becomes fully developed even in long bends. Although decay of the longitudinal velocity distribution occurs equal and opposite to the development, it may still take much longer. That is because the development is assisted by the spiral flow, which is not the case with decay. Predicting the distance required for this decay is important in the consideration of where to end bank protection works.

1.3 BOUNDARY SHEAR STRESS DISTRIBUTION IN OPEN CHANNEL BENDS

Of prime importance in the consideration of bank erosion is the redistribution of the boundary shear stress through the bend. In the straight reach upstream of a bend the shear stress exhibits a fairly uniform distribution, as do the longitudinal velocities. In fact the two are closely related, and as Bathurst et.al. (1979) report, the redistribution of the boundary shear stress follows that of the longitudinal velocity. Ippen et.al. (1962), McCrea (1983) and Steffler (1984) all confirm this tendency. This occurs because the magnitude of the boundary shear stress is directly proportional

to the velocity gradient near the boundary. Because zones of high velocity must lead to a compression of the velocity isovels near the boundary, a local increase in the boundary shear stress results.

Ippen et.al. (1962) investigated the shear stress distribution in both smooth and rough trapezoidal channels, and found the distribution of boundary shear stress around the bend to be very dependant upon the stream geometry. Increased stream curvature was associated with higher stresses developed both along the inside of the bend in the upstream portion of the curve, and along the outer bank past the bend. Increased curvature and depth were also found to be associated with the upstream movement of the location of the maximum shear stress , from the outside of the bend to the inside. Decreasing curvature was found to lead to decreased average shear stress, and a tendency for the inner bank shear stress to diminish as well.

The comparison of their results from the smooth and rough channels indicated that, for the latter case, there was a much quicker transfer of the stream momentum to the outside bank, and a general increase in the maximum observed shear stress. Both were attributed to the fact that in a rough channel there is a greater thickness of fluid slowed by the boundary roughness. As a consequence, more fluid can be induced to move toward the inside of the bend by the transverse pressure gradient. This accelerates the crossover and manifests itself in a overall increase in the attack along the outside bank. They concluded that, in natural streams, even greater variation could be expected.

Bathurst et.al. (1979) also found that the boundary shear stress distribution in natural river bends was affected by stream geometry parameters such as: bend curvature; arc angle of the bend; and width to depth ratio. They also observed that increased curvature was associated with increasing maximum shear stress. They found that the strength of the shear stress seemed to be related to Reynolds number as well. In cases of low and high flow, where the secondary circulation was observed to be weak, they compared it with shear stress distribution in straight reaches.

Another interesting finding of their study was the relationship between shear stress peaks and the reverse circulation cells (observed adjacent to steep outside banks). These shear stress peaks were found to be associated with the downwelling region at the junction of the main secondary cell and the counter rotating cell, for low and medium discharges. At high flows, where the primary velocities were strong the peaks appeared to be associated with maximum velocity instead.

2. PART TWO - EXPERIMENTAL STUDY

2.1 INTRODUCTION

The fundamental purpose of this study was to investigate the distribution of shear stress and velocity along a sloped bank around a bend, in order to gain information which might be valuable in the design of riprap armouring for bank protection. Specifically the objective was to investigate the feasibility of zoning riprap sizes up a bank and around a bend, rather than using one large size throughout. An additional purpose of this study was to provide further experimental data to augment that obtained by previous investigators.

With these in mind, the following experimental objectives could be defined:

1. That the model itself should be of realistic proportions and should operate at a natural Froude number and an adequate Reynolds number such that is could be considered representative of actual river bends.

2. That detailed lateral and longitudinal velocities should be measured, along with their corresponding turbulence intensities; and that such measurements should facilitate the evaluation of boundary shear stresses and any other pertinent characteristics of flow.

3. That the model should cover a range of side slopes realistic to its application to riprap armoured banks.

The experimental facility used was designed specifically for use with the DISA Laser Doppler Anaemometer (LDA) in the University of Alberta's T. Blench Hydraulics Lab. Six runs were conducted with a combination of two side slopes and three flow depths.

2.2 FACILITIES AND PROCEDURES

2.2.1 Flume

The flume was constructed of galvanized sheet metal on steel supports. Plexiglass was substituted for the sheet metal at each measurement section, to allow the laser light beams to enter the flow from below. The original flume itself was rectangular in shape 1.07 metres (m) wide and 0.20 m deep, with a radius of curvature to the centreline of the channel section of 3.66 m. The side slope was constructed inside the rectangular flume, along the outside of bank using flexible plexiglass on wooden supports. Figure 1 illustrates the channel sections for each of the two side slopes.

Two side slopes were used, first 3 to 1 (horizontal to vertical) then 2 to 1. An even steeper side slope was desirable, but due to the physical limitations of the existing flume a 1 to 1 side slope would have afforded inadequate room to manipulate the LDA and still obtain a reasonable quantity of information on this sloped bank. It was felt that investigation of more flow depths at the two practical side slopes, would provide more valuable information.

Figure 2 shows the flume layout and test locations. The curve consisted of a 13.4 m long entrance section, a 17.2 m curved segment

covering an arc of 270°, and a 2.4 m straight exit section. The slope of the flume was set constant for all runs at 0.00083 (1/1200). This was sufficiently small that the change in elevation from one end of the flume to the other was inadequate to allow clearance for the recirculation of the flow, therefore the exit section terminated in a drop box. Flow circulation was facilitated by pumping from a level regulated sump to the bottom of the head box. The head box itself was equipped with a gate which regulated overflow back into the sump, thus allowing the control of the flow depth. The exit section was equipped with a tailgate to prevent drawdown of the flow.

2.2.2 Co-ordinate System

Figure 3 defines the co-ordinate system adopted for this study. x, y, and z represent co-ordinates of length along the flume centreline, across the flume perpendicular to the flow, and up from the bed of the flume, respectively. x is positive in the downstream direction with its origin at the beginning of the curve and y is positive out from the centreline of the original rectangular flume. This y origin was chosen to provide a consistent reference point for all runs, as Figure 1 illustrates. z is positive up from the boundary. u and v are the velocities corresponding to the x and y directions, respectively. Figure 4 illustrates the measurement convention in the z direction.

2.2.3 Laser Doppler Anaemometer

As stated already, the laser light beams entered the flow through the plexiglass observation stations from below the flume. The location of the measuring point was moved by traversing the plane mirror and focusing lens on threaded tracks. This traversing mechanism was motor driven and controlled by a computer. The laser and optics did not move during this traversing process. Positioning of the light measuring point was accurate to +0.01 mm. The threaded tracks had a maximum range of 0.6 m therefore two setups were required for each section. This involved manually moving the trolley carrying the LDA system. Alignment of the measurements was facilitated by means of a string through the centre of the curve and a reflecting surface above the flow.

The laser itself was a 4W Argon-Ion laser, run using 500-600 mW. Two focal lengths were used for the study, 160 mm for Runs 1 to 5 and 80 mm for Run 6.

Figure 3 illustrates schematically the flow of information for the LDA setup. The laser beam was split into three light beams: blue, green and mixed, which intersected at the measuring point. These three beams excited the optics parallel to and concentric about its axis. These optics were aligned such that the blue/mixed lined up tangential to the channel axis, and the green/mixed lined up normal to the channel axis, facilitating direct measurement of longitudinal and lateral velocities. The optics also collected the scattered light which was then separated by colour sensitive mirrors, converted into electric signals by separate

photo-multipliers, and fed to the frequency shifter. This in turn passed the signal on to two counters (one for each direction) that evaluated the Doppler frequency. The coincidence filter assured that the measurements from each of the two directions occurred close enough together to be considered simultaneous.

Scattering of light was accomplished by seeding the flow with latex paint (concentration less than 2 ppm). Cornstarch was tried for this purpose as well, but it was found to be too heavy to stay in suspension at the velocities encountered.

2.2.4 Data Acquisition and Reduction

Steffler (1984) provides a detailed description of the acquisition and reduction techniques used. Longitudinal velocity and its mean square turbulence intensity were measured by the green/mixed beams, while secondary velocity and its mean square turbulence intensity were measured by the blue/mixed beams. The Doppler frequencies were analyzed according to residence time in the measuring volume, using the total number of fringes in a burst. This information was provided by one of the counters. A minimum sample size of 10,000 readings, with individual readings not more than 4 standard deviations away from the mean, was collected at each measuring point.

At each cross section thirteen vertical profiles were taken, in a direction perpendicular to the boundary. Four to five of these profiles were located on the sloped outside bank. These measurements were started as close to the boundary as possible and

were spaced at increasing increments up toward the surface. These data were stored on floppy disk for later transfer to the University of Alberta main computer for analysis.

The vertical co-ordinates had to be adjusted for refraction. The formula used was:

$$z = (z' - z'_0) \left\{ \frac{n}{\cos (\theta/2)} \right\} \left\{ \frac{1 - \sin^2 (\theta/2)}{n^2} \right\}^{1/2} \qquad (2)$$

where:

z = actual measuring point distance above the bed;

z' = traverse reading;

z'_0 = traverse reading when beam intersection was on the inside of the wall;

n = refractive index of water = 1.33; and

θ = beam intersection angle.

2.3 EXPERIMENTAL RESULTS

2.3.1 Introduction

Six runs were conducted for this investigation the significant details for which are given in Table 1.

The model was designed to realistically represent an actual river bend, as the details in Table 1 show. Of prime importance is a valid Froude number. Values for Alberta rivers were obtained by examining the data presented by Kellerhals et.al. (1972). The majority of natural Froude numbers were found to range between 0.1

Table 1. Significant Details of the Experiments

Run No.	R_o (m)	Side Slope	B (m)	D (m)	V (m/s)	S_o	B/R_o	β	D/R_o	F_R	R_e ($\times 10^{-4}$)
1	3.59	3:1	0.934	0.080	0.44	0.00083	0.260	11.7	0.0222	0.504	2.9
2	3.58	3:1	0.910	0.069	0.34	0.00083	0.254	13.2	0.0192	0.416	1.9
3	3.57	3:1	0.896	0.055	0.35	0.00083	0.250	16.1	0.0155	0.473	1.6
4	3.57	2:1	0.890	0.083	0.41	0.00083	0.250	10.7	0.0232	0.455	2.9
5	3.57	2:1	0.880	0.075	0.40	0.00083	0.246	11.7	0.0211	0.471	3.0
6	3.56	2:1	0.862	0.060	0.37	0.00083	0.242	14.2	0.0170	0.478	2.2

to 0.6 at bankfull discharge (a typical design flow), thus the experimental range of about 0.4 to 0.5 given in Table 1 can be considered reasonable.

Also of importance are parameters such as bed slope, aspect ratio (β), and width to radius of curvature ratio. Typical values for the first two items were also obtained from the data on Alberta rivers given by Kellerhals et.al. (1972). Values for those rivers investigated ranged from about 0.00004 to 0.02 for the bed slope, and from about 5 to 80 for the aspect ratio. Both the bed slope and the aspect ratios used in the experiments were within these ranges, however the latter, ranging from about 10 to 16 would be catagorized as narrow streams, such as the Swan River, Little Paddle River and Vermilion River. Aerial photographs of these rivers were used to obtain estimates for typical values of the width to radius of curvature ratio. Characteristic values ranged from about 0.1 to 0.3. Again Table 1 indicates that the model was realistically proportioned.

The Reynolds number ranged from 1.6×10^4 to 3.0×10^4, which assured fully turbulent flow. Thus viscosity effects remained negligible in the redistribution of the flow characteristics. The entrance section was sufficiently long to assure a fully developed turbulent boundary layer by the time the flow reached Section 1. This can be checked by estimating the boundary layer thickness, (δ), using the Blasius equation, and assuming turbulent conditions exist at the channel entrance (Ippen et.al., 1979):

$$\frac{\delta}{x} = \frac{0.38}{\left(\frac{V\,x}{\nu}\right)^{1/5}} \tag{3}$$

where:

x = distance from channel entrance;

V = cross sectionally averaged longitudinal velocity; and

ν = kinematic viscosity of the flow.

Substituting: x = 13 m; v = 0.44 m/s; and ν = 10^{-6}; yields a value of δ = 0.2 m, confirming that the turbulent boundary layer was developed for all six runs.

2.3.2 Velocity Distributions

Figures 6 through 9 illustrate the longitudinal velocity profiles at Sections 1 to 4, for Run 6. Figures 10 and 11 show the velocity distributions at each section for Runs 1 and 6. These figures show quite clearly the redistribution of the longitudinal velocity pattern, as the flow progresses through the bend. It should be remembered when viewing Figures 10 and 11, that the y origin represents the centreline of the rectangular section into which the side slopes were built, as the actual channel centreline for the trapezoidal section varied from run to run due to the channels' assymetric shape (see Figure 1).

At Section 1 just upstream of the curve (x = -0.75 m), the flow distribution was relatively uniform (again keeping in mind the assymetric channel shape) showing a slight tendency for higher velocities near the inside bank in the case of Run 6. Velocities on

the side slope were much lower than in the rest of the channel and
they decreased up the bank. By Section 2 (x = 5.75 m), the
maximum velocity had moved to the outside bank, with a corresponding
decrease in velocity along the inside bank, as Figure 10 shows. By
Section 3 (x = 11.5 m) the flow was strongly skewed to the outside,
and the maximum channel velocity was increasing. This tendency
continued at Section 4, just downstream of the curve (x = 17.5).

Comparison of the velocity profiles for the four sections shows
not only the skewing of the velocity distribution, but also the
changing shape of these profiles as the flow proceeded around the
bend, (Figures 6 to 9). Compared to the straight upstream section
(Section 1), the other profiles showed a marked increase in the
velocity gradient near the boundary. This effect was observed first
to occur on the side slope at Section 2, which stands to reason as
an increase in the velocities in that area must result in a
compression of the velocity isovels. At Sections 3 and 4, where the
maximum channel velocity showed an increasing trend, profiles near
the slope showed this effect as well as those on the slope.

Comparing the two side slopes, there appeared to be a slight
tendency for the longitudinal velocity to skew outward more quickly
in the case of the steeper side slope. This was especially evident
when comparing results for Section 4. For the 2 to 1 side slope
(Run 6), the location of the maximum velocity isovel remained at the
very outside, however, this was not the case for the 3 to 1 side
slope (Run 1).

Figures 12 through 15 illustrate the development of the spiral flow by depicting the lateral velocity profiles at Sections 1 to 4 for Run 6. At Section 1, in the straight reach, the magnitude of the lateral velocities were found to be very small; typically the maximum observed values were in the order of 2 to 5 percent of the average longitudinal velocity. They usually occurred near the walls and were directed toward the centre. At Section 1, Run 6 showed much more scatter at the top of those profiles nearest the inside wall, than did other runs. An extreme peak velocity of about 8 percent of the channel average in the longitudinal direction was observed, as Figure 12 illustrates.

The spiral flow pattern was well established by Section 2, as Figure 13 shows. Large lateral velocities were apparent, especially the inward component near the bed. Values near the walls were somewhat lower in magnitude.

By Section 3 the spiral flow appeared quite fully developed, with maximum lateral velocities near the surface of the same order of magnitude as those near the bed, however, somewhat smaller than those at Section 2, indicating the decay of the secondary circulation. Again circulation near the walls was not as strong as near the centre, as evidenced by the spreading of the velocity profiles shown in Figure 14. Typically, by Section 4, a further decrease occurred in the magnitude of the lateral velocities.

There was some evidence of counter rotating cells near the outside wall at Section 3 in Run 1, and to a much smaller extent at Section 4. Evidence of such a cell at the outside of Section 4 was

also observed during Run 4.

2.3.3 Turbulent Fluctuation Intensities

The turbulent intensity fluctuation distributions in the longitudinal direction $(\overline{u'^2})$ for Run 6 are shown in Figures 16 through 19 for Sections 1 to 4, respectively. At Section 1 the profiles characteristically showed a peak near the bed and a gradual reduction near the surface. These peaks near the bed support the concept of the occurrence of a high boundary shear stress. Peaks on the sloped bank were of a similar magnitude, although they were somewhat smaller than those near the bed, and not as well defined. At Section 2 the profiles showed a similar tendency, however the peak values along the wall (slope) were increased such that they were about the same as those on the bed. These peaks were also much more sharply defined. This general trend towards increasing peak values of $\overline{u'^2}$ continued through Sections 3 and 4.

Figures 20 through 23 show the turbulent intensity distributions in the lateral direction $(\overline{v'^2})$ for Run 6, Sections 1 to 4, respectively. They appeared to be somewhat similar in shape to those in the longitudinal direction, having a maximum value near the bed and showing a gradual reduction toward the water surface. However, the peak was much more rounded and typically about half to two thirds as large as the corresponding values in the longitudinal direction. Peak values up the slope were similar to those elsewhere at all sections, although they appeared not to decrease as much near

the surface. Considering the variation around the bend, there again appeared to be a trend towards increasing peak values, and 'peakier' shapes.

2.4 ANALYSIS OF RESULTS

2.4.1 Velocities

Averages of the longitudinal and lateral velocities were determined at each profile by numerical intergration. Values on the outer bank represent an average through a profile perpendicular to the slope rather than a vertical (as Figure 4 illustrates), as these profiles were oriented to facilitate computation of the boundary shear stress. True averages through vertical profiles could have been obtained using interpolated values determined between profiles, however, it was felt that the perpendicular profiles were adequate, as they still indicated behavioral tendencies up the slope, and either method would be approximate.

2.4.2 Boundary Shear Stress

The boundary shear stress in the longitudinal direction was determined using the mean velocity results, and is expressed in the form of a shear velocity, u_*. The longitudinal velocity profiles were fitted to a semi-logarithmic distribution defined by the following equation:

$$\frac{u}{u_\star} = 5.75 \log \left(\frac{z \ u_\star}{\nu}\right) + B \qquad\qquad (4)$$

where:

u = longitudinal velocity at depth z;

z = location of measurement point above the bed;

ν = kinematic viscosity of water; and

B = a constant.

The value of $u_\star$ was initially estimated using the first ten values of velocity above the 3 mm depth; 60 percent of the flow depth was taken as an upper limit (Schlichting, 1979). A semi-logarithmic line was then fitted through these points expressed non-dimensionally as u/u versus log z/zmax, where u represents the depth averaged longitudinal velocity, and zmax represents the maximum z value at that profile (as shown in Figure 4). This first value of $u_\star$ was then used to eliminate all points less than 70 /$u_\star$ (Schlichting, 1979). A second value of $u_\star$ was computed and the procedure was repeated until there was no change in $u_\star$. This procedure was not particularly well suited to computer analysis as some judgement was required. Therefore, visual examinations of the semi-logarithmic plots were conducted to confirm and refine the results. Figures 24 through 27 show semi-logarithmic plots of $u/u_\star$ vs. $zu_\star/\nu$. They confirm that the assumption of a semi-logarithmic distribution is valid over the range indicated. Equation 4 is plotted on these figures as well, for comparative purposes. A value of B = 5.5 was used (Schlichting, 1979).

Figures 28 through 33 show the distribution of the boundary shear stress for each section of Run 1 to Run 6. As expected, they show the same tendencies as the longitudinal velocity distributions. At Section 1 the distribution was rather uniform, with values on the slope being lower than those on the bed. As the flow progressed around the bend the trend was to increasing values along the outside of the bend, especially on the side slopes, with a corresponding decrease on the bed near the inside of the bend. There appeared to be no significant difference in the magnitude of the shear stress experienced by the different side slopes, for corresponding flow depths.

Polar plots of the longitudinal and lateral velocities indicated that the total bed stress vector could reasonably be assumed to lie in the same path as the resultant velocity vector. The orientation of the velocity vector near the bed was determined by best line fit of points below:

$$\frac{u}{u_*} < 12 \tag{5}$$

which is an upper limit recommended by Nash and Patel (1972). In many cases there were insufficient points below this limit to allow this determination, however those that did allow it indicated a tendency for the angle to decrease up the slope. With respect to the variation around the bend no strong conclusion could be drawn, however, there did seem to be some evidence that all angles tended to increase at Sections 2 and 3 and decrease by about a half by Section 4. Values were found to be near zero at Section 1, as might

be expected.

Figure 34 shows a polar plot of the velocities at Section 3 of Run 6, illustrating this straight line tendency and the trend toward a decreasing angle up the bank. Figure 35 illustrates the variation of the bed stress angle up the slope for Sections 2 and 3 of Run 6. tan I represents the bed stress angle at the centre of the section and tan o represents the local bed stress angle; zmax represents the total depth at the profile and Zmax represents the maximum depth in the channel as shown in Figure 4.

3. PART THREE - DISCUSSION OF RESULTS

3.1 INTRODUCTION

As stated earlier, the prime objective of this study was to observe the variation of shear and velocity distributions along sloped banks with particular focus on characteristic variations up the bank and the effects of varying side slope. Variations along the slope through the bend were to be considered as well. It was intended that a better understanding of these behaviors will lead to fewer failures of bank erosion protection works, and yet will at the same time decrease construction costs once these variations are understood sufficiently to improve riprap design techniques.

There are two typical criteria used for determining the size of rock required to resist movement, one based on allowable attack velocity and the other based on tractive force theory. These are fundamentally the same and should therefore yield the same results. With these two approaches in mind, this section discusses the variation of the shear and velocity distributions along the sloped bank. Other important factors such as the secondary circulation and the turbulent fluctuation intensities are considered as well, however, in necessarily more qualitative terms.

3.2 LONGITUDINAL VELOCITIES

Consideration of an allowable attack velocity is probably the most common criteria used by practicing engineers, perhaps because it is easier to identify with than shear stress. Typically a design

attack velocity is determined by using the average approach channel velocity as a base in some empirical equation. There are numerous approaches, perhaps the simplest is taking 4/3 times the average channel velocity to be the attack velocity along the bank (California Department of Transportation, 1970). Whatever the empirical equation, the next step is to relate this attack velocity to rock size using a table or figure. Such a table or figure may be developed from tractive force theory, however, once the relationship between velocity and rock size has been developed, tractive force is not considered again. Quite often such a relationship is based purely on results of laboratory measurements where the velocity required to initiate movement was the actual measured quantity, leading to an empirical relationship between critical velocity and rock size.

Using an empirical equation eliminates the need to precisely define attack velocity, however, it must be determinable when trying to apply distributions measured in the lab to prototype situations. There are likely two rational approaches, one would be to take the depth averaged longitudinal velocity, (perhaps modified by some safety factor) or alternatively, to consider the velocity at some distance above the bed where it would be considered to have maximum influence on rock movement. The latter actually approaches a boundary shear stress consideration, and as such will not be pursued further here. The former, which will be discussed next, would still be highly empirical in application and is therefore, perhaps, somewhat less desirable.

Figures 36 to 39 illustrate the variation of the longitudinal velocity up the 3 to 1 side slope for Sections 1 to 4, respectively. Figures 40 to 43 do the same for the 2 to 1 side slope. Again (as in Figure 35), zmax/Zmax indicates relative position up the bank; $\bar{u}/V$ is the ratio of depth averaged longitudinal velocity to the cross sectionally averaged longitudinal velocity at that section. At Section 1, in the straight reach upstream of the curve (Figures 36 and 40), $\bar{u}/V$ appeared to gradually decrease up the slope, with a maximum near the bottom of about 1 to 1.1. Generally there did not seem to be a strong variation for the different discharges, although there was more scatter for the 3 to 1 side slope. Comparison of the results for the two side slopes indicated that values for the steeper side slope did not appear higher in this straight section.

At Section 2 (Figures 37 and 41), the runs on the 3 to 1 side slope showed a great deal of scatter, especially Runs 2 and 3. It should be noted that some problems developed with Runs 2 and 3 due to inexperience with the complex LDA equipment, possibly accounting for this scatter. Results on the 2 to 1 side slope indicated a much more defined relationship which appeared to show good agreement with Run 1 on the 3 to 1 side slope. Again there was an indication that $\bar{u}/V$ versus zmax/Zmax did not depend much on discharge (Figure 41), and values on the 2 to 1 side slope were slightly higher than on the flatter slope (as would be expected). By a zmax/Zmax of 0.4 or (40 percent of the way down the slope), $\bar{u}/V$ was already about 0.9 (except for the scattered runs), indicating that the potential for

zoning riprap sizes up the bank could be limited. This will be discussed further later on. The maximum $\bar{u}/V$ was about 1.1, which agrees well with Yen (1965) for his investigation in a 90^0 bend.

Figures 38 and 42 for Section 3, illustrated a relatively steep gradient of $\bar{u}/V$ versus zmax/Zmax, as well as a definite tendency for those values on the 2 to 1 side slope to be higher than on the flatter 3 to 1 side slope (by about five percent). By a zmax/Zmax of 0.4, $\bar{u}/V$ was about 1. As for previous sections the relationship did not appear to depend significantly on discharge. The maximum $\bar{u}/V$ was about 1.2.

At Section 4 (Figures 39 and 43) there appeared to be more spread between runs for both side slopes, indicating perhaps some dependence on discharge. Values for the 2 to 1 slope were up to 20 percent higher than those on the 3 to 1 slope, and in both cases values of $\bar{u}/V$ increased quickly down from the top of the slope. By a zmax/Zmax of 0.4 values of $\bar{u}/V$ were 0.95 to 1.2 for the 3 to 1 side slope, and 1.2 to 1.4 on the 3 to 1 side slope. The maximum observed was 1.45.

These figures illustrated a limited capability of zoning of rock sizes up a slope. Even near the upstream end of the bend where $\bar{u}/V$ increases more gradually, it has to be remembered that $\bar{u}$ must still be related to some attack velocity. Such decreases in $\bar{u}$ up the slope might be counteracted by the fact that flow depth is decreasing and therefore velocity isovels might be more compressed near the boundary. The only way to determine this is by considering the velocity gradient at the boundary, which is then the

consideration of boundary shear stress.

Figures 44 through 49 show the $\bar{u}/V$ versus zmax/Zmax relationship in a slightly different way, by run rather than by section. These figures indicate the potential for zoning of rock sizes around a bend to be high, as expected. They also illustrate the comparison between side slopes (as already discussed), where there does not appear to be a radical difference until at least Section 3 or 4.

3.3 BOUNDARY SHEAR STRESS

It appears that the most direct approach towards sizing riprap protection would be the consideration of tractive force theory in combination with a predicted distribution of boundary shear stress. This is particularly necessary if designers hope to zone rock sizes, considering the difficulties encountered when trying to ascertain the actual attack velocity.

Figures 50 to 53 illustrate the variation of the longitudinal shear velocity up the 3 to 1 side slope for Sections 1 to 4, respectively. Figures 54 to 57 do the same for the 2 to 1 side slope. Again zmax/Zmax indicates the relative position up the bank; u_*/U_* is the ratio of the shear velocity at a point on the bank to the average shear velocity in the straight section upstream of the curve.

Shear velocity varies as a direct function of the boundary shear stress such that:

$$u_* = \sqrt{\tau_0/\rho} \tag{6}$$

where:

τ_0 = total boundary shear stress; and

ρ = mass density of water.

The shear velocity at a point was determined as discussed in Section 2.4.2. The average shear velocity in the straight section upstream of the curve was determined using the equation:

$$U_* = \sqrt{g R S} \tag{6}$$

where:

g = acceleration due to gravity;

R = channel hydraulic radius (area/wetted perimeter); and

S = slope of the energy grade line.

At Section 1, in the straight section upstream of the curve (Figures 50 and 54), there appeared to be tendency for the boundary shear stress to decrease up the slope, especially for the 3 to 1 side slope. As in the case of the velocities, there did not appear to be excessive spread between runs, indicating that there was not a strong dependence on discharge. Also there did not seem to be much variation between the two side slopes. The maximum value of u_*/U_* at Section 1 was about 1.15.

As might be expected at Section 2, the plots for the 3 to 1 side slope, in Figure 51, showed a great deal of scatter. This is likely due to the difficulties outlined in the previous section. Also Run 1, on the 3 to 1 side slope, behaved in accordance with the results for the 2 to 1 side slope shown in Figure 55. A significant feature

of the results at this section was the fact that the shear stress remained almost constant, at or near its maximum value, up most of the slope, indicating that no potential for zoning sizes up the bank exists. Excluding the questionable points, it appeared that u_*/U_* was slightly lower than at Section 1, although there still did not seem to be a significant difference between the side slopes, or a dependence on discharge. The maximum observed value of u_*/U_* at this section was just over one.

The boundary shear stress showed some increase by Section 3, as Figures 52 and 56 illustrate. Again there appeared no significant difference between the two side slopes. An interesting feature at this section was that the highest stresses were found to be near the top of the bank, although typically there was not a lot of variation over the bank. Again the runs did not show much spread, indicating that the relationship may not be strongly dependant on discharge. Typically u_*/U_Q peaked at about 1.2 to 1.4 for most runs.

At Section 4 u_*/U_* peaked at just over 1.5, as shown in Figure 57. In general the distributions were found to be much more variable over the slope as seen in Figures 53 and 57. Values did not seem significantly higher on the 2 to 1 side slope, and the shear stress appeared to show a marked decrease near the base of the bank. Generally the maximum observed values of u_*/U_* ranged from about 1.2 to 1.5 at Section 4.

These results appear to be in general agreement with Ippen et.al. (1962), who found the ratio of the local boundary shear

stress to the average, to range from about 0.6 near the upstream end of the bend, to about 2 at the downstream end just past the bend (for the smooth channels). Bathurst et.al. (1979) found that shear stresses associated with the cores of maximum velocity were about 1.5 to 2.5 times the mean. Those associated with regions of strong downwelling and counter rotating cells at the outer bank were found to be higher, up to 3. Yen (1965) found somewhat lower values, in the order of 1.2. However, in his investigations the redistribution of boundary shear stress did not fully develop, and in fact the location of the maximum shear stress stayed to the inside of the channel centreline, although it displayed an outward skewing tendency.

Figures 58 through 63 illustrate the same information by run, rather than by section. These are somewhat less definitive than the corresponding plots for longitudinal velocity. They illustrate the redistribution of the shear stress around the bend, however, indicating that the potential exists for zoning riprap sizes around the bend.

3.4 LATERAL VELOCITIES

Secondary circulation will have a significant effect on the erosion along the outside bank of the bend, and comparably will contribute to the instability of rock armour material placed to protect that bank. Examination of the development pattern of the lateral velocities could feasibly lead to at least a qualitative indication of how the sizing of this rock could be refined,

especially considering their effect on the longitudinal velocity redistribution.

As discussed in Section 2.4.1, mean lateral velocities at a profile were determined through direct numerical intergration. This analysis also provided values for the net lateral flow at a profile, and led to an indication of the degree of development of the longitudinal velocity redistribution through the bend.

As expected, all runs showed the net lateral flow to be near zero at Section 1. By Section 2, Runs 2, 3, 5 and 6 exhibited a tendency toward a slight outward net flow. This indicates that the spiral flow was already developed by Section 2. In these runs the magnitude of the net transverse flow was found to be relatively uniform from profile to profile (across the channel section). Profiles taken at Section 2 in Runs 1 and 4 showed a slight inward net flow, especially those profiles nearest the inside wall. Therefore the spiral flow might not have been fully developed by Section 2 in these runs.

By Section 3 the spiral flow had been fully developed in all runs and in fact, some deterioration in the strength of the lateral velocities was noted. Most profiles had consistent lateral movement of the flow across the section, which still showed a slight outward tendency. It can therefore be said that the spiral flow had developed quickly, however, the redistribution of the longitudinal velocities was still developing by Section 3. Values of net transverse flow at those profiles on the side slope were found to be slightly lower than in the rest of the channel.

By Section 4, Runs 1 and 4 appeared to indicate a net outward movement of the flow and a slight tendency for profiles at the walls to have higher values of net flow. Runs 2, 3, 5 and 6·showed the lateral flow to be nearly balanced, and individual profiles across the section exhibited consistent values of net flow except on the slope where they were slightly lower.

Interpretation of these results is not simple. In general, it was found that the spiral flow developed and decayed quickly. In comparison, the longitudinal velocity redistribution never did become fully developed. There appeared to be a general tendency for the net lateral transfer of flow to be consistent across the channel, and somewhat less up the slope, once the spiral flow had become fully developed. The results seem to indicate that in the case of higher aspect ratio, the spiral flow developed more quickly than those of lower aspect ratio. This reflects Equation 1 which expressed this development length as being directly proportional to flow depth. It is interesting to note that Runs 1 and 4 (lowest aspect ratios) were associated with cells of reverse circulation along the outside bank, which might be related to the deterioration of the spiral flow. Unfortunately, there did not appear to be any pattern in the magnitude of the net flow for the profiles on the slope that might indicate the effect of varying the side slope.

3.5 TURBULENT FLUCTUATION INTENSITIES

Turbulent fluctuations, if high enough, can lead to failure of riprap protection by vibrating individual rocks loose. Although

$\overline{u'v'}$ was not directly measured in the experiments, comparison of $\overline{u'^2}$ and $\overline{v'^2}$ to similar values for straight reaches should indicate if turbulent fluctuation intensities are significantly higher along the sloped bank in the curved channel.

Figure 64 illustrates the peak longitudinal turbulence fluctuation for Run 6, non-dimensionalized by u_*. Typical values on the slope ranged from 2 to 3.5, only slightly higher than the maxima of up to 3.0 observed in a straight rectangular channel by Steffler (1983). In general, the peak value at a section appeared to move down the slope as the flow progressed around the bends, however, it is difficult to conclude much based on one run. Unfortunately, difficulty in getting good data near the bed, where the peaks tended to occur, meant that no significant results could be extracted from the other runs.

Peak values of the lateral turbulence intensity on the slope were typically e-half to two-thirds of corresponding values in the longitudinal direction, which concur with the findings of Steffler (1983).

3.6 PRACTICAL APPLICATION OF THE RESULTS

Direct application of the results of this study must necessarily be limited. Actual riprapped banks have localized protrusions into the flow which have effects on the redistribution of velocity and boundary shear stress, not considered in this smooth boundary model. Nonetheless, some valuable general applications are possible.

The most notable result was the indication that it is probably

not practical to consider zoning rock sizes up a bar , although significant potential for zoning the sizes around the bend does exist. The next step should be to try to determine typical distributions for a rough boundary (simulating the riprap surface), considering different curvatures, and a wider range of aspect ratios. The tendency for the distributions to be independent of discharge indicates that zoning could be accomplished by relating local shear stress to an average straight reach value. The major difficulty would be determining how points around a natural bend correspond to those in a model. It is likely that refinements of riprap design such as zoning will require extensive field investigation before apply prediction techniques with any confidence. If riprap zoning does become viable in the future, it will have to be done through consideration of boundary shear stress rather than velocity, due to the difficulty in defining attack velocities in anything but empirical terms.

An important question, as yet unanswered, is where to begin and end the bank protection works. Nouh et.al. (1979) provided some insight into the distance required to develop the spiral flow, which is indicative of where protection should begin. However, the effects of the longitudinal velocity redistribution persist much longer than the spiral flow, therefore more investigation is required into the flow downstream of a bend.

Although results from this study did not show significant differences in the magnitudes of velocities, and especially shear stresses, between the two side slopes, particle stability itself

increases with flatter slopes. Strength of the downwelling flow caused by the secondary circulation, and the turbulent fluctuation intensities will contribute to particle instability, however, the results in this respect were somewhat inconclusive.

It is interesting to note that those runs of higher aspect ratio appeared to show quicker development of the spiral flow. Since the aspect ratio is the ratio of width to depth this effect would be expected, as both Rosovskii (1961) and Nouh and Townsend (1979) predict the development length of the spiral flow to be directly proportional to the depth. Lower aspect ratios seemed to exhibit a slight tendency to develop counter rotating cells along the outer bank.

CONCLUSIONS

The purpose of this study was to examine the shear and velocity distribution along a sloped bank in a curved channel, with the objective of investigating the potential for zoning rock sizes up a bank and around a bend when designing riprap bank protection. A detailed experimental investigation was conducted involving measurement of longitudinal and lateral velocities, and turbulent fluctuations in a smooth, 270 bend with a sloped outer bank. Boundary shear stresses and boundary stress angles were also determined.

This study concludes that there is little, if any, potential for zoning rock sizes up a bank in river bend, however, zoning around the bend would be quite feasible. It was found that there was not a significant difference in the relative size of velocities and shear stresses on the sloped bank as the curved flow developed. However, no conclusive results were obtained comparing the strength of the downwelling flow, or the turbulence fluctuation intensities, for the two side slopes.

It was found that the secondary circulation developed quite quickly for the runs with higher aspect ratios, while counter rotating cells along the outer bank seemed to be associated with the runs lower aspect ratios.

Future studies using rough boundaries to simulate the riprap should be conducted for varying curvatures, and a wider range of aspect ratios. These studies must utilize more measurement sections and longer exit channels if more information is to be gained as to

where to start and stop bank protection works. More field measurements are needed as well, if model studies are to be related to field situations with any confidence.

In conclusion, this study presents the results of a detailed investigation of the flow near a sloped bank in a curved channel, thus providing a contribution to the ongoing research into flow in curved channels.
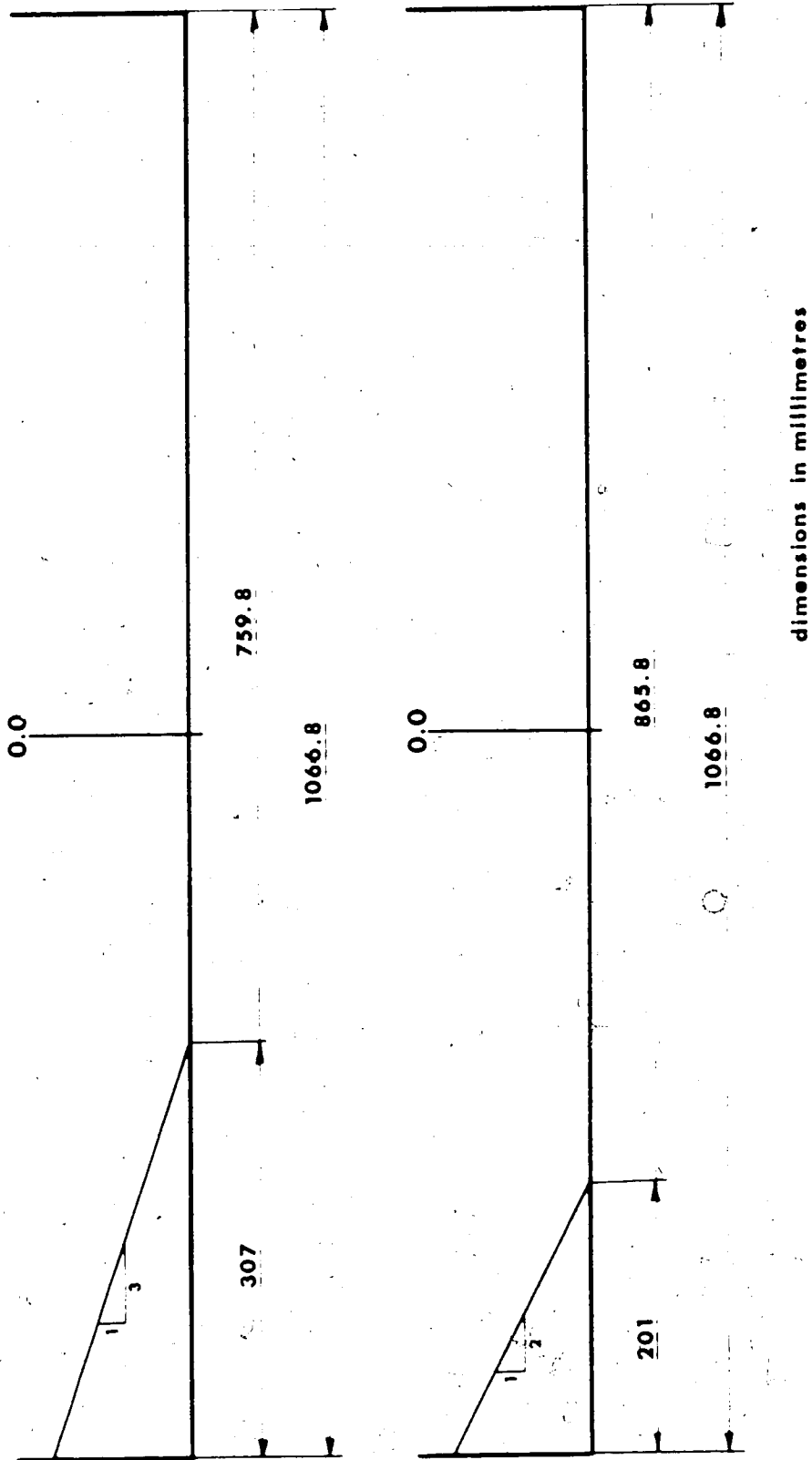
Figure 1. Dimensions of the Channel Sections for Each of the Two Side Slopes

dimensions in millimetres

42
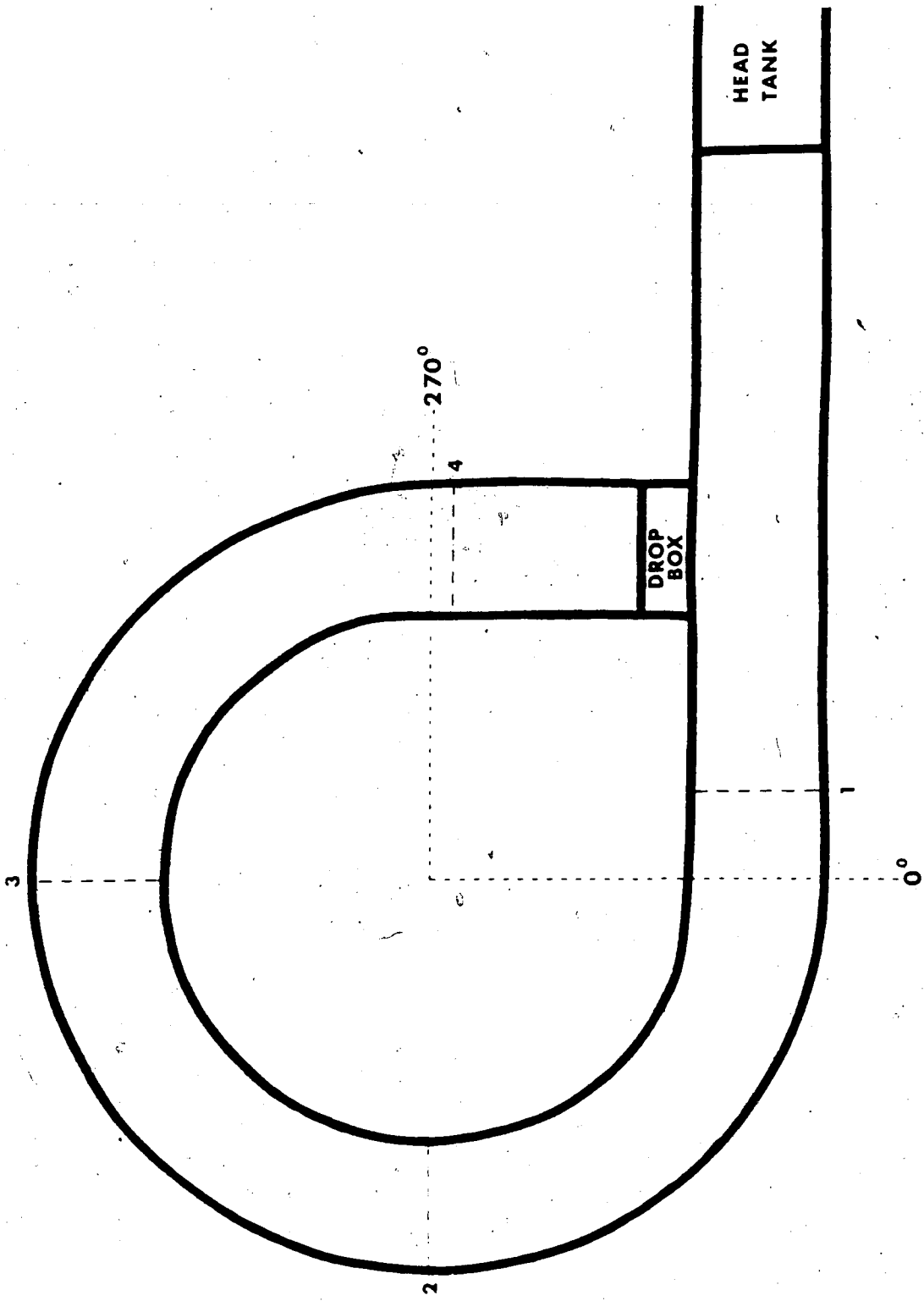
Figure 2. Flume and Test Locations
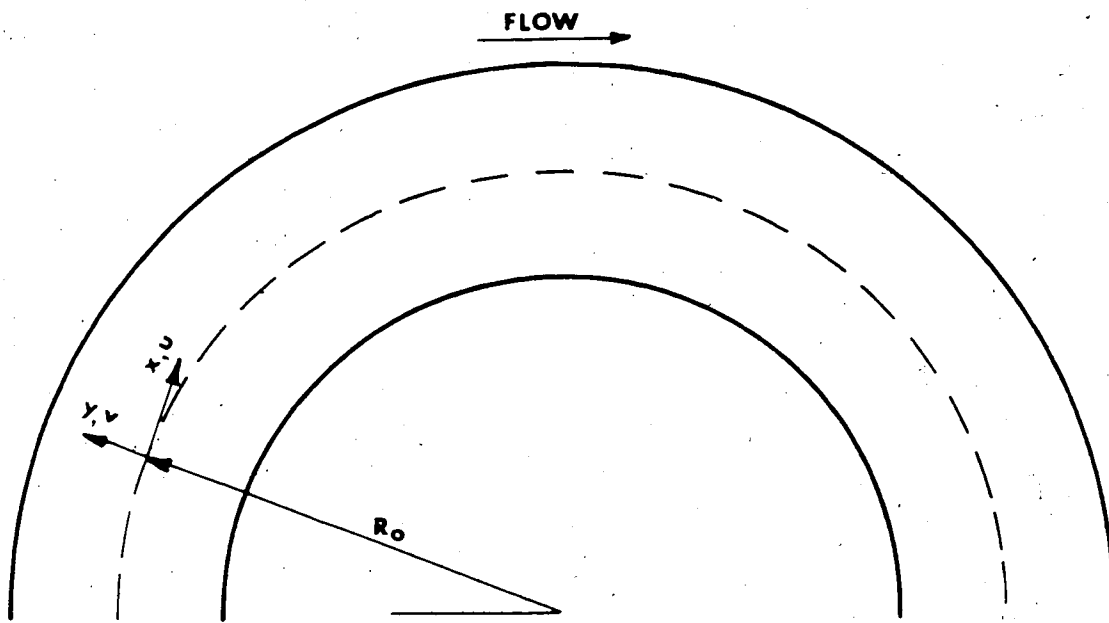
Figure 3. Co-ordinate System
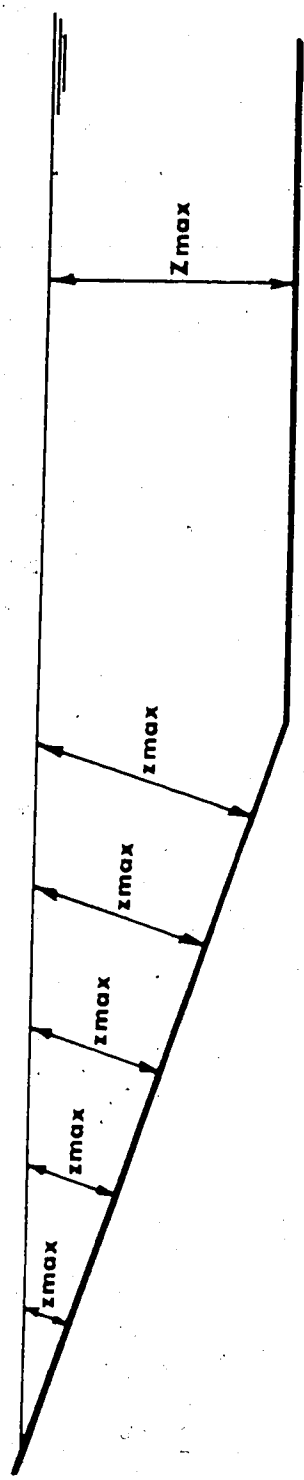
Figure 4. Definition Sketch for Measurements
in the z Direction
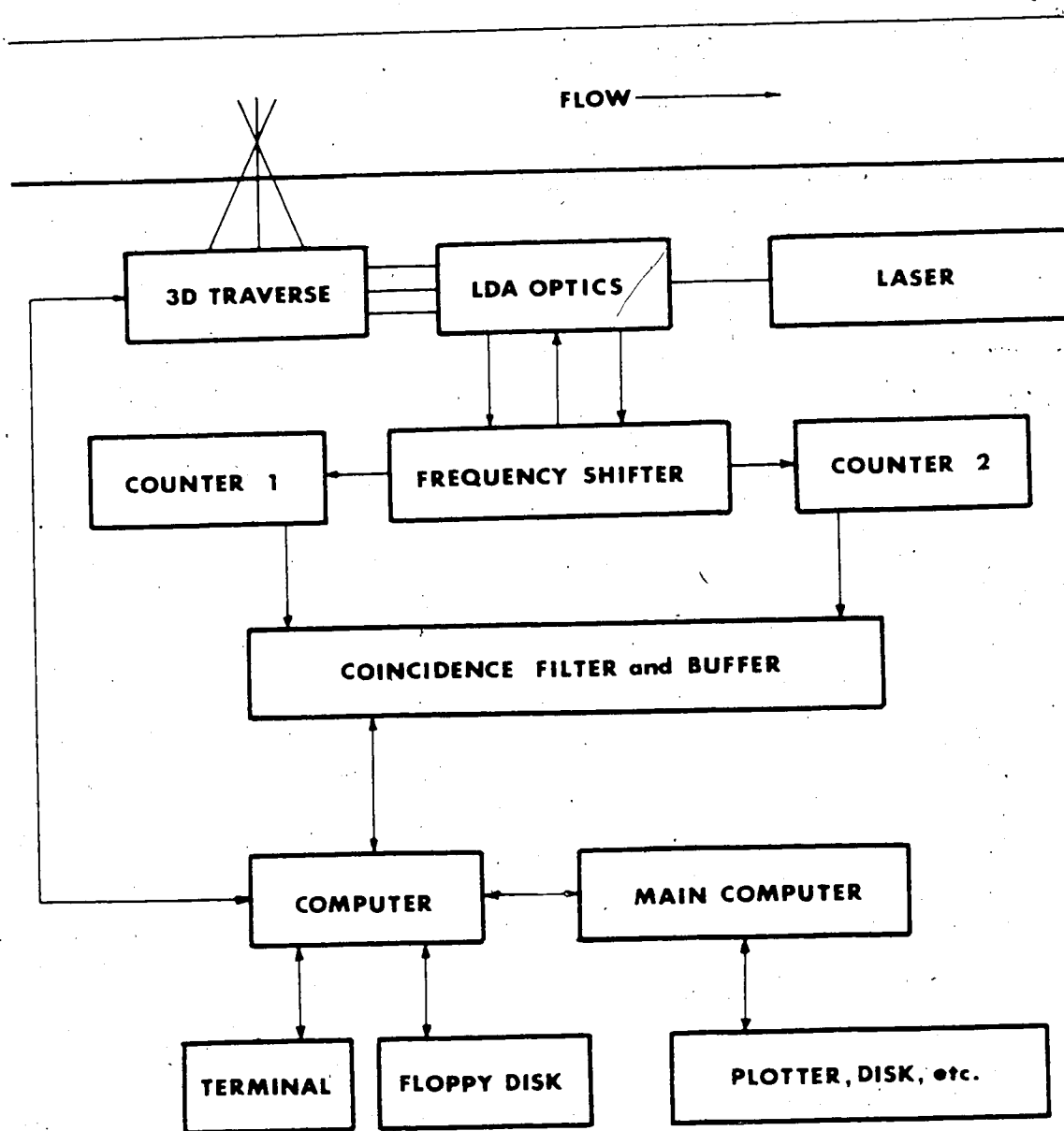
Figure 5.   Schematic Diagram of LDA Setup
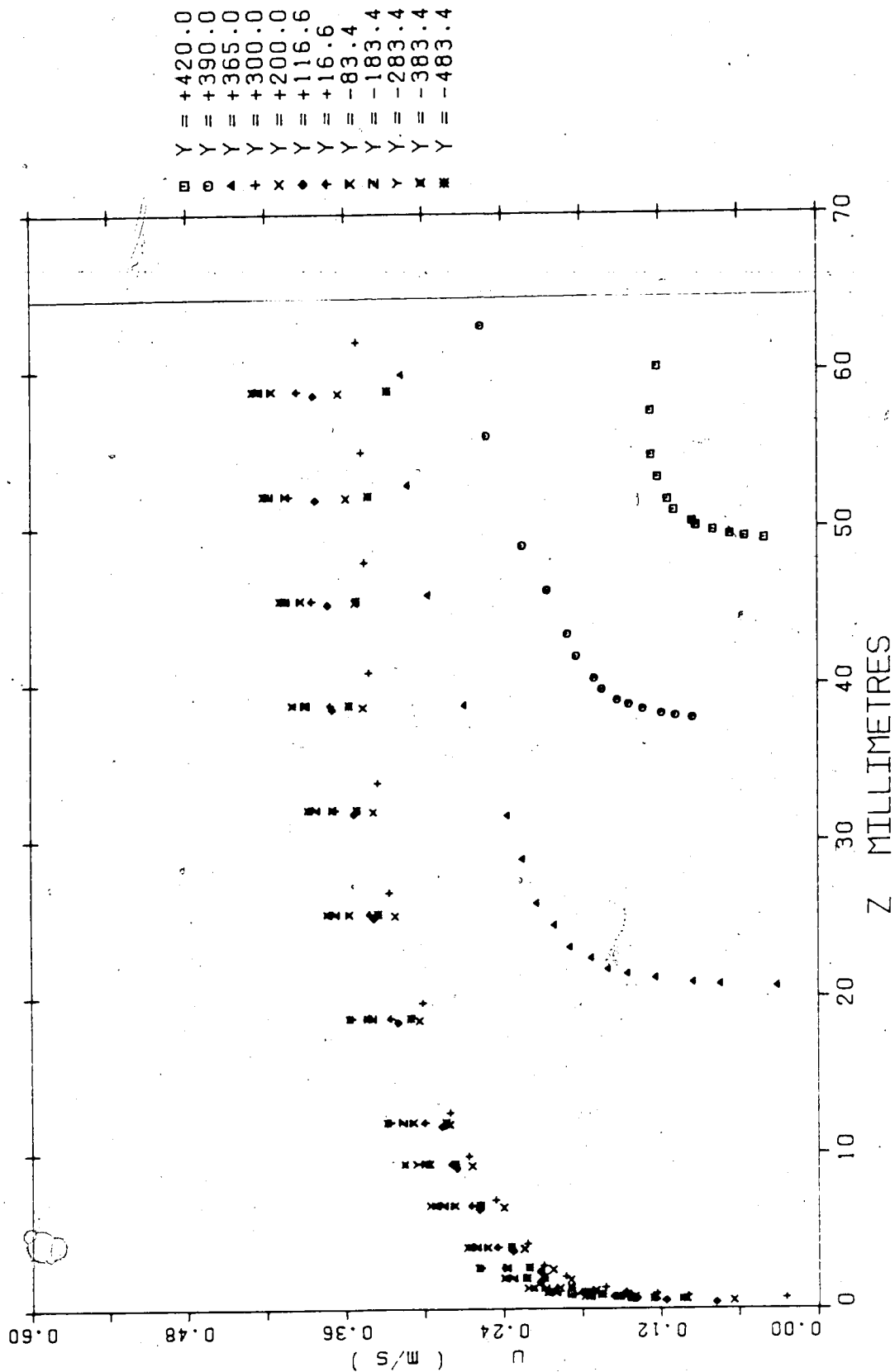
Figure 6.   u Velocity Distribution (Section 1, Run 6)
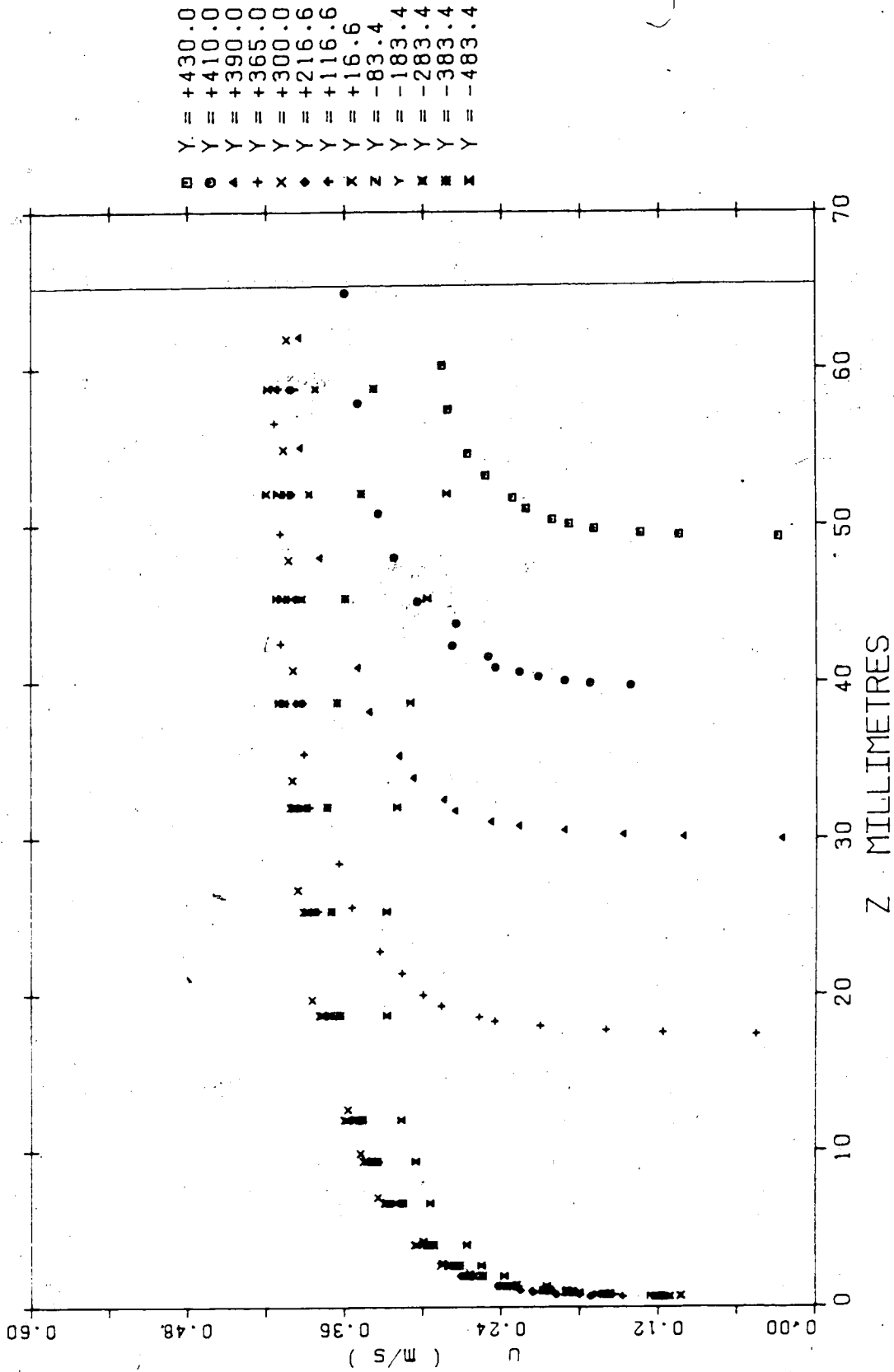
Figure 7.   u Velocity Distribution (Section 2, Run 6)
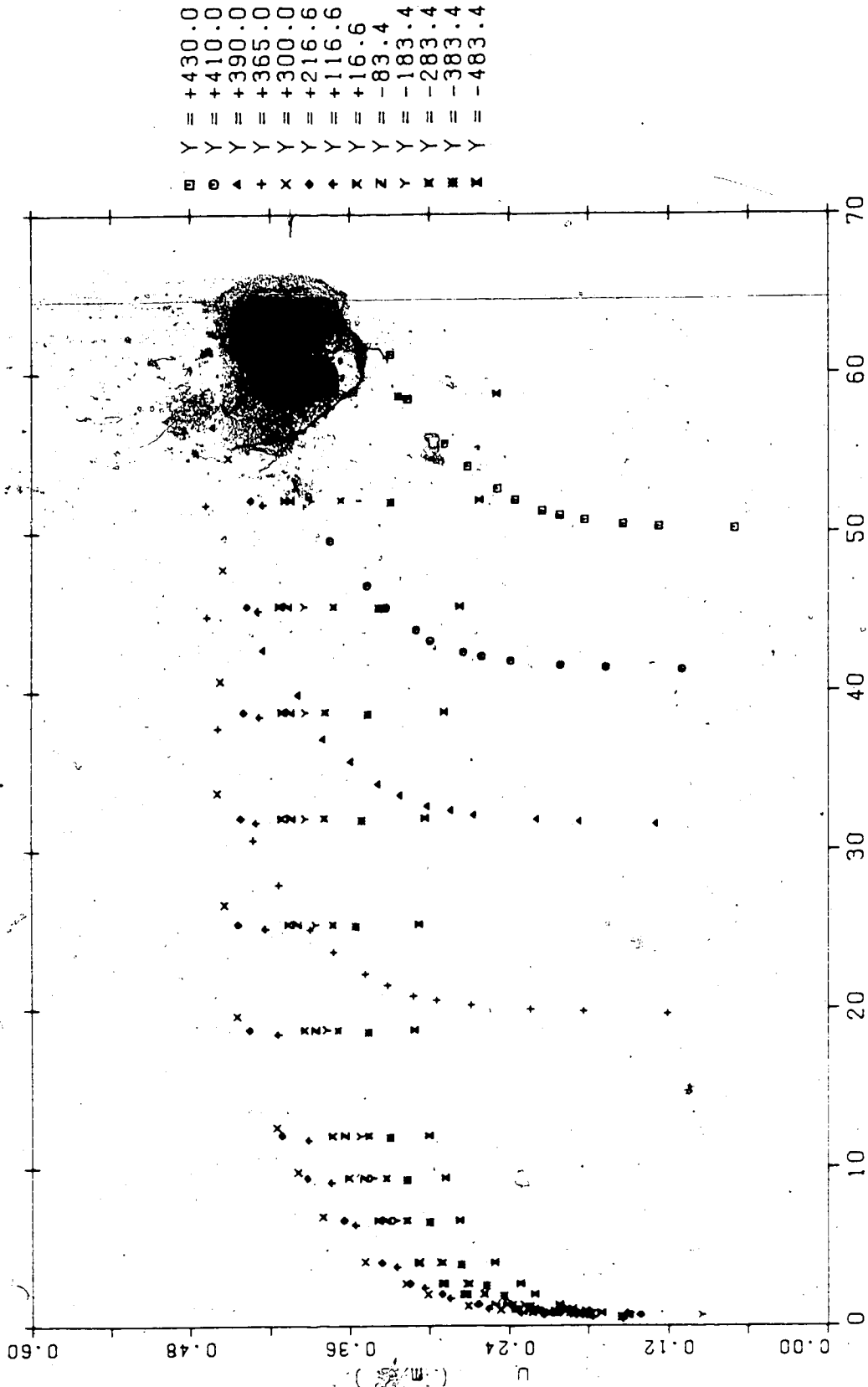
Figure 8. u Velocity Distribution (Section 3, Run 6)

Y = +430.0
Y = +410.0
Y = +390.0
Y = +365.0
Y = +300.0
Y = +216.6
Y = +116.6
Y = +16.6
Y = -83.4
Y = -183.4
Y = -283.4
Y = -383.4
Y = -483.4
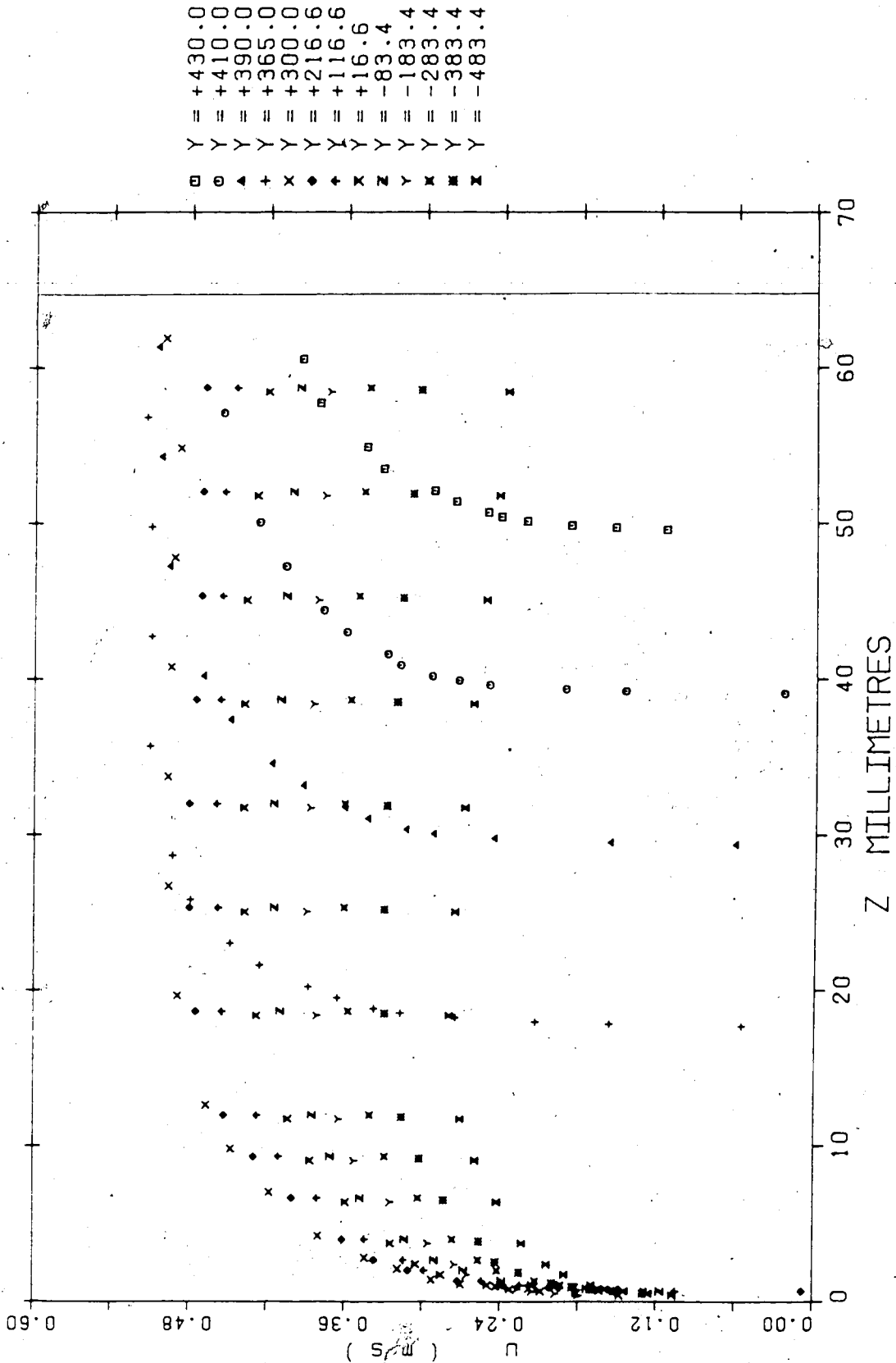
Figure 9. u Velocity Distribution (Section 4, Run 6)

SECTION 1

SECTION 2

SECTION 3

0.00 0.05 0.10
scale
(m)

SECTION 4

velocities in mm/s
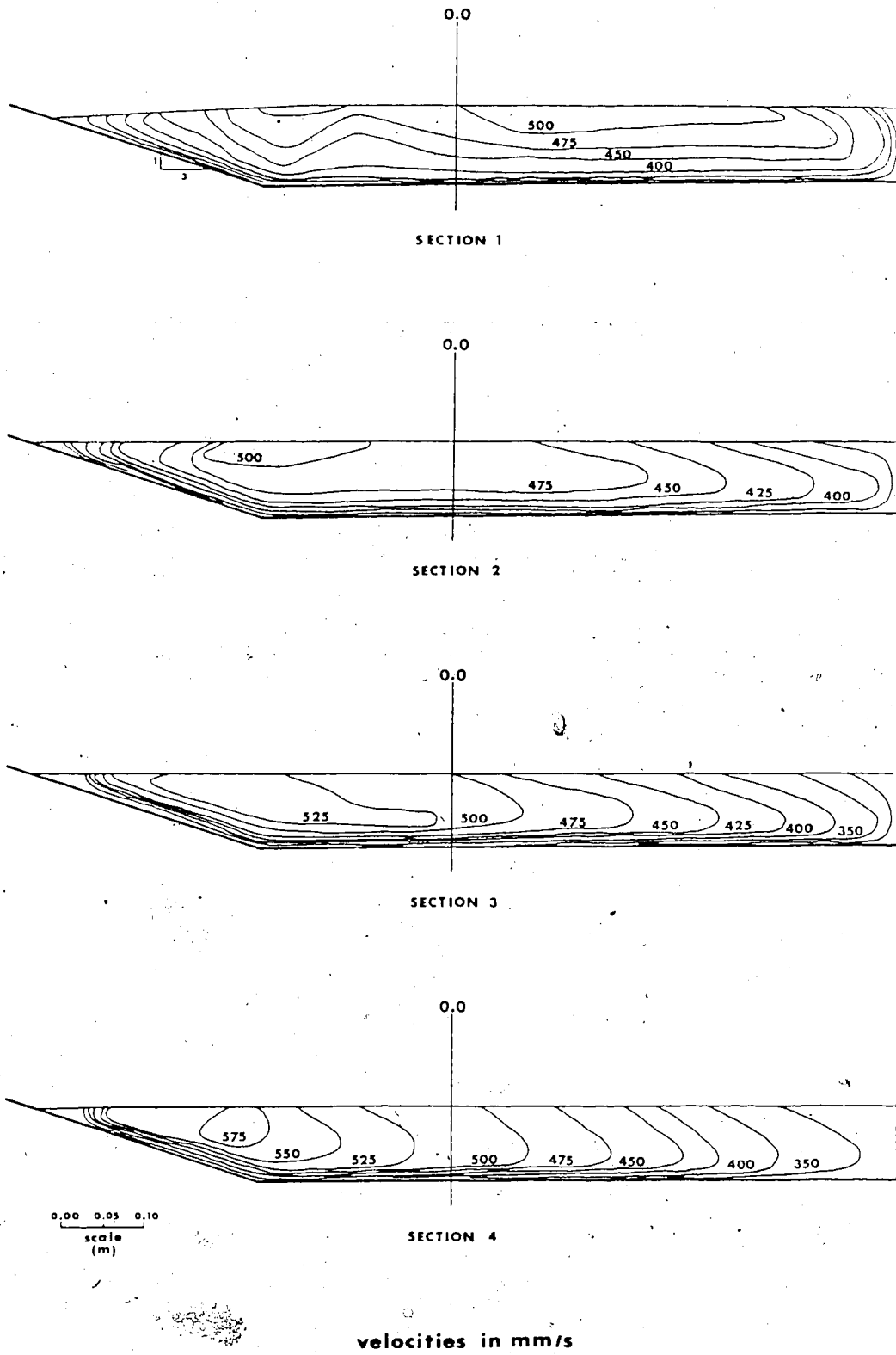
Figure 10. Longitudinal Velocity Distributions (Run 1)

52
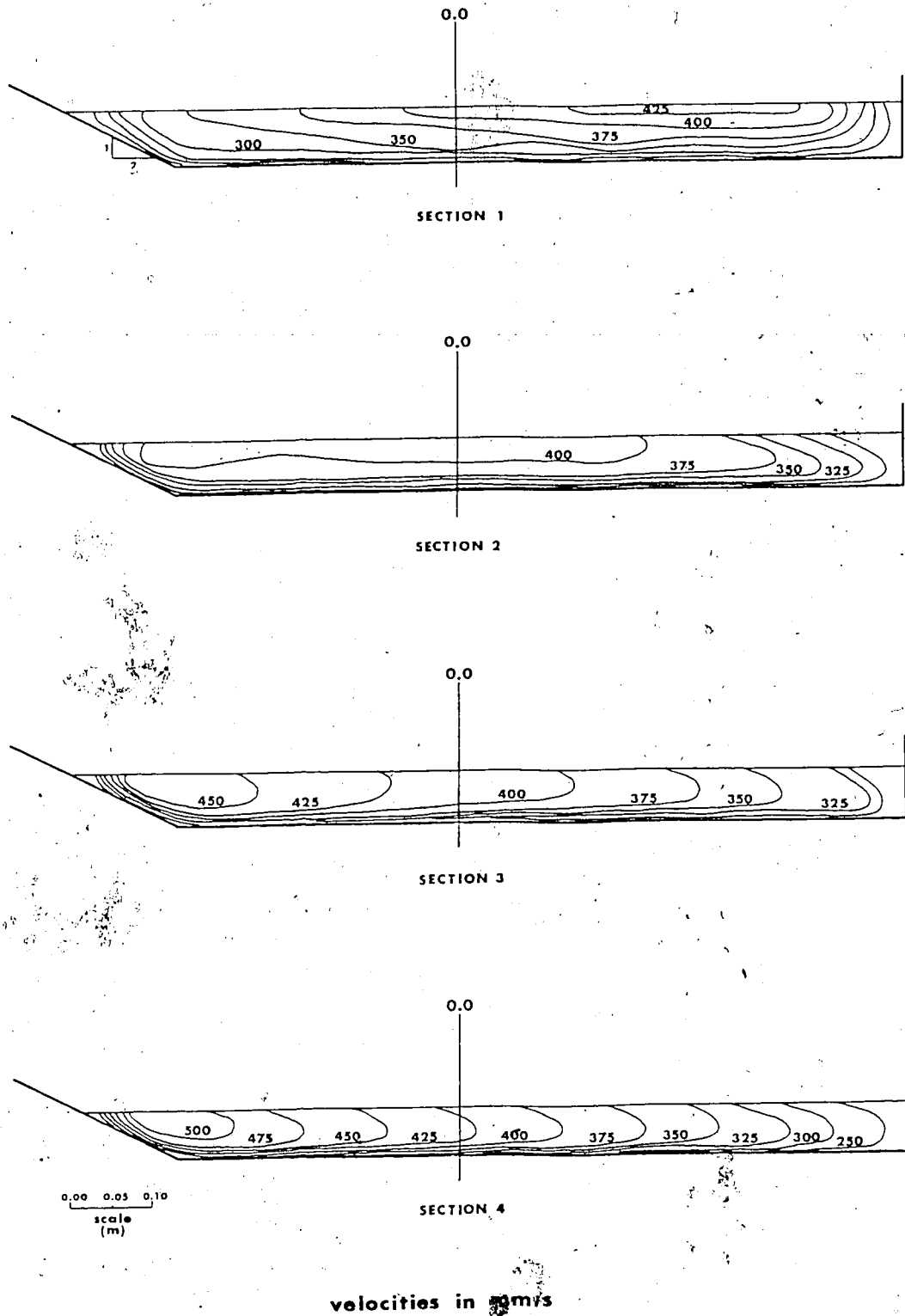
Figure 11. Longitudinal Velocity Distributions (Run 6)

Y = +420.0
Y = +390.0
Y = +365.0
Y = +300.0
Y = +200.0
Y = +116.6
Y = + 16.6
Y = − 83.4
Y = −183.4
Y = −283.4
Y = −383.4
Y = −483.4

Z MILLIMETRES

V (m/s)

0.090 0.060 0.030 0.000 -0.030 -0.060

0   10   20   30   40   50   60   70

Figure 12. V Velocity Distribution (Section 1, Run 6)
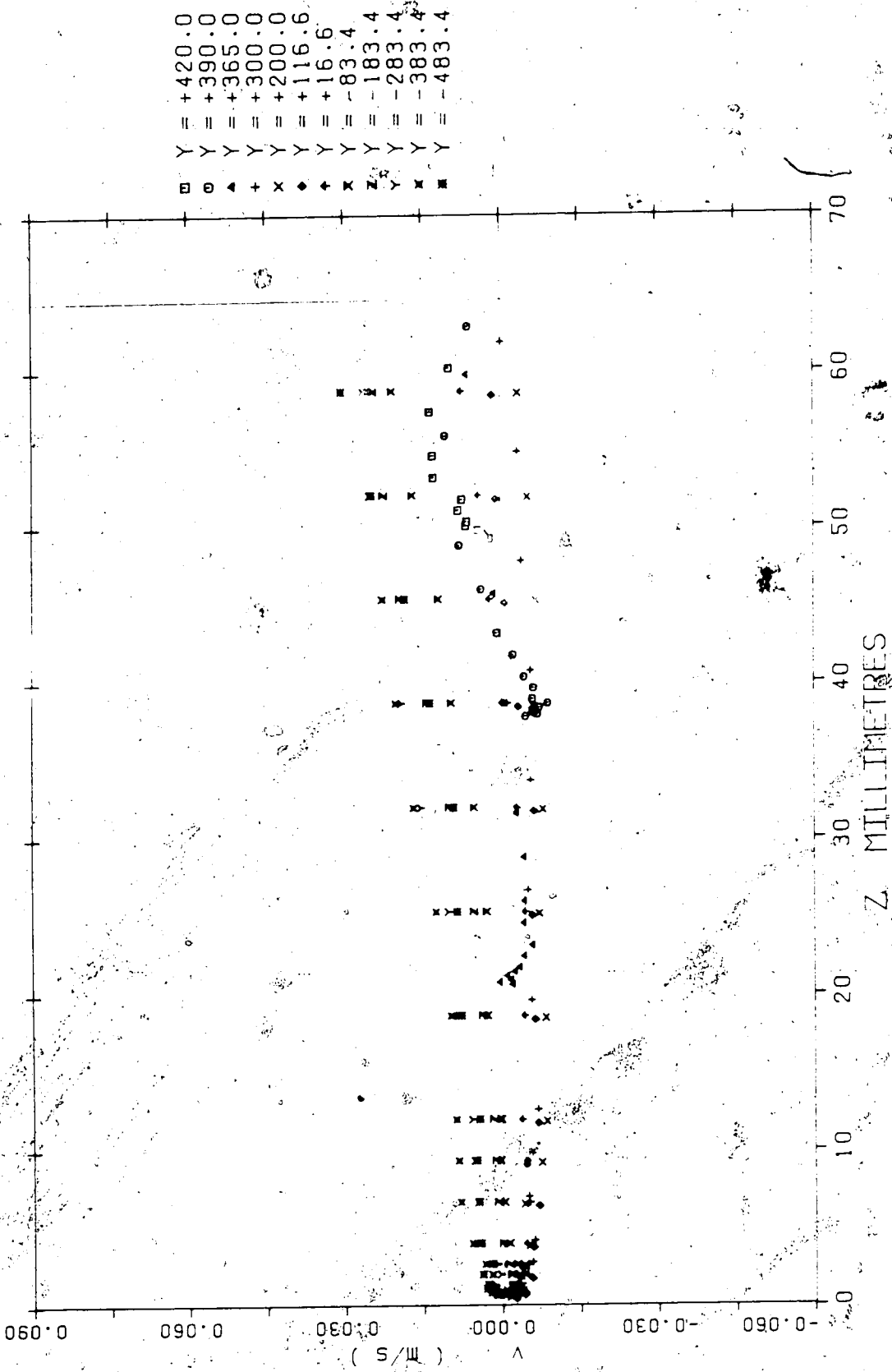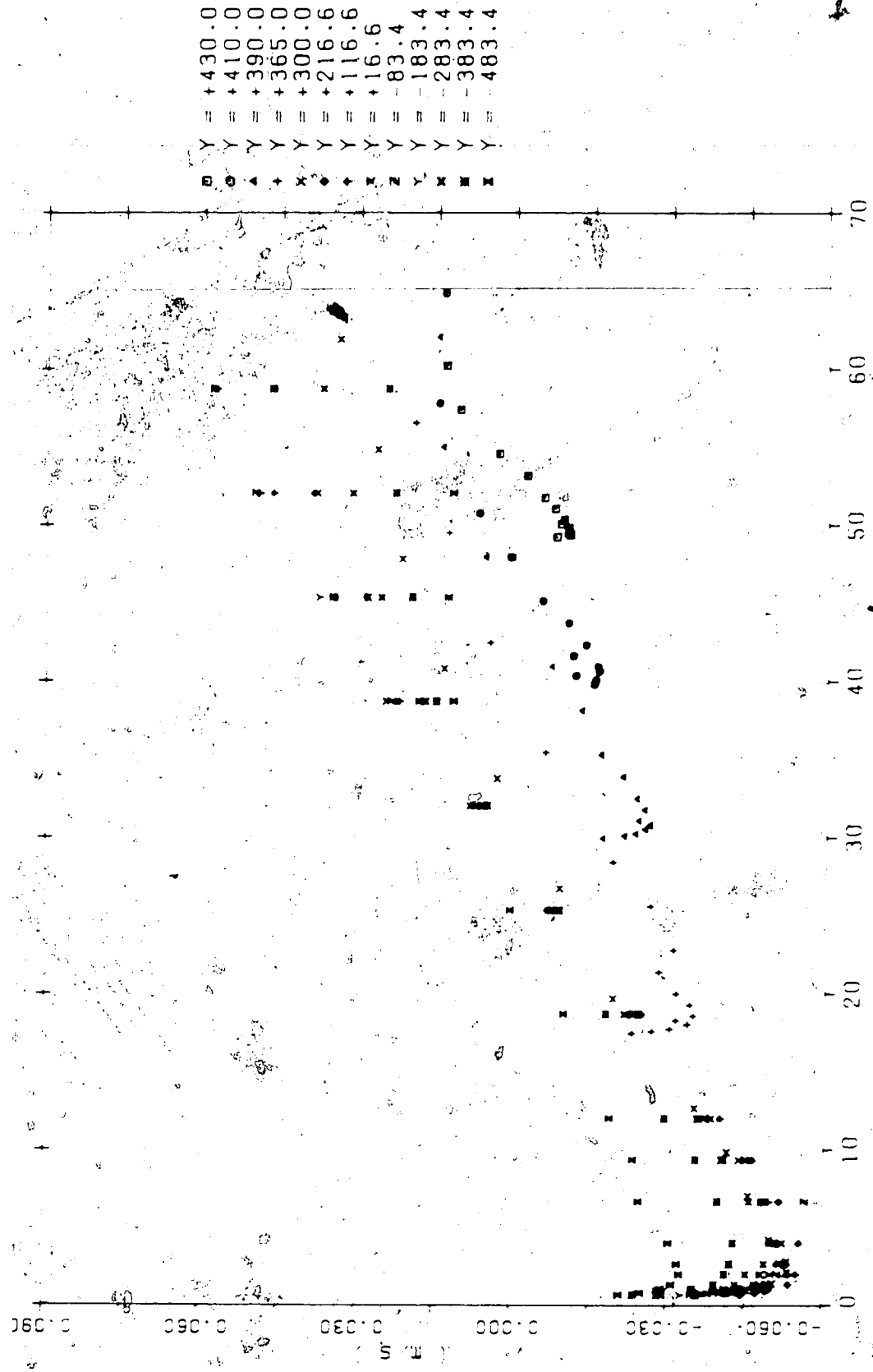
Figure 13. v Velocity Distribution (Section 2, Run 6).

Y = +430.0
Y = +410.0
Y = +390.0
Y = +365.0
Y = +300.0
Y = +216.6
Y = +116.6
Y = +16.6
Y = 83.4
Y = 18?.4
Y = -283.4
Y = -383.4
Y = -48?.4

Z MILLIMETRES

m s
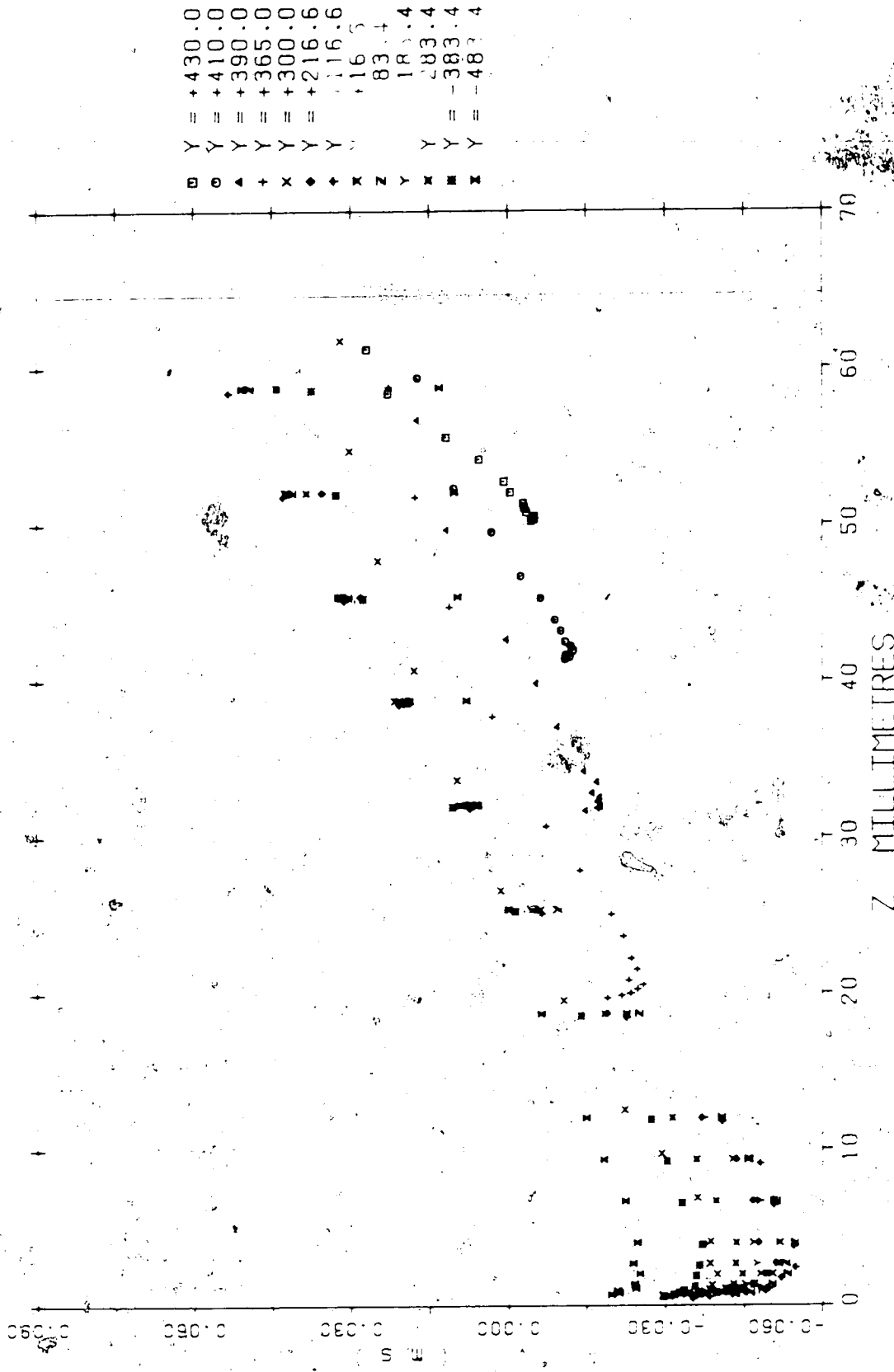
Figure 14. v Velocity Distribution (Section 3, Run 6)
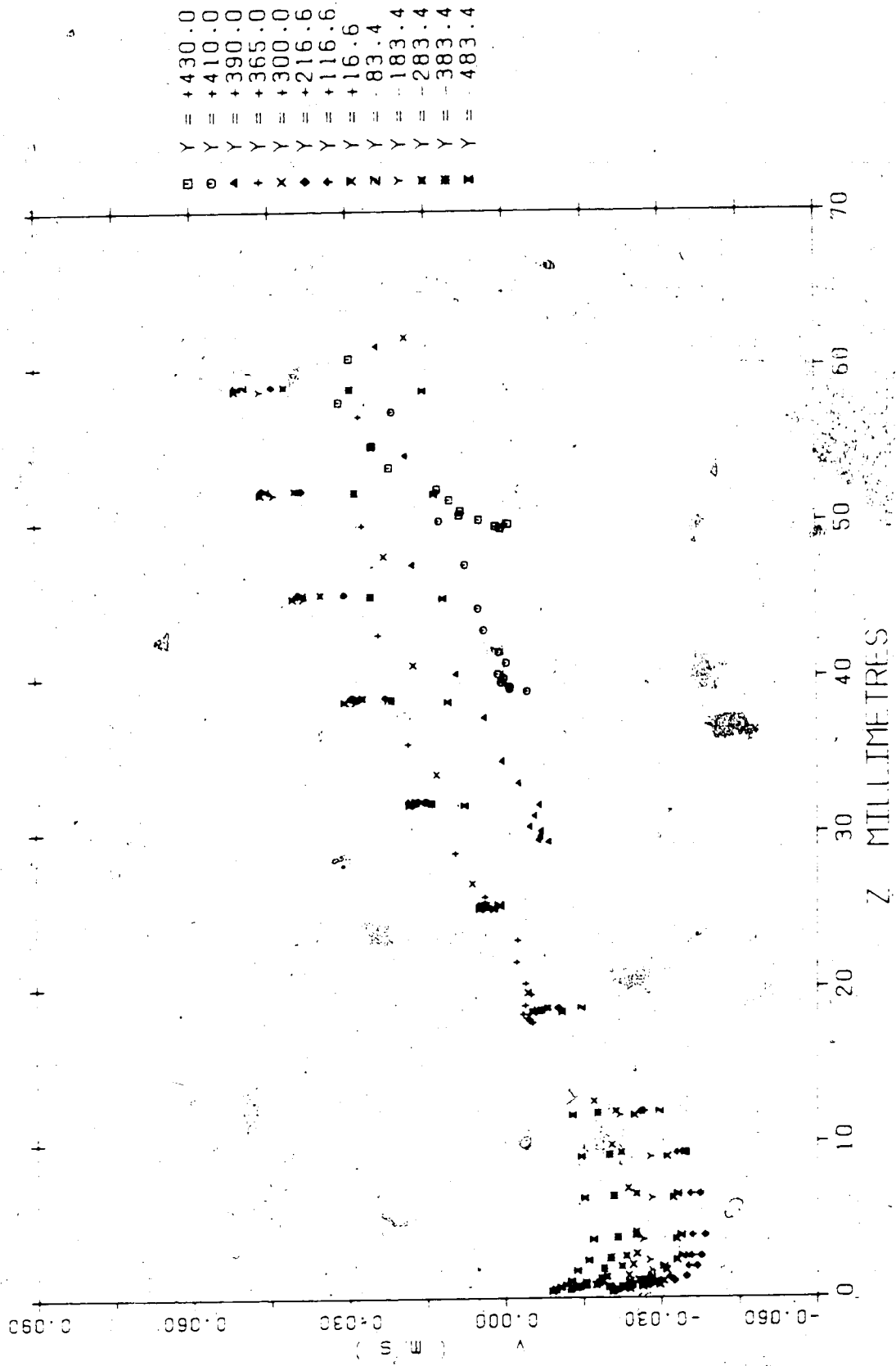
Figure. 15.   v Velocity Distribution (Section 4, Run 6)
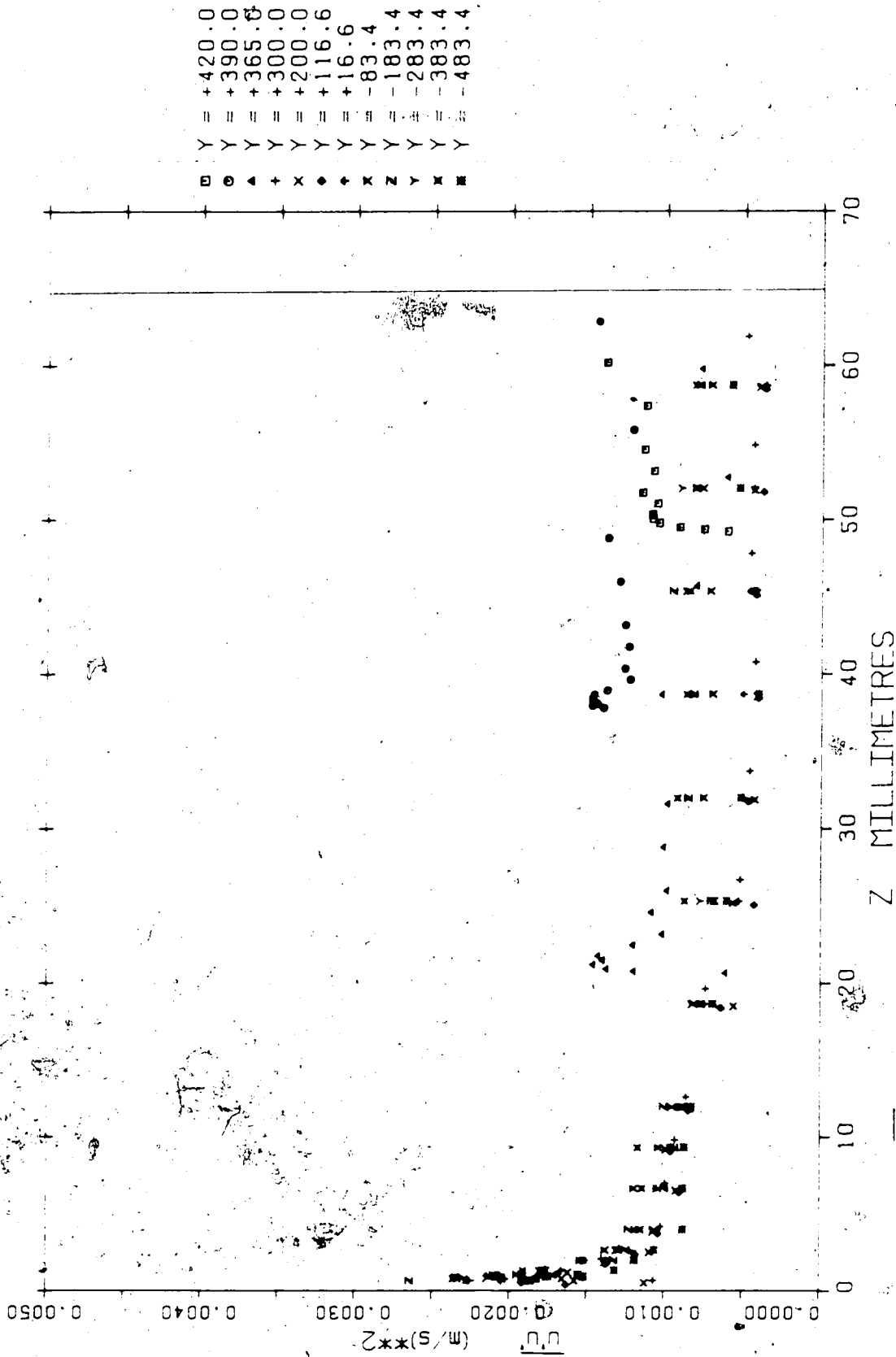
Figure 16. $\overline{u'^2}$ Turbulence Intensity Distribution (Section 1, Run 6)
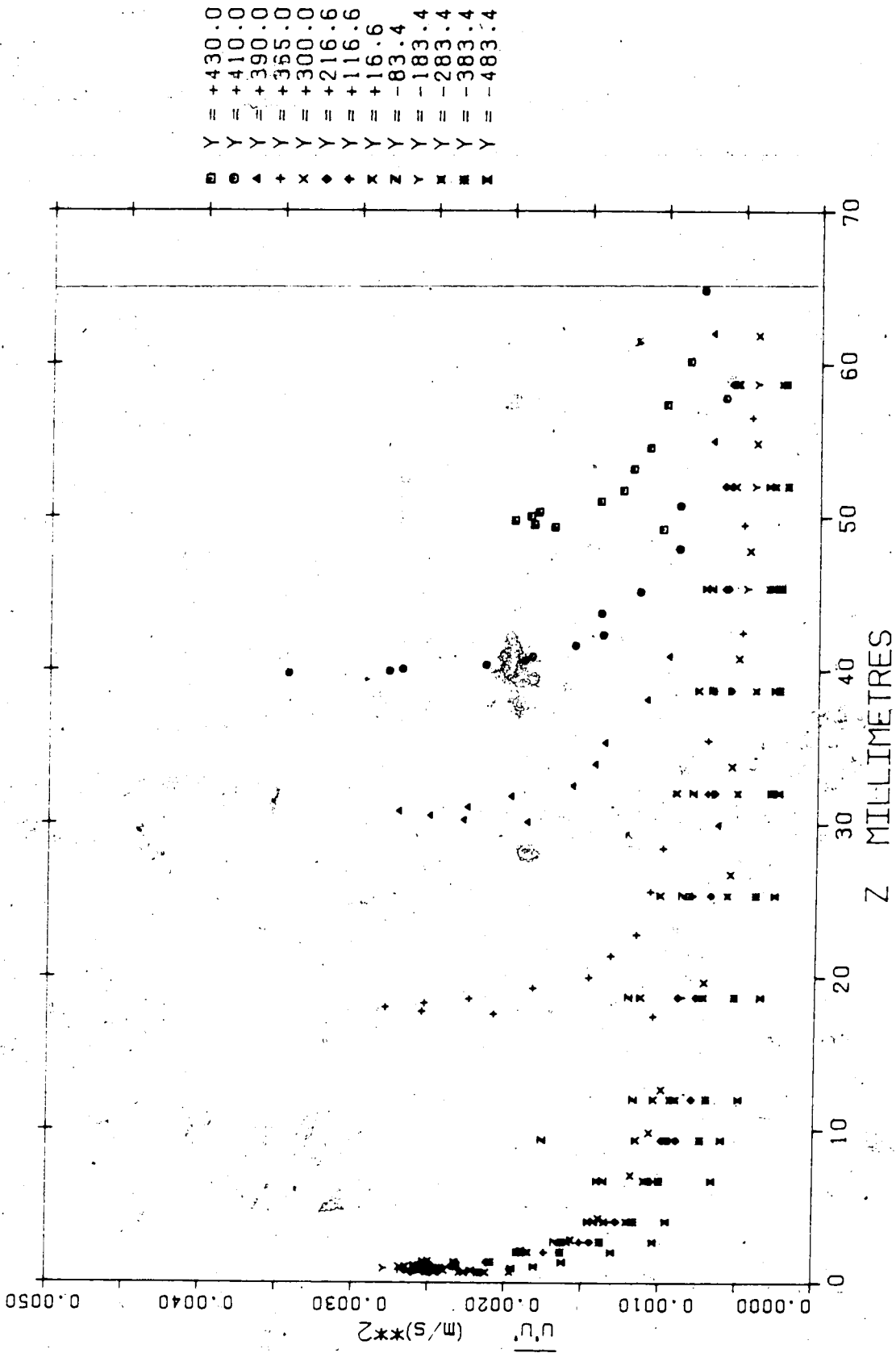
Figure 17. $\overline{u'^2}$ Turbulence Intensity Distribution (Section 2, Run 6)
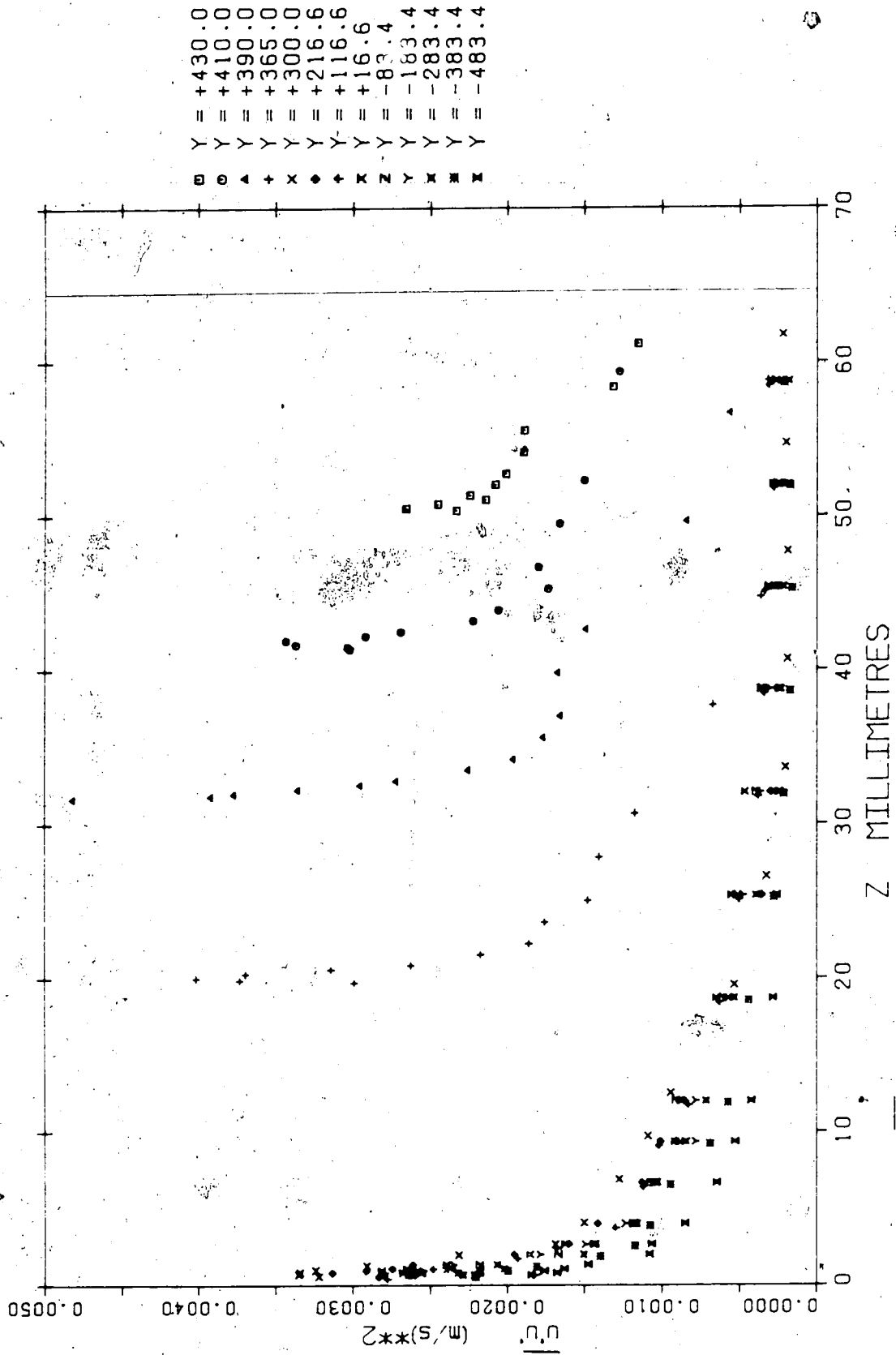
Figure 18. $\overline{u'^2}$ Turbulence Intensity Distribution (Section 3, Run 6)
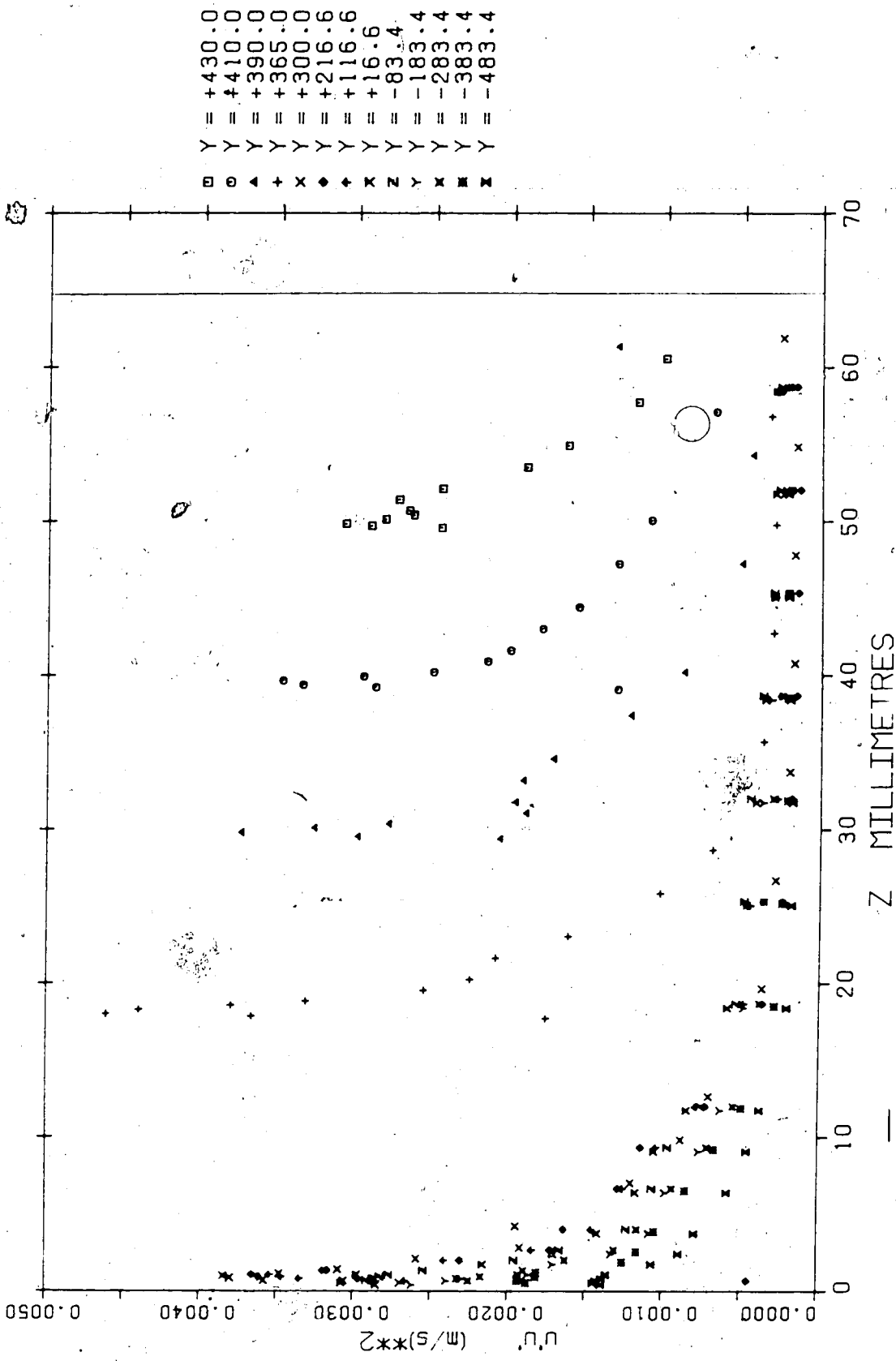
Figure 19. $\overline{u'^2}$ Turbulence Intensity Distribution (Section 4, Run 6)
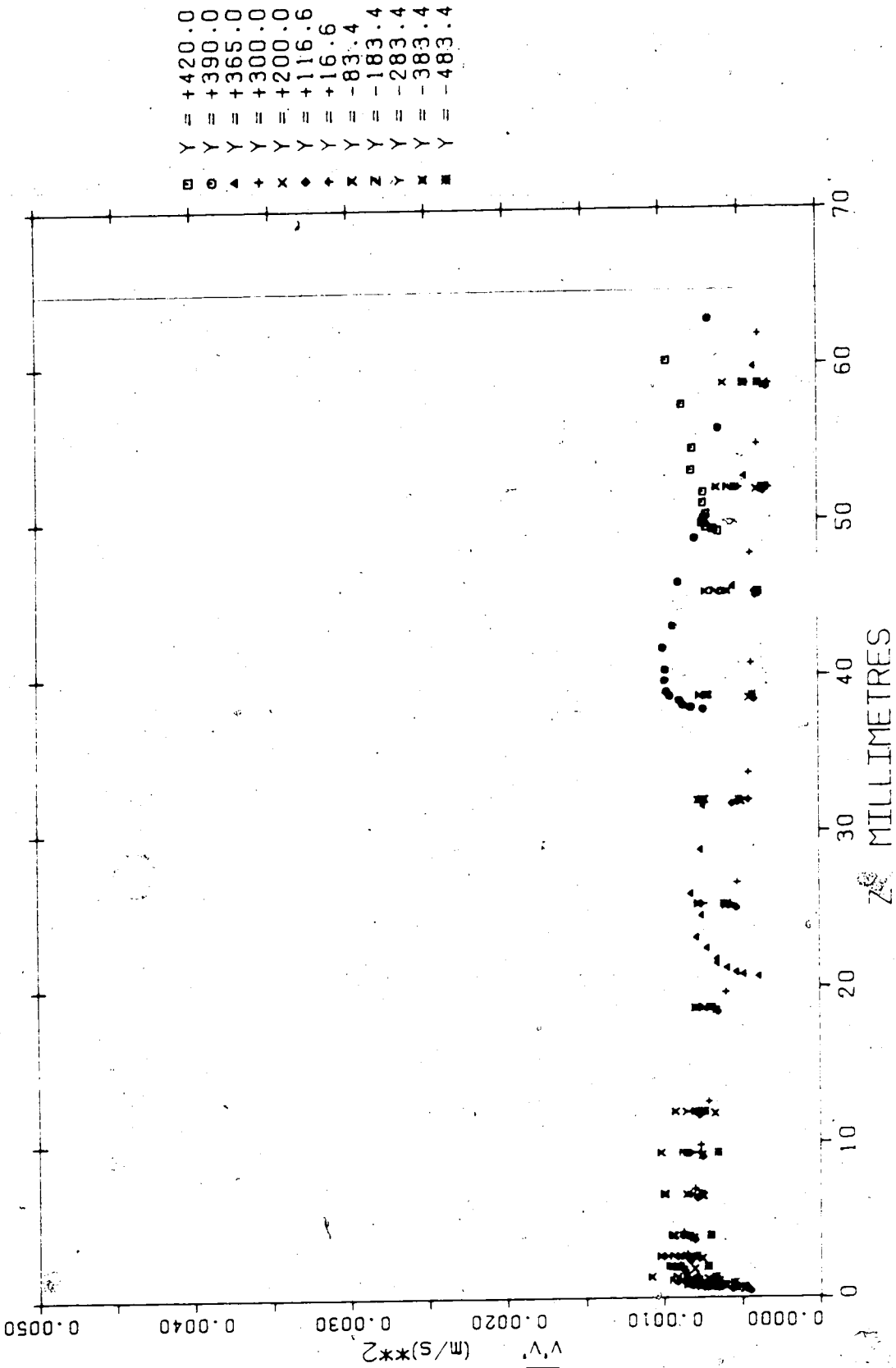
Figure 20. $\overline{v'^2}$ Turbulence Intensity Distribution (Section 1, Run 6)
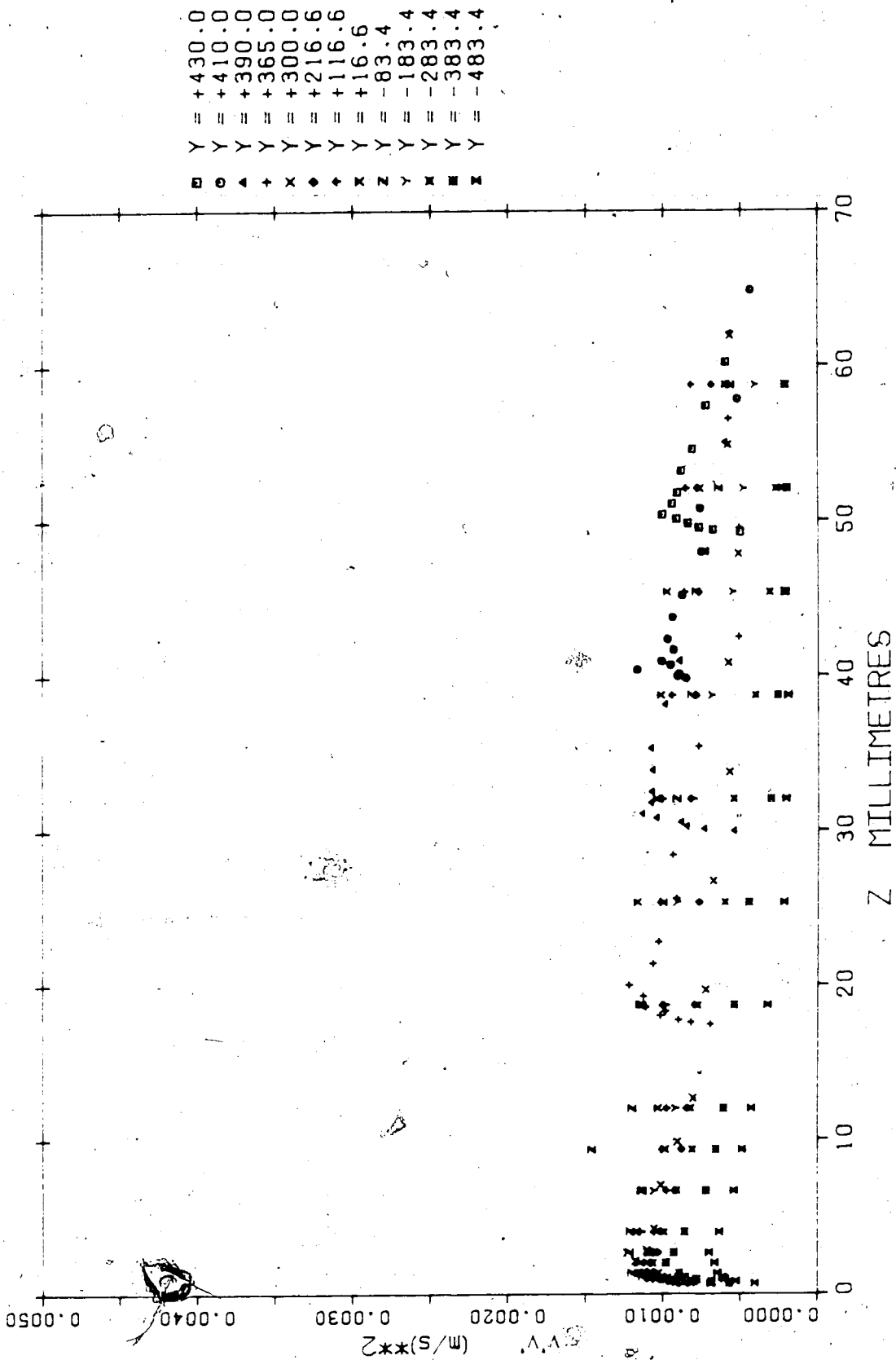
Figure 21. $\overline{v'^2}$ Turbulence Intensity Distribution (Section 2, Run 6)
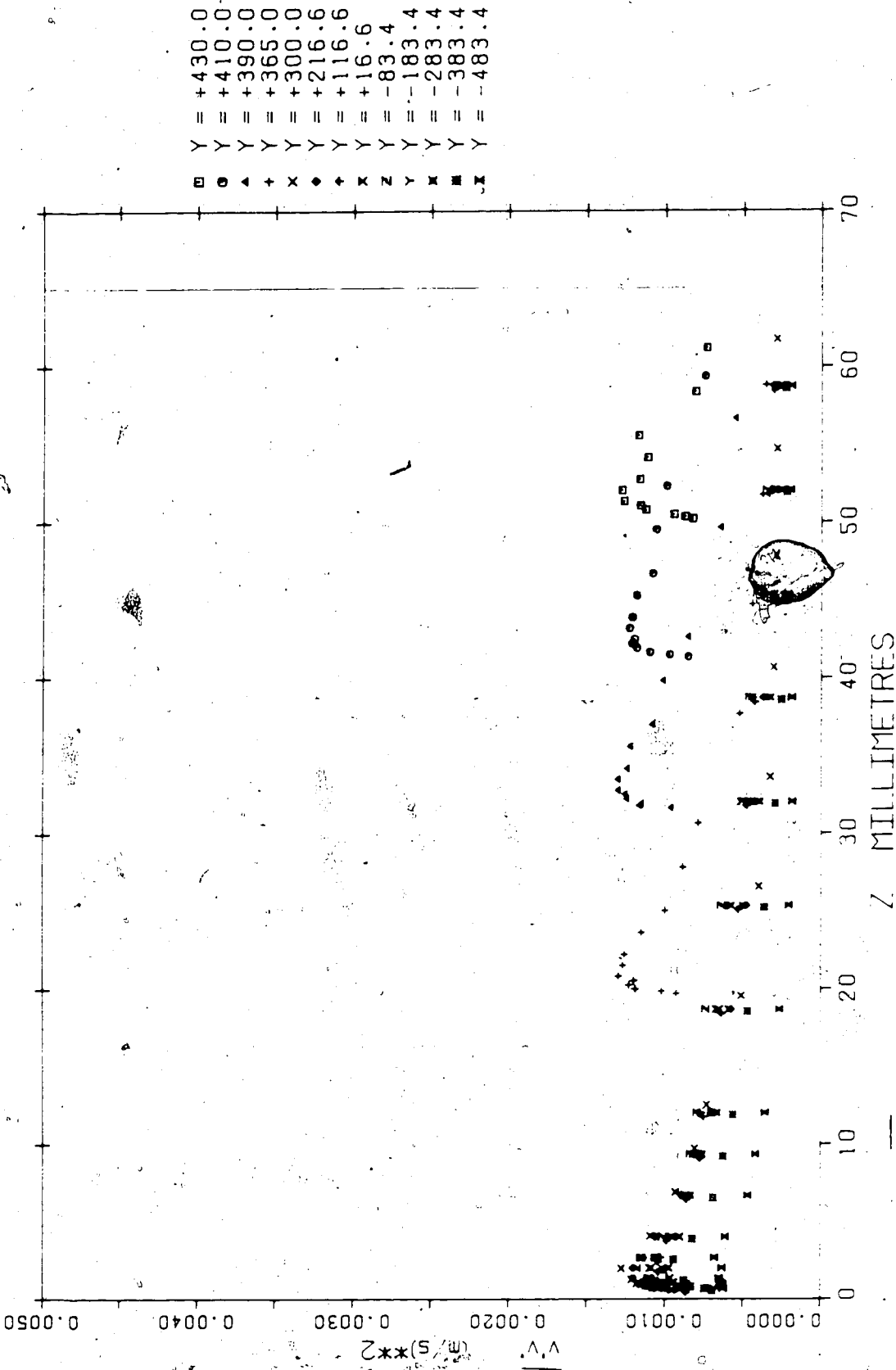
Y = +430.0
Y = +410.0
Y = +390.0
Y = +365.0
Y = +300.0
Y = +216.6
Y = +116.6
Y = +16.6
Y = -83.4
Y = -183.4
Y = -283.4
Y = -383.4
Y = -483.4

Z. MILLIMETRES

$\overline{v'v'}$ (m/s)**2

Figure 22.. $\overline{v'^2}$ Turbulence Intensity Distribution (Section 3, Run)
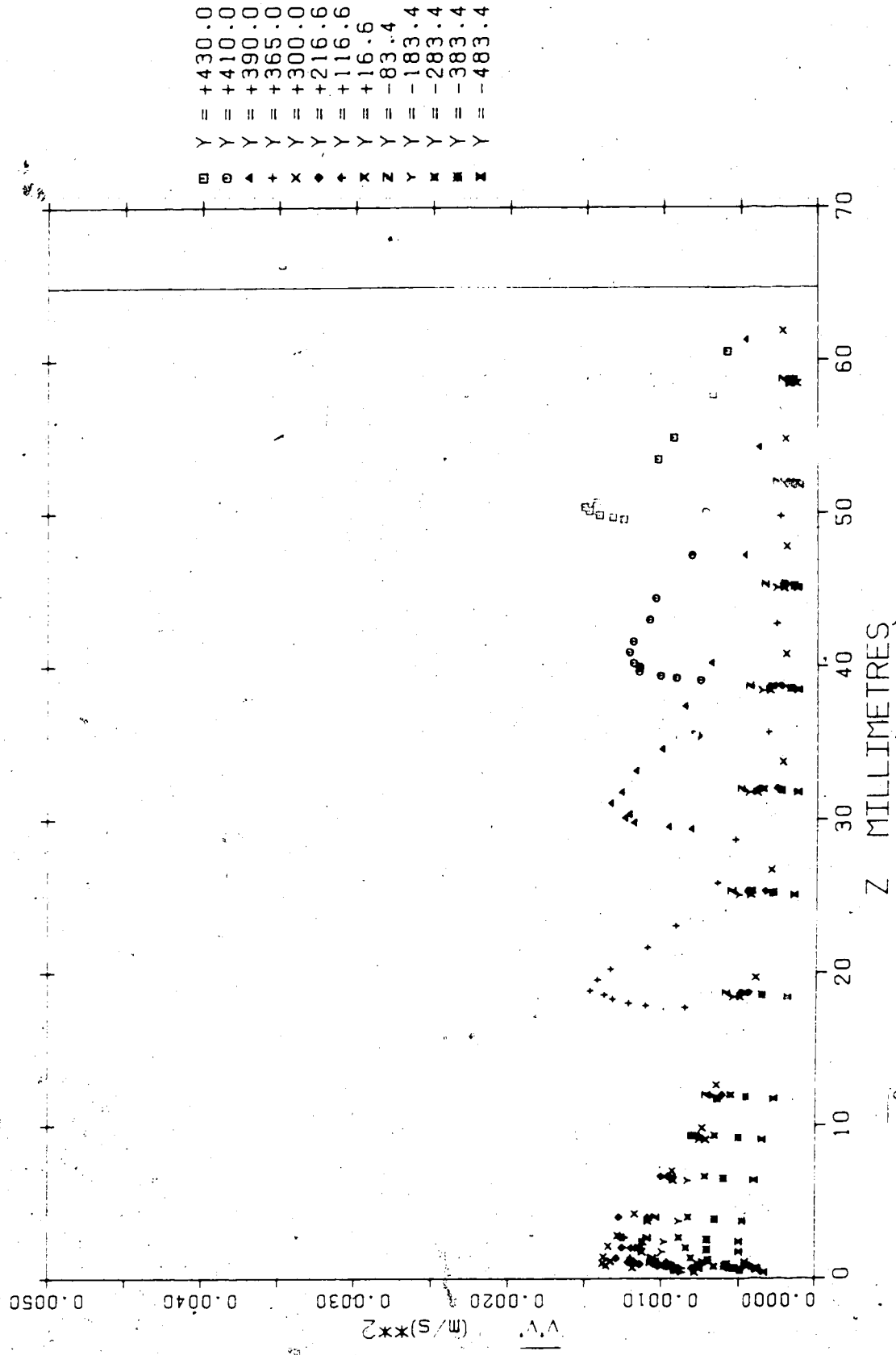
Figure 23. $\overline{v'^2}$ Turbulence Intensity Distribution (Section 4, Run 6)
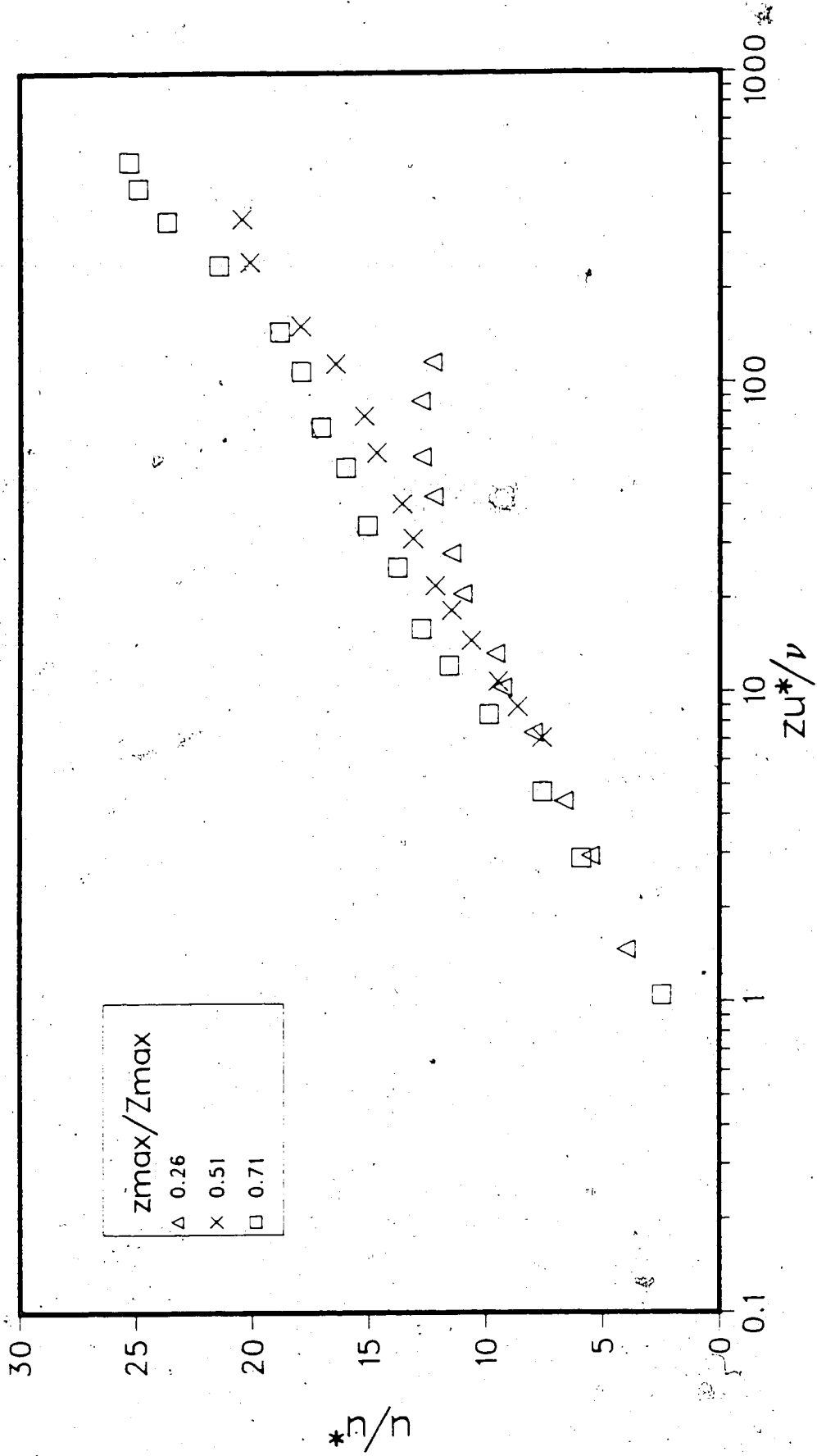
Figure 24. Semi-logarithmic Plot of u/u∗ vs. zu∗/ν (Section 1, Run 6)

65
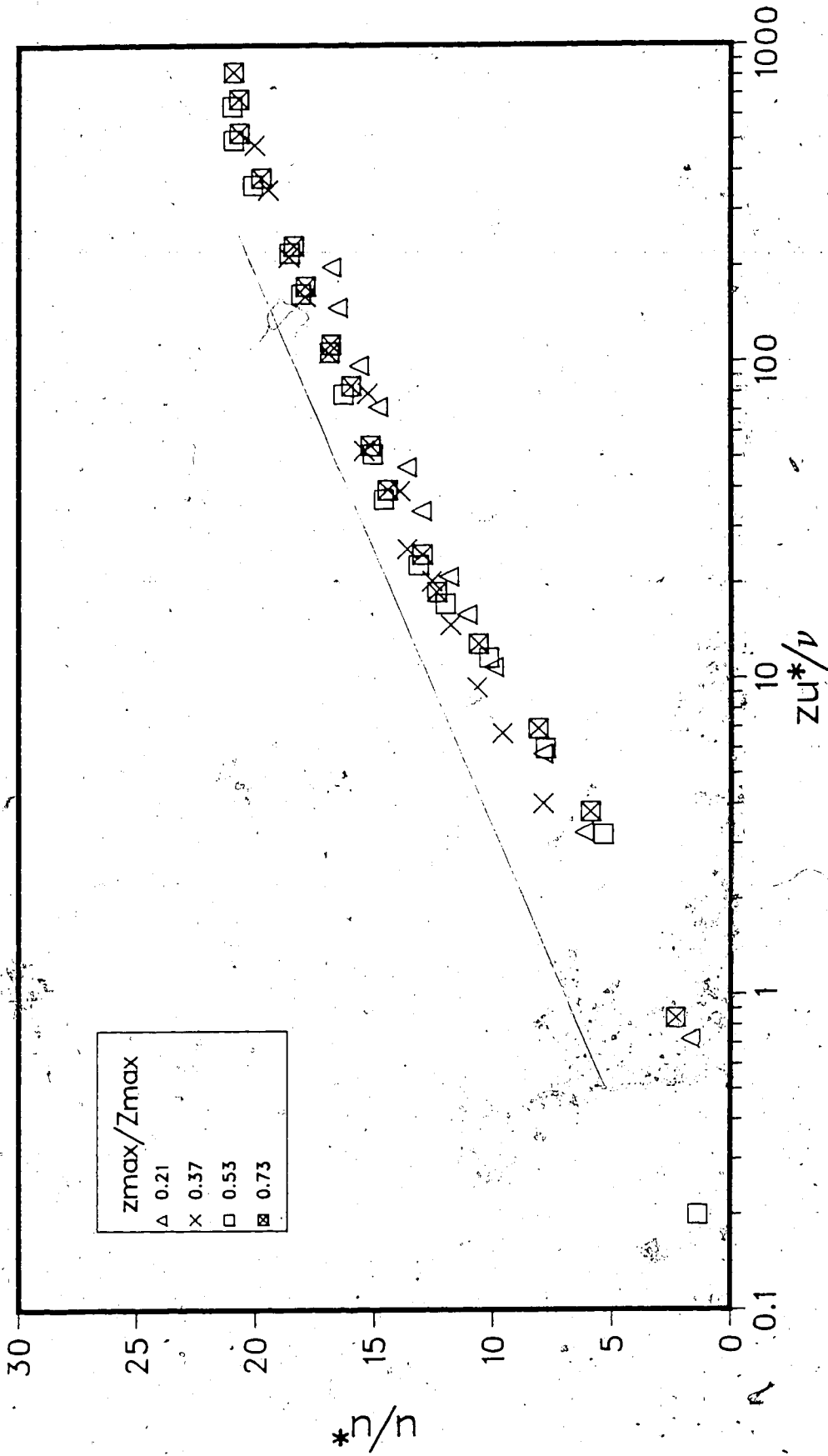
Figure 25. Semi-logarithmic Plot of u/u* vs. zu*/ν (Section 2, Run 6).
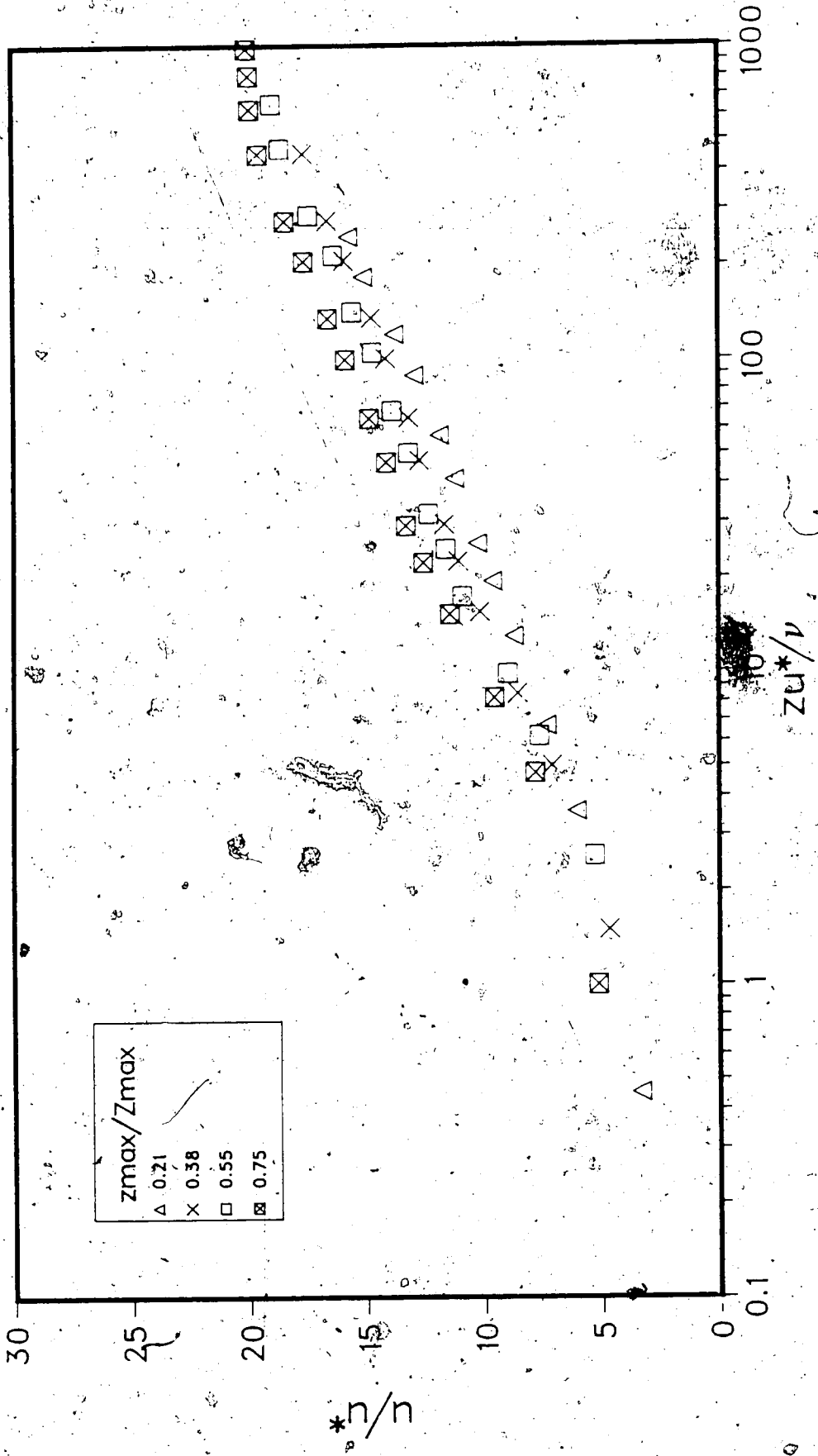
Figure 26. Semi-logarithmic Plot of u/u* vs. zu*/ν
(Section 3, Run 6)
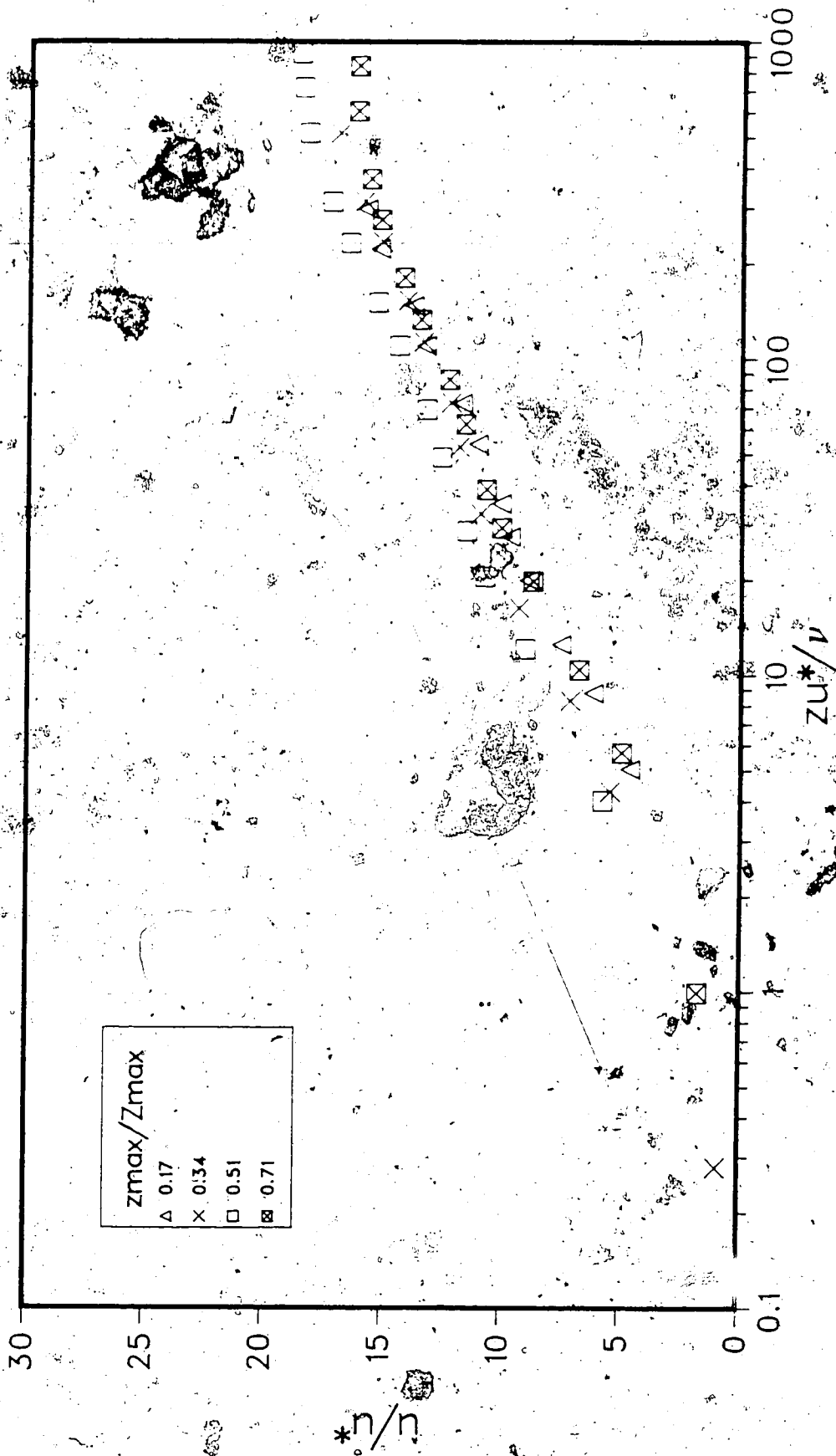
Figure 27. Semi-logarithmic Plot of u/u_* vs. zu_*/ν (Section 4, Run 6)
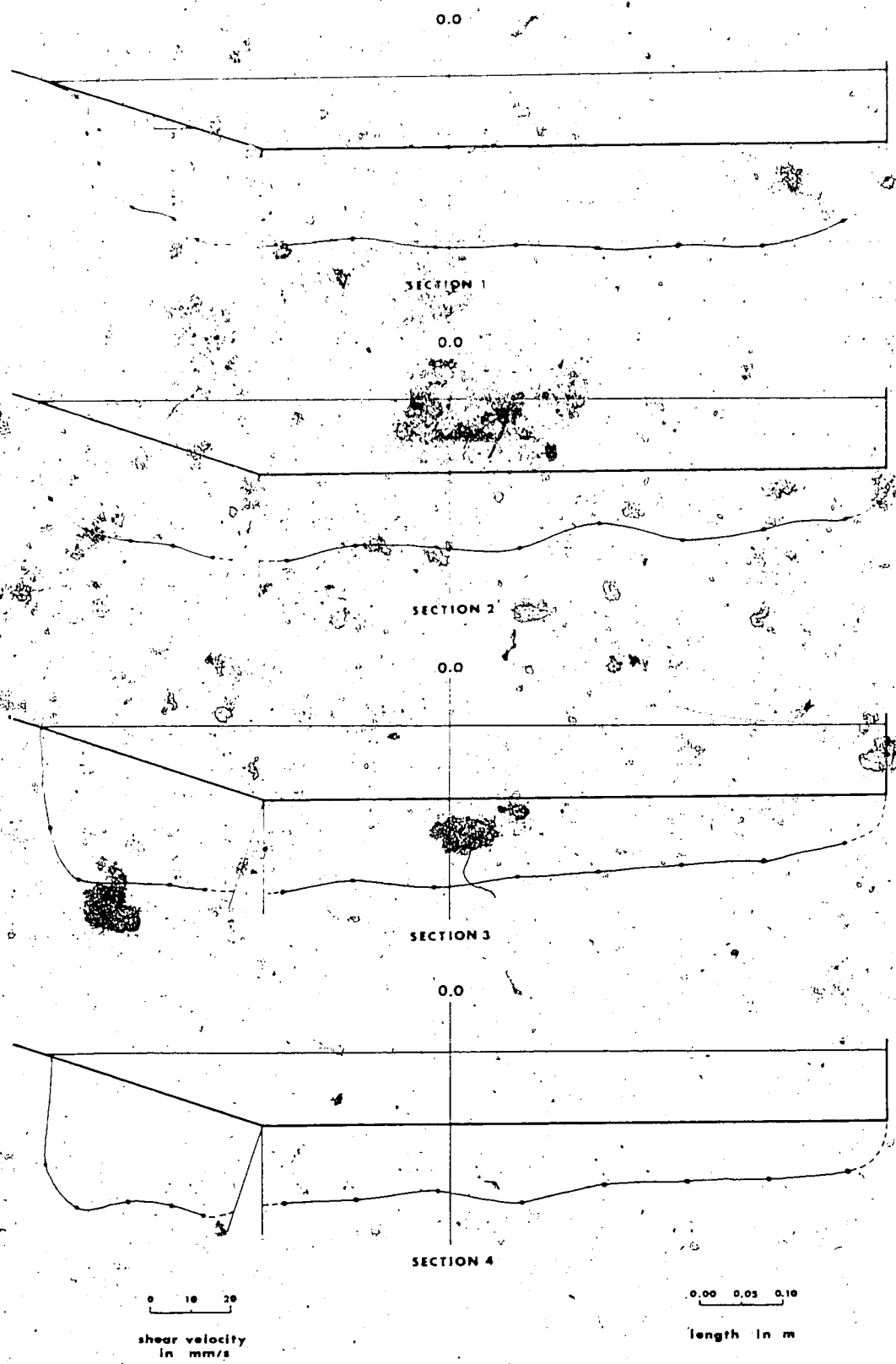
Figure 28. Distribution of Longitudinal Boundary
Shear Stress (Run 1)

0.0

SECTION 1

0.0

SECTION 2

0.0

SECTION 3

0.0

SECTION 4

0   10   20

shear velocity
in   mm/s

0.00   0.05   0.10

length in   m
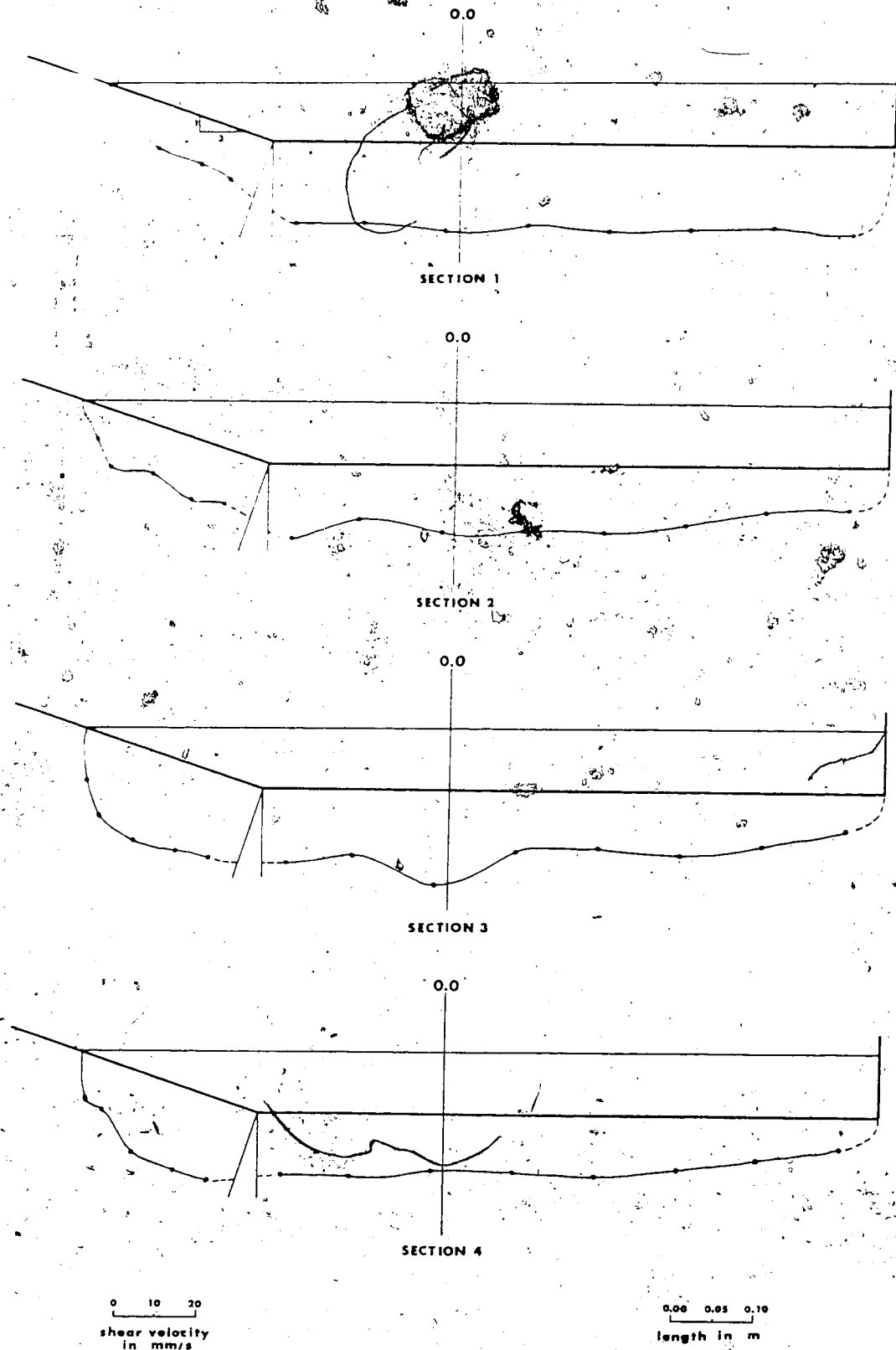
Figure 29. Distribution of Longitudinal Boundary
            Shear Stress (Run 2)

SECTION 1

SECTION 2

SECTION 3

SECTION 4

0 10 20

shear velocity
in mm/s

0.00 0.05 0.10

length in m
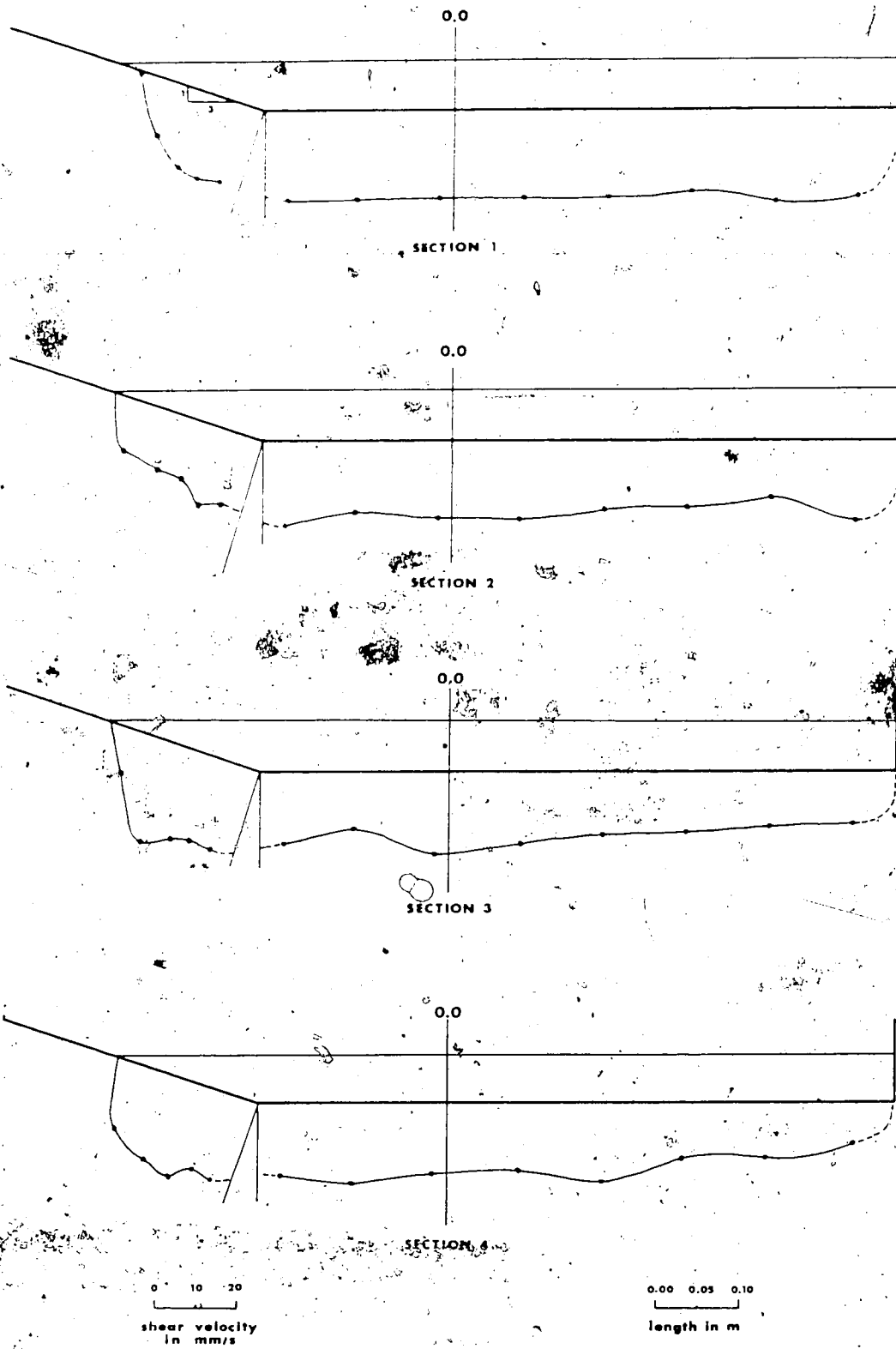
Figure 30. Distribution of Lonigitudinal Boundary
Shear Stress (Run 3)

0.0

SECTION 1

0.0

SECTION 2

SECTION 3

0.0

SECTION 4

0   10   20

shear velocity
in mm/s

0.00 0.05 0.10

length in m
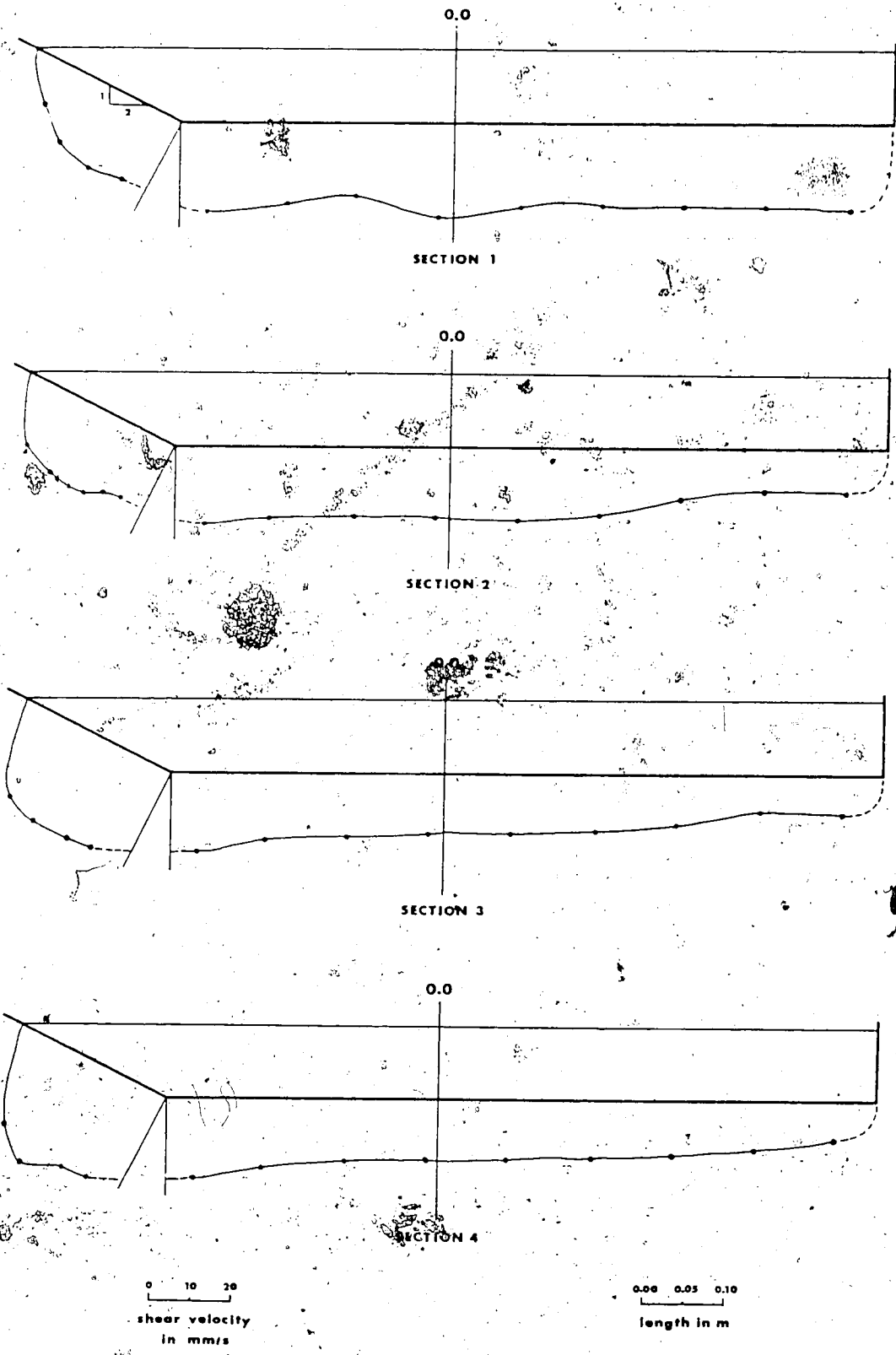
Figure 31. Distribution of Longitudinal Boundary
            Shear Stress (Run 4)

0.0

SECTION 1

0.0

SECTION 2

0.0

SECTION 3

0.0

SECTION 4

0   10   20

shear velocity
in mm/s

0.00   0.05   0.10

length in m
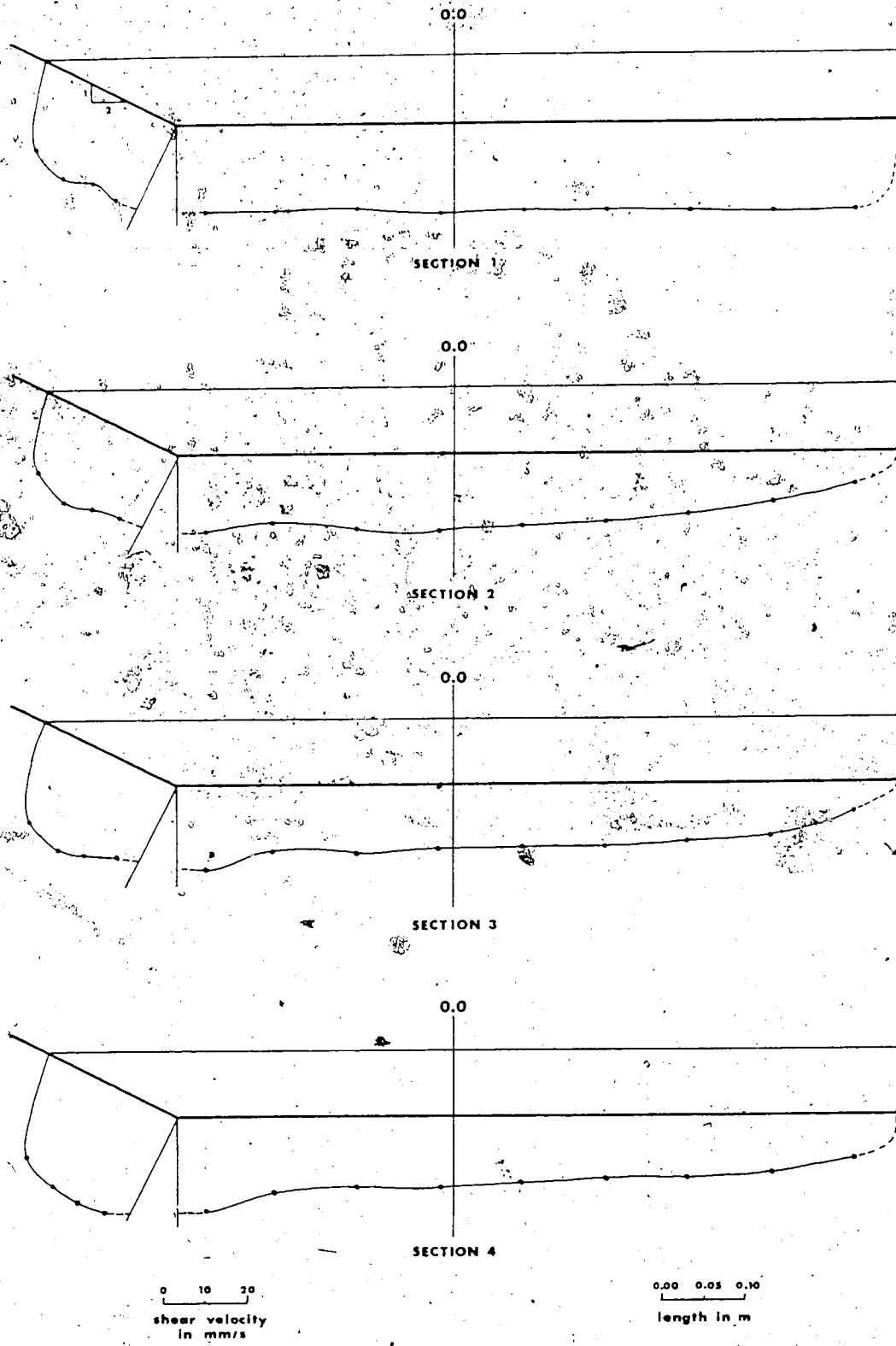
Figure 32. Distribution of Longitudinal Boundary
Shear Stress (Run 5)
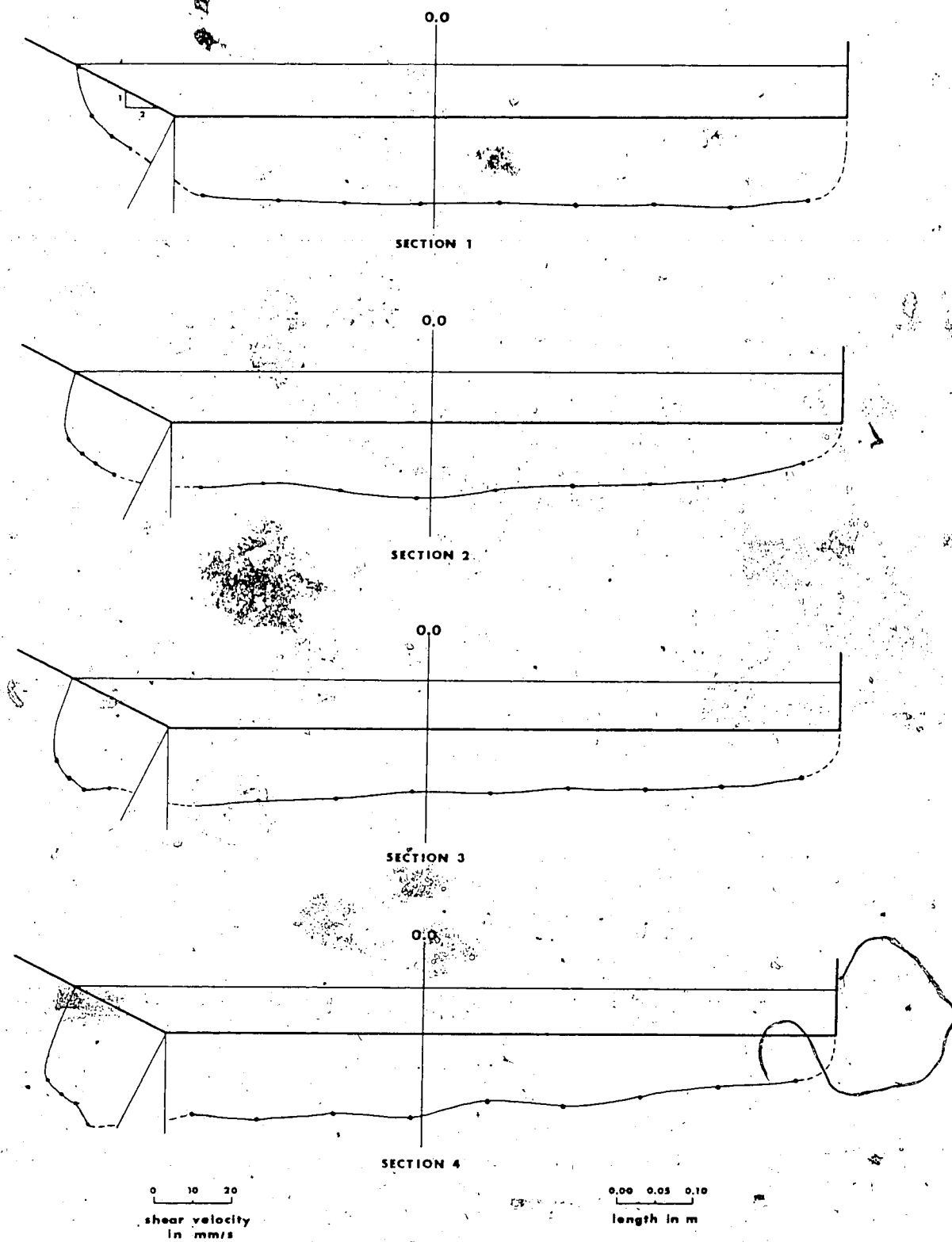
Figure 33. Distribution of Longitudinal Boundary
Shear Stress (Run 6)
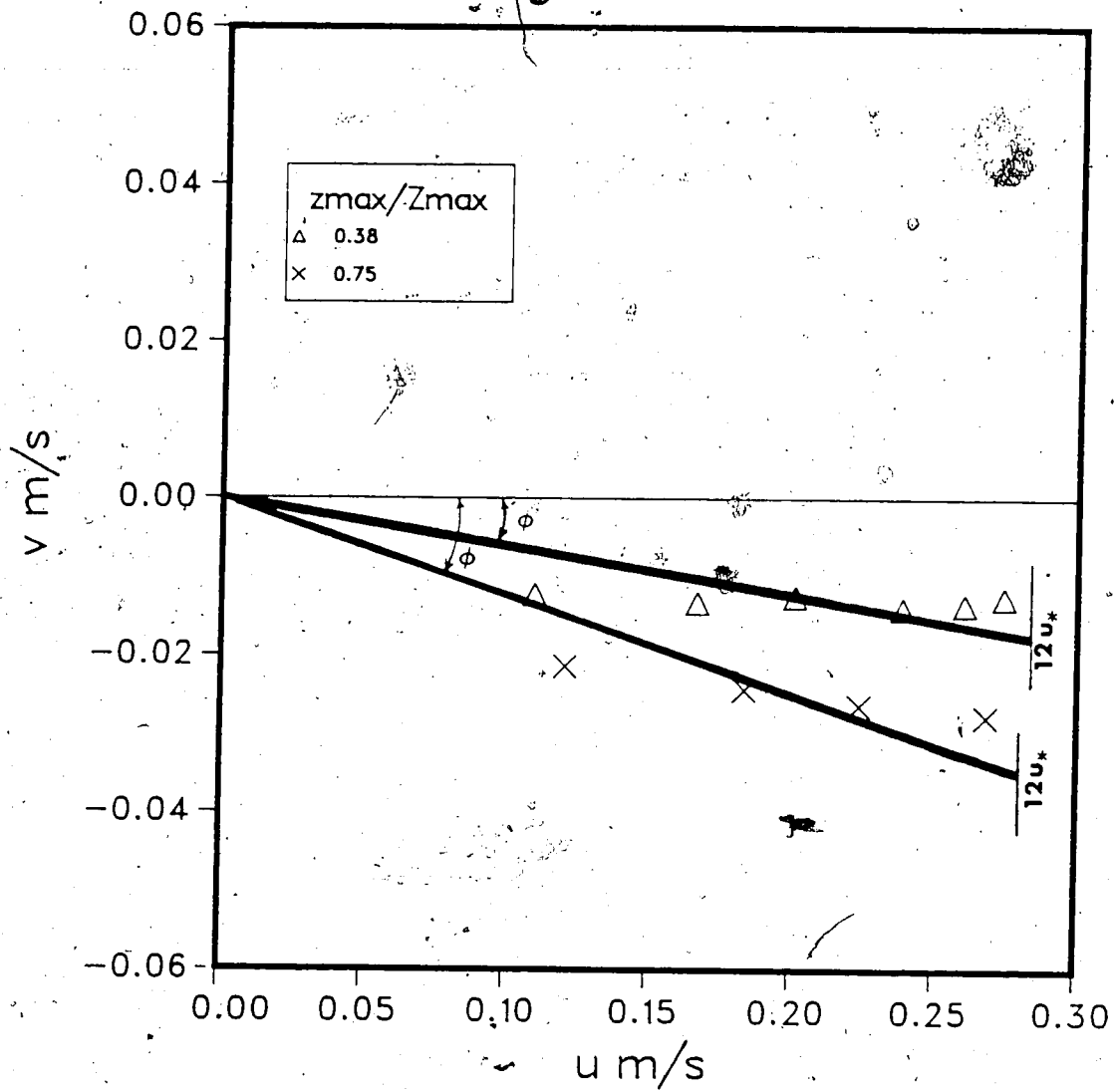
Figure 34. Polar Plot of Velocities (Section 3, Run 6)
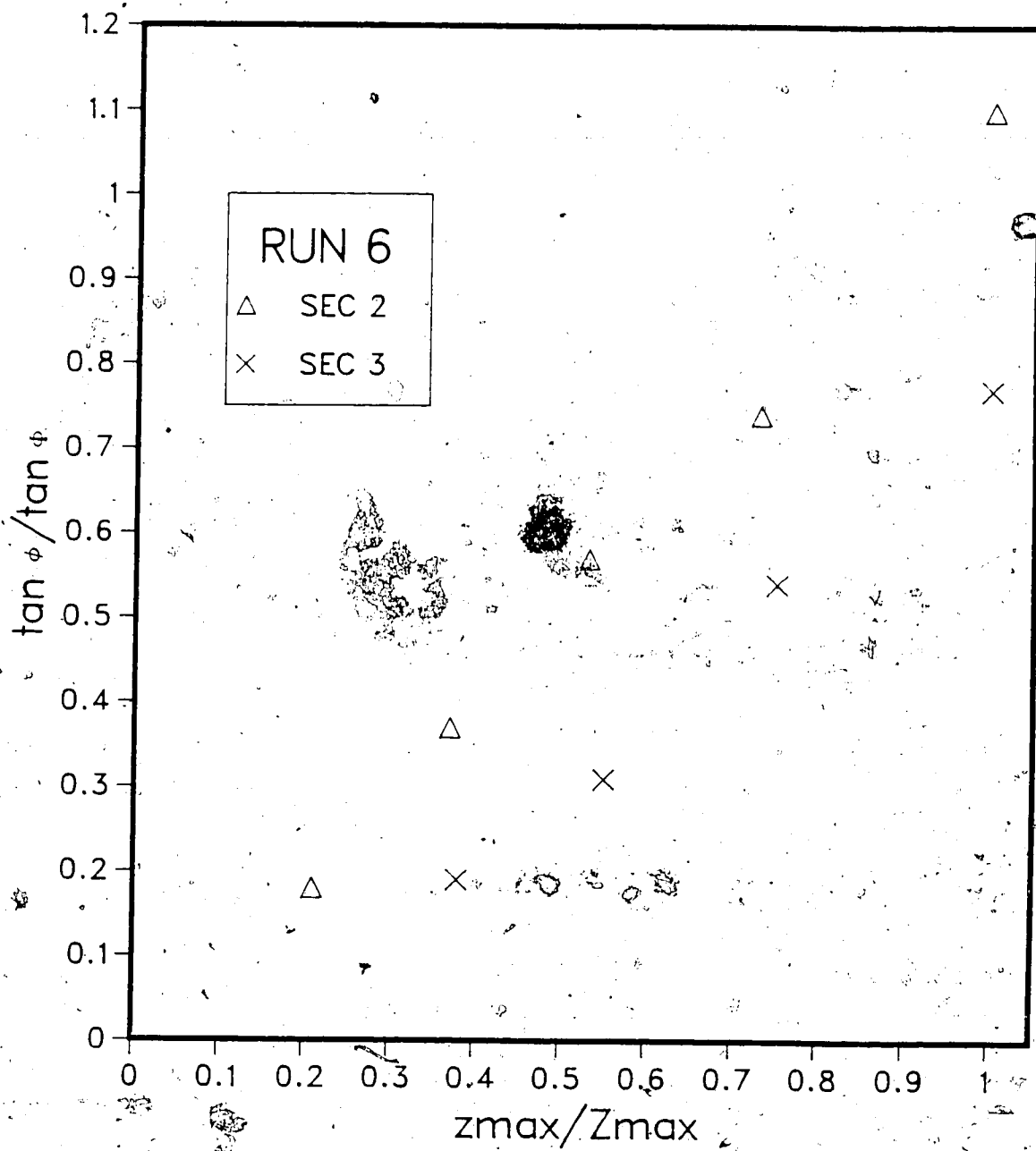
Figure 35. Variation of Bed Stress Angle up the Slope (Run 6)
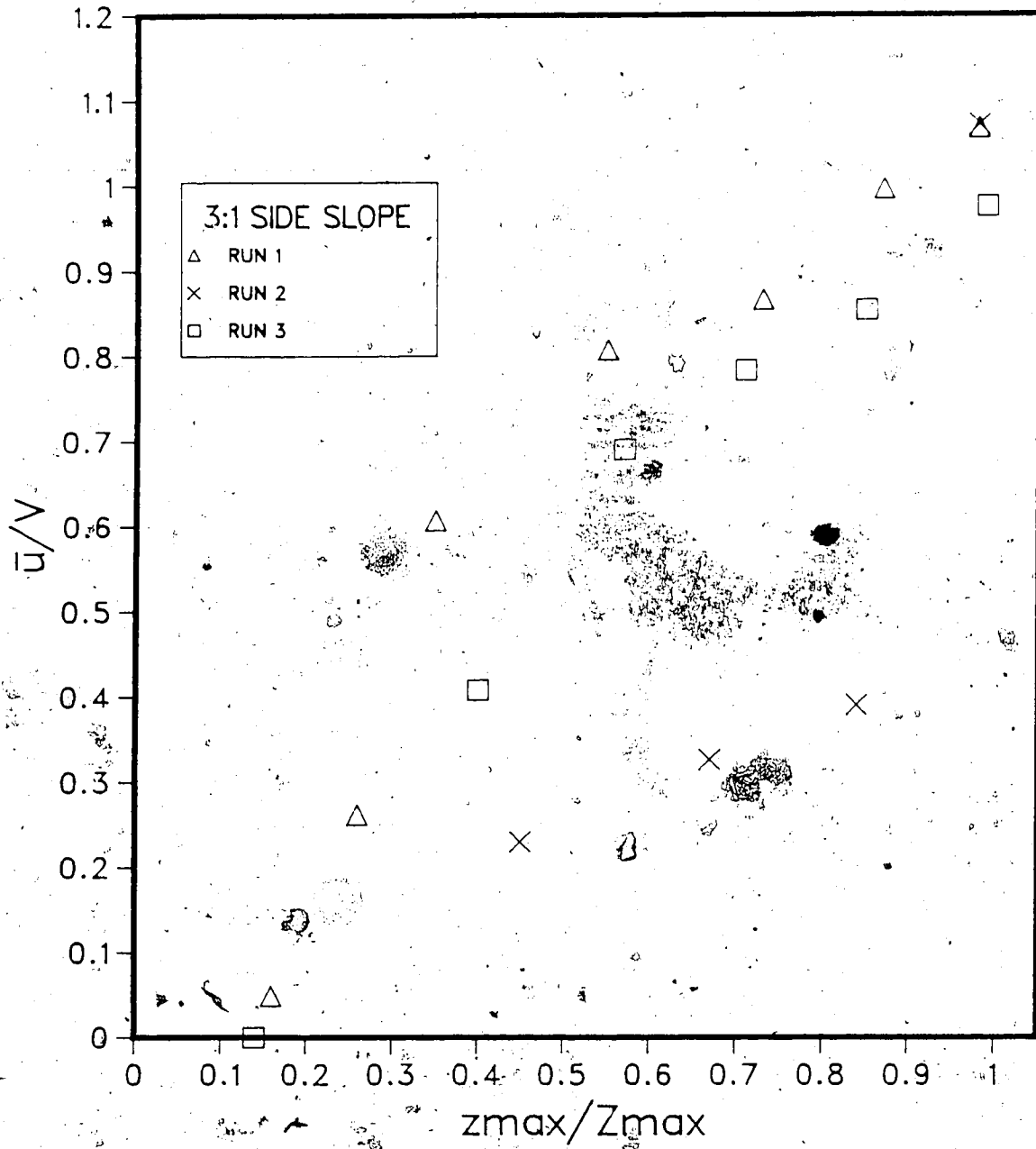
Figure 36. Variation of Longitudinal Velocity up the 3 to 1 Slope
          (Section 1)
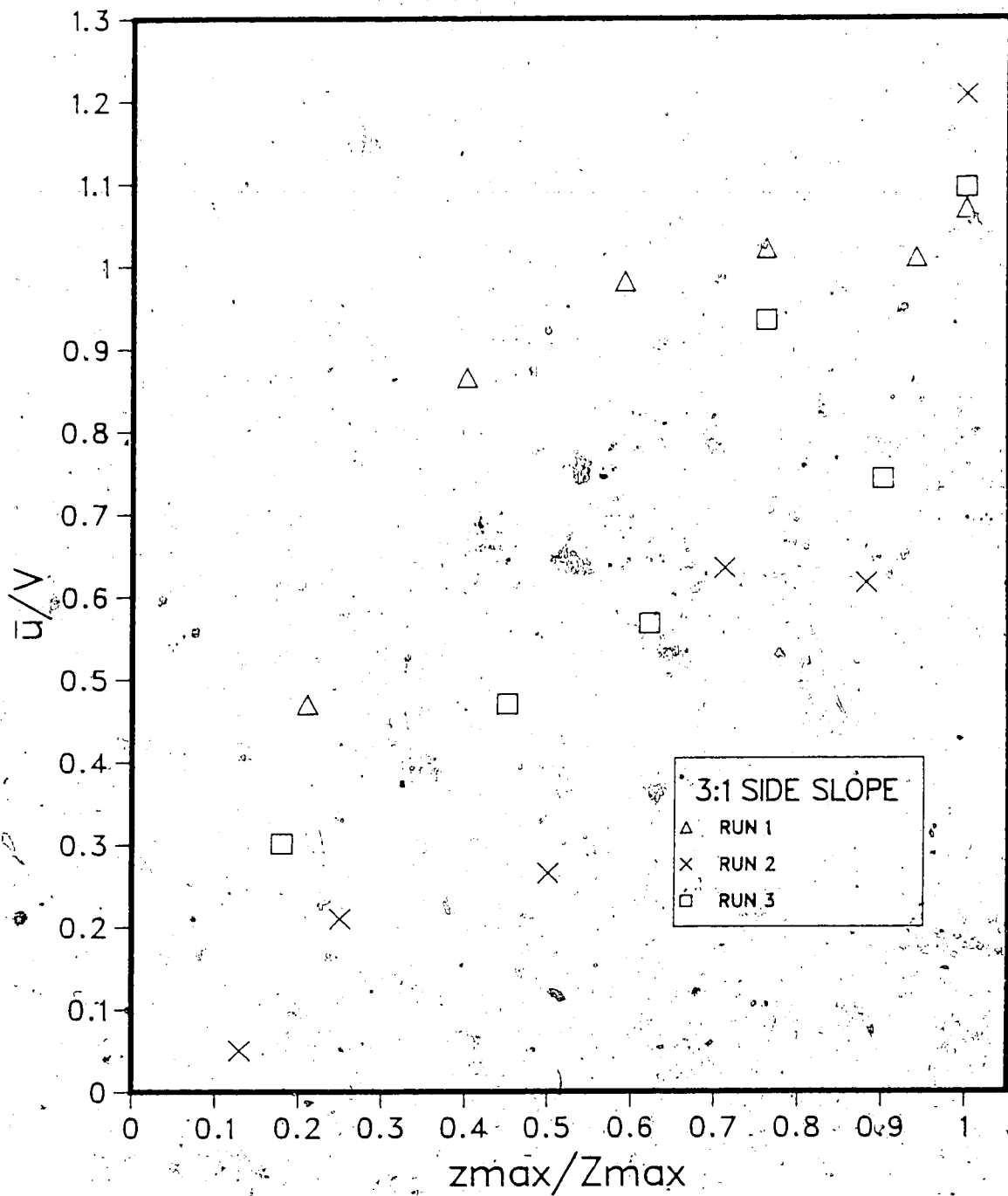
Figure 37. Variation of Longitudinal Velocity up the 3 to 1 Slope
(Section 2)
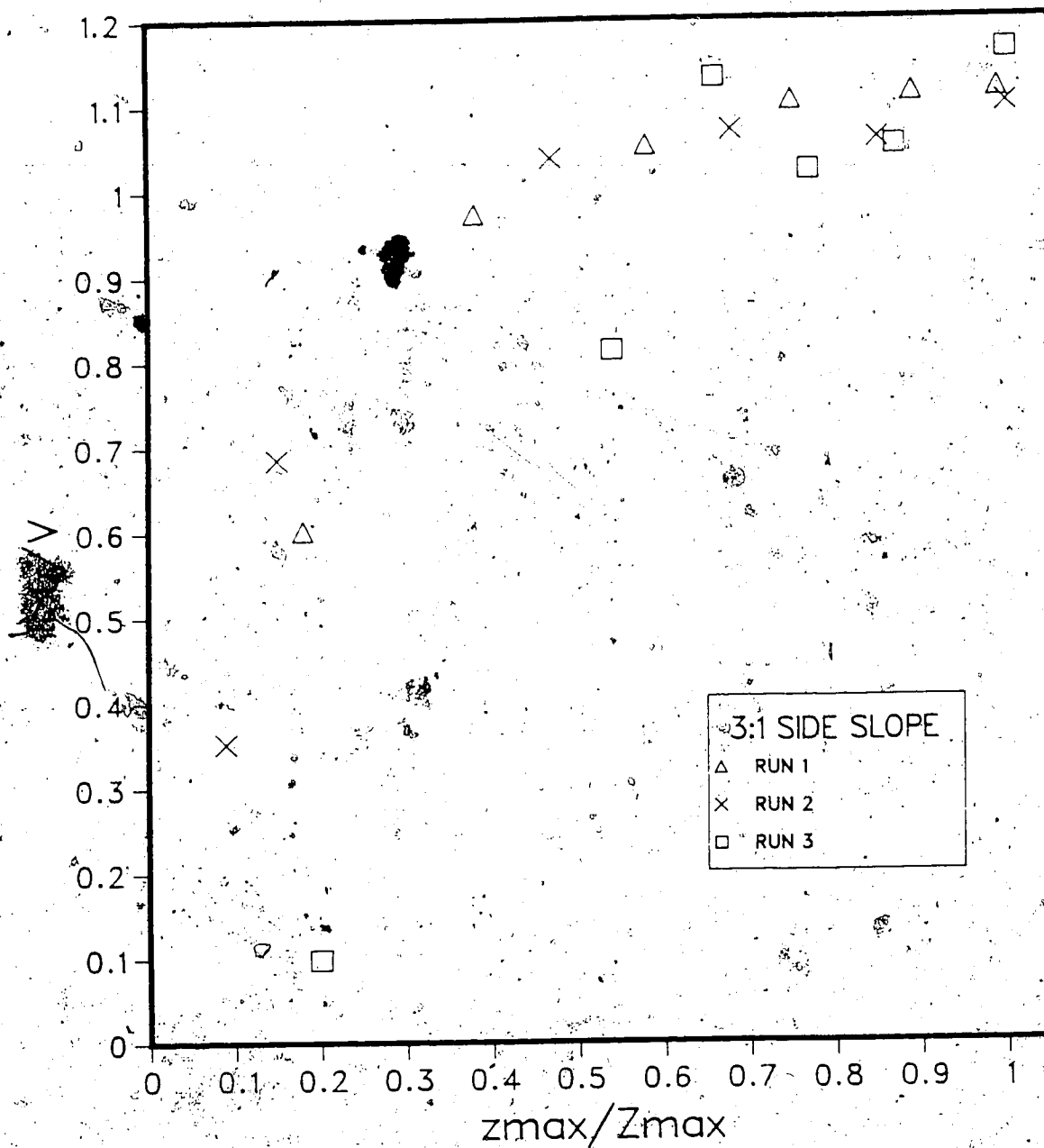
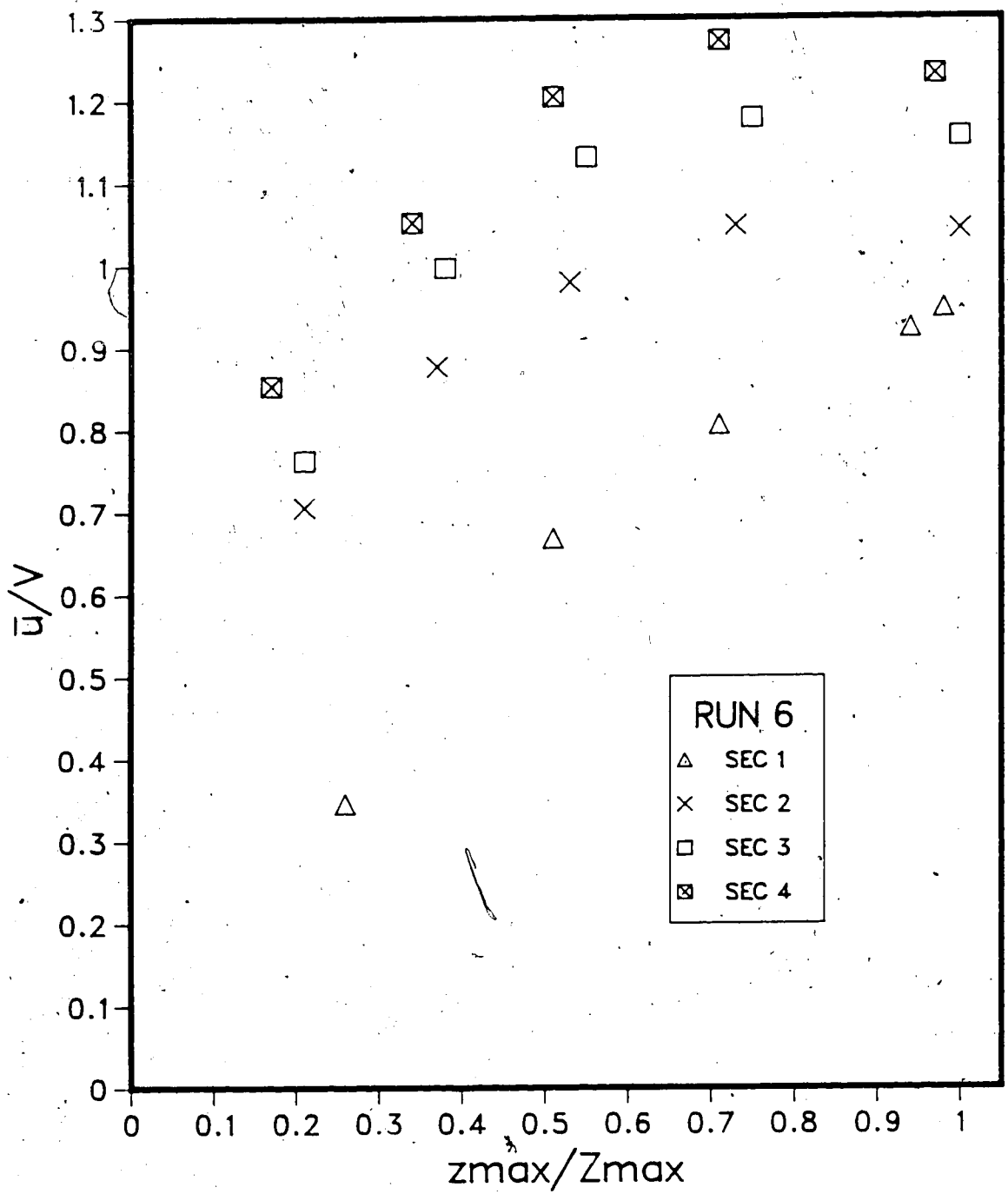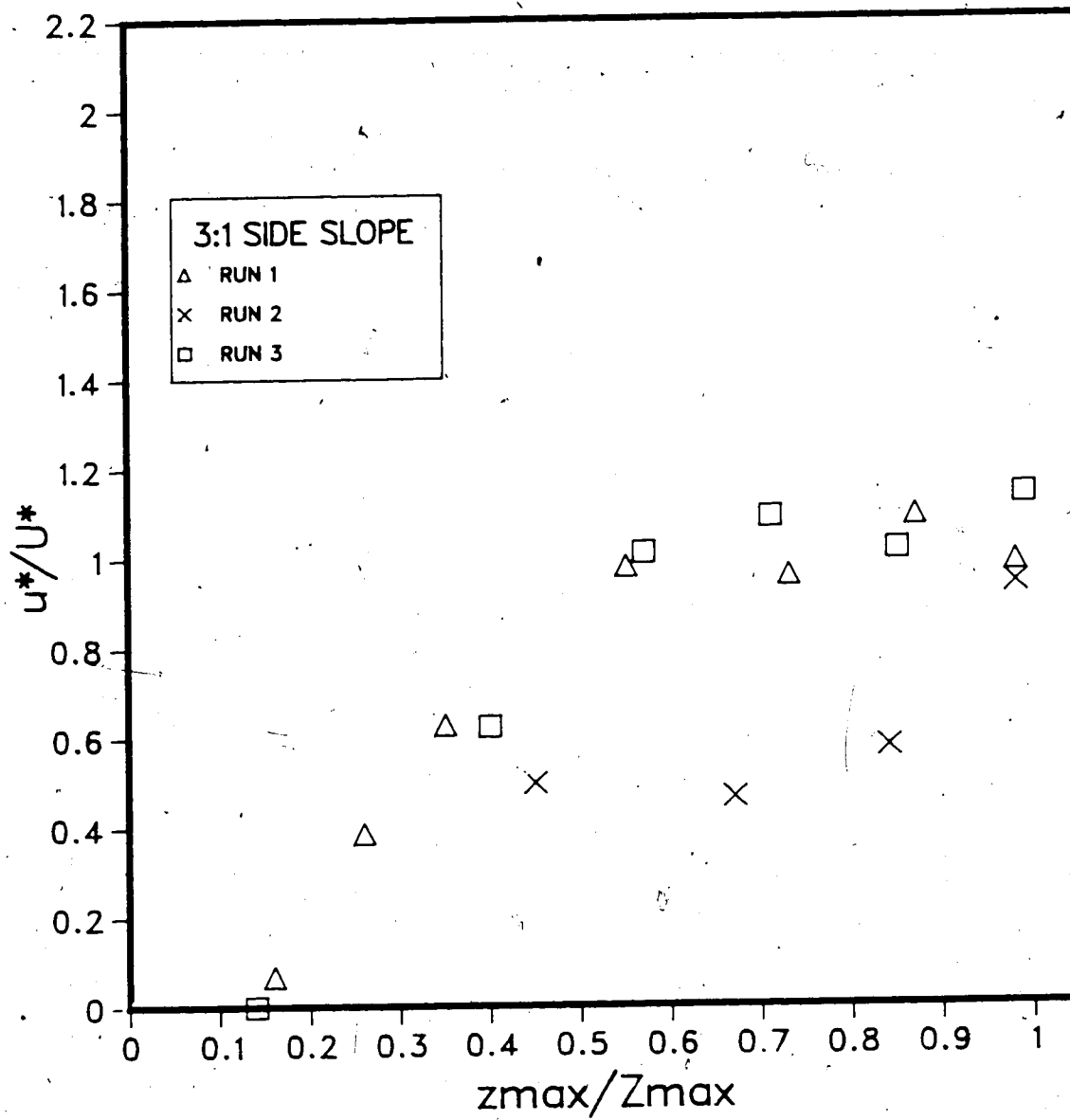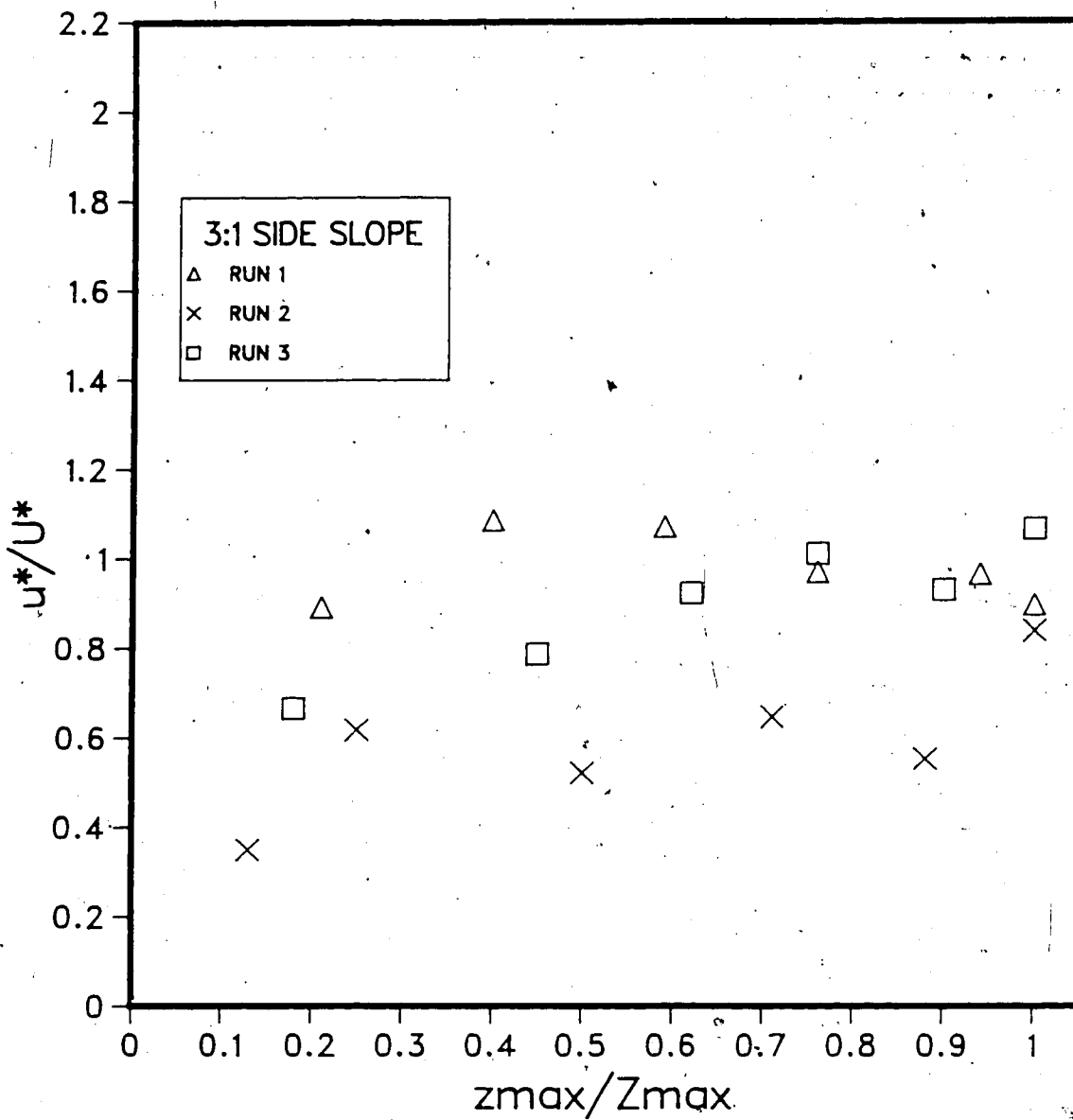Figure 38. Variation of Longitudinal Velocity up the 3 to 1 Slope
            (Section 3)
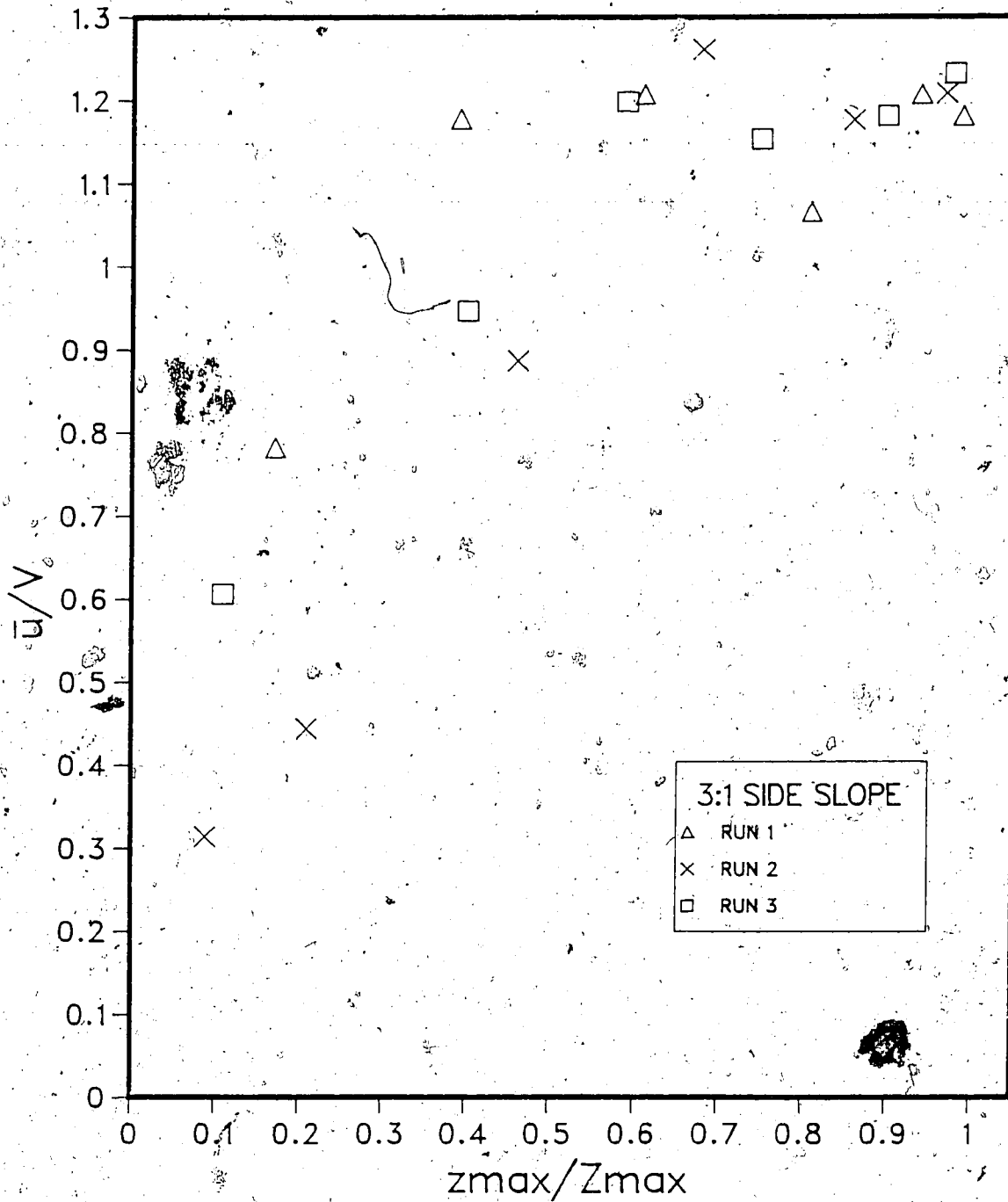
Figure 39. Variation of Longitudinal Velocity up the 3 to 1 Slope (Section 4)
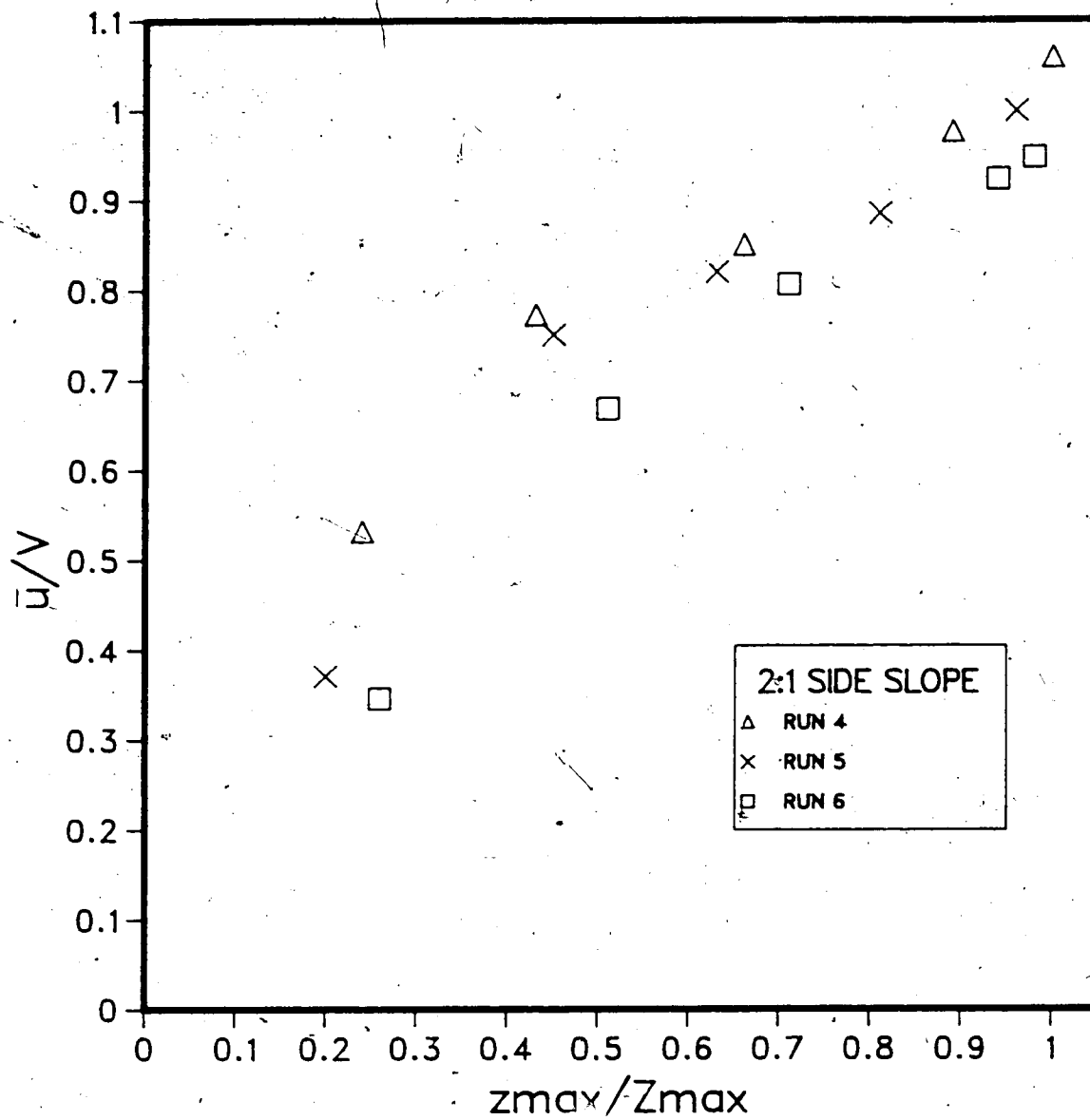
Figure 40. Variation of Longitudinal Velocity up the 2 to 1 Slope (Section 1)
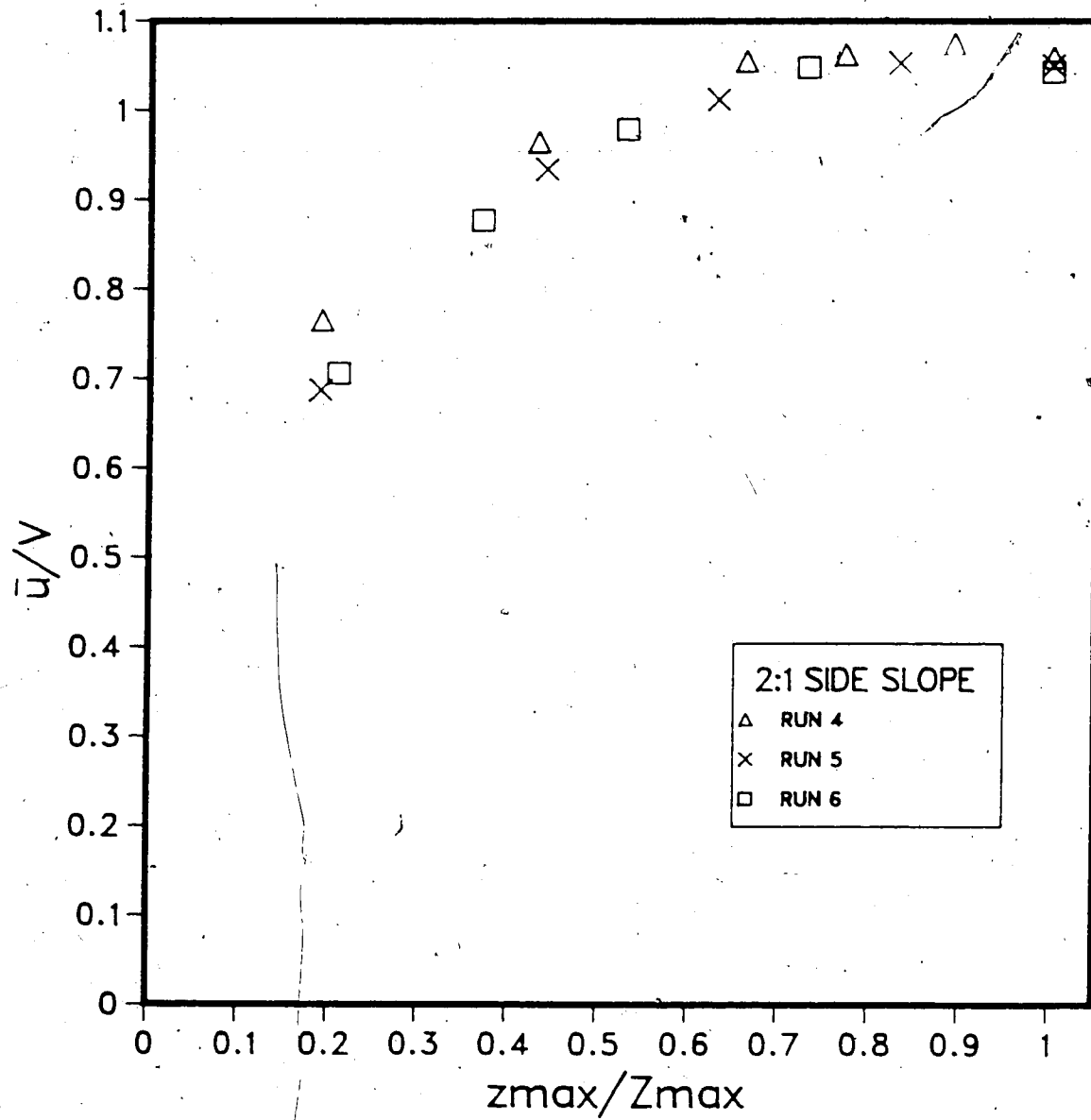
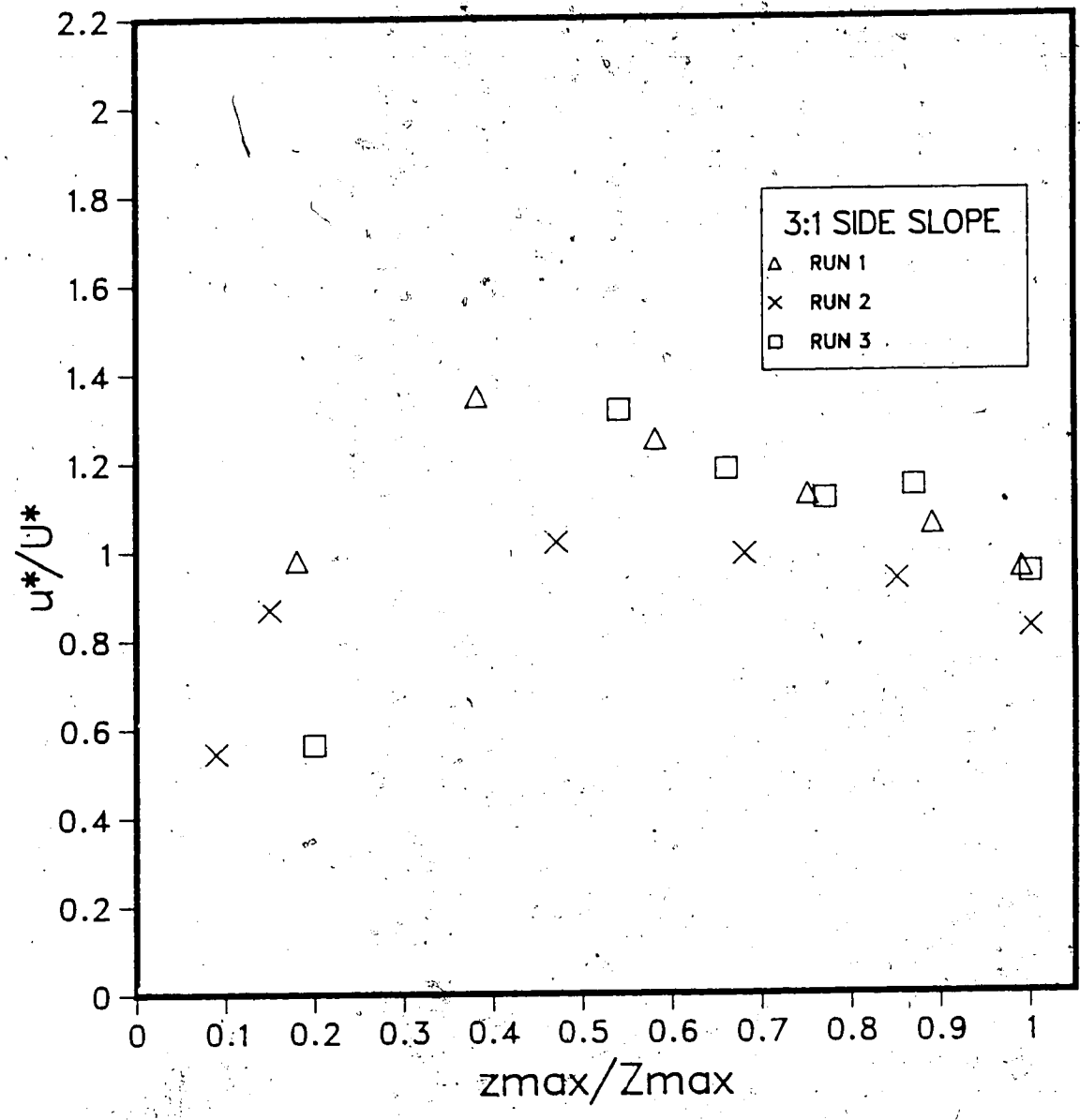Figure 41. Variation of Longitudinal Velocity up the 2 to 1 Slope
(Section 2)
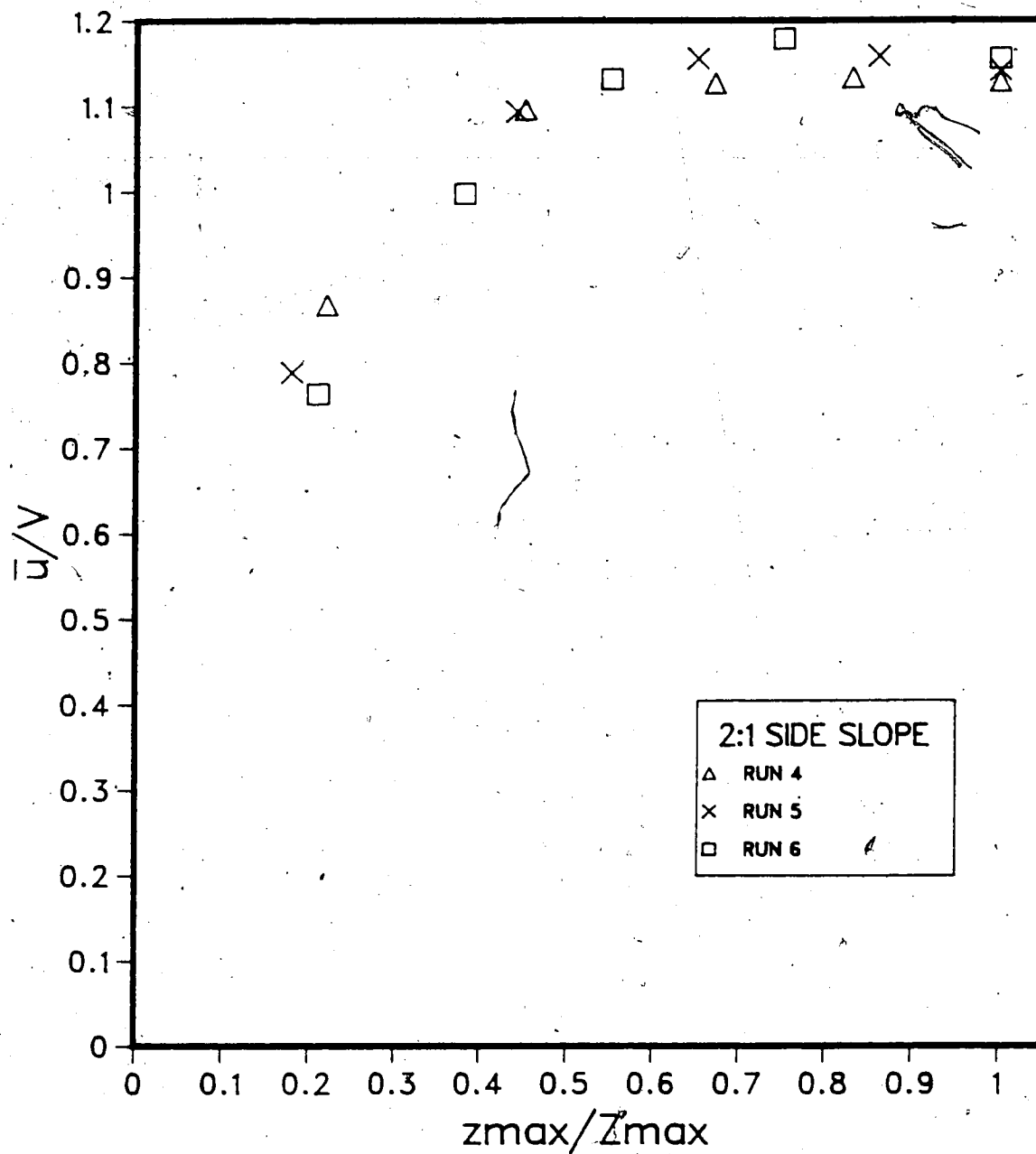
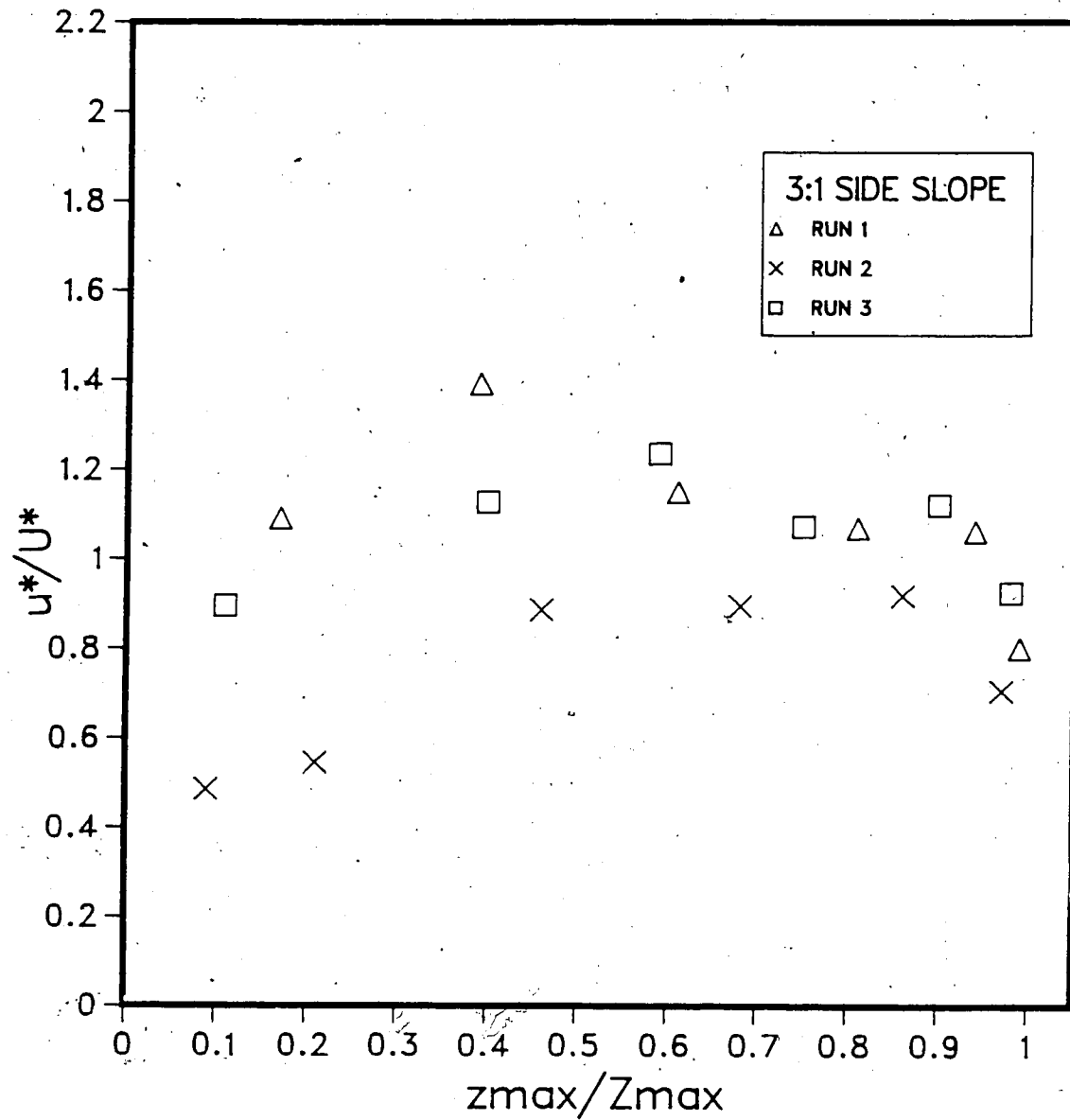Figure 42. Variation of Longitudinal Velocity up the 2 to 1 Slope
(Section 3)
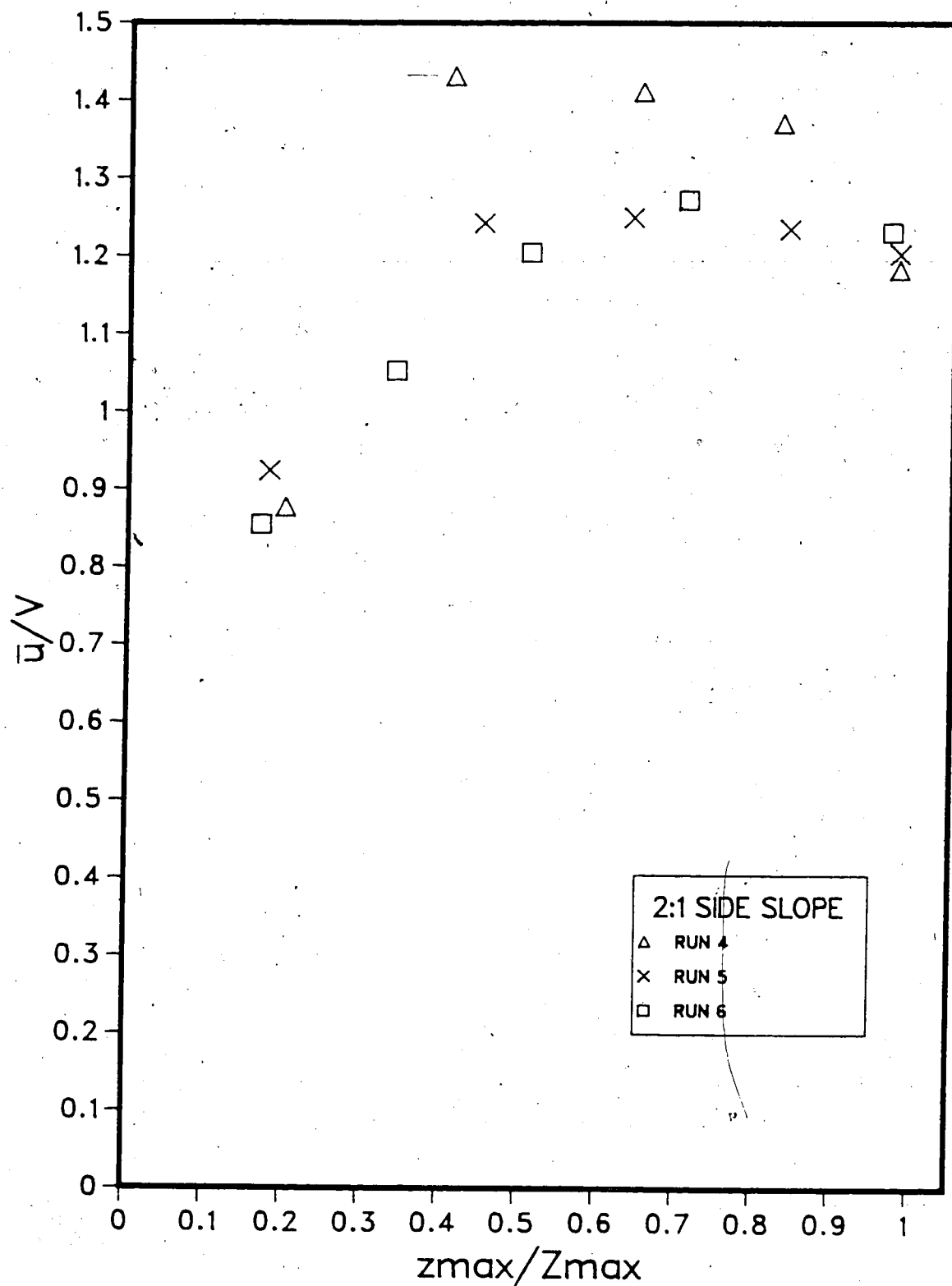
Figure 43. Variation of Longitudinal Velocity up the 2 to 1 Slope (Section 4)
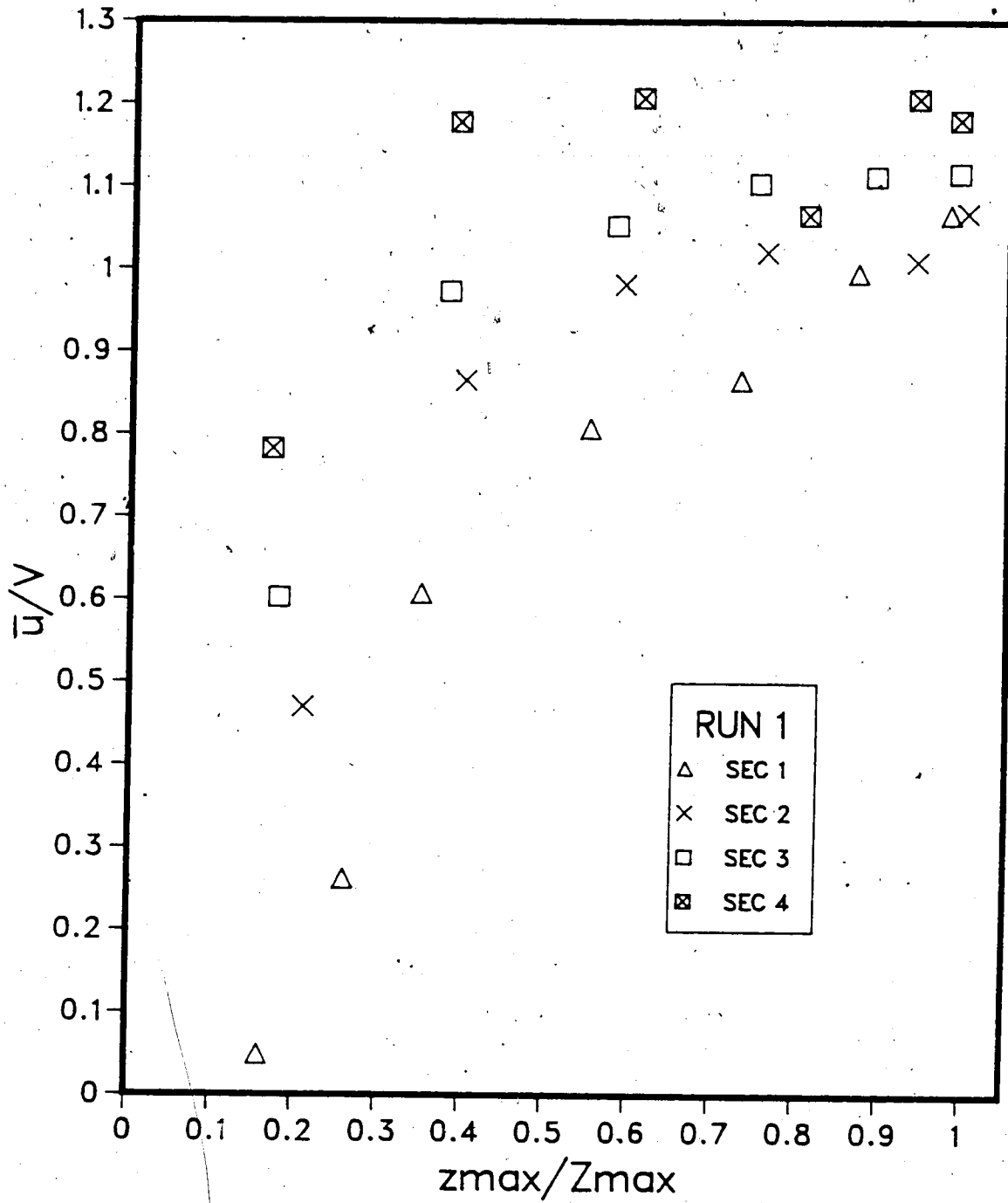
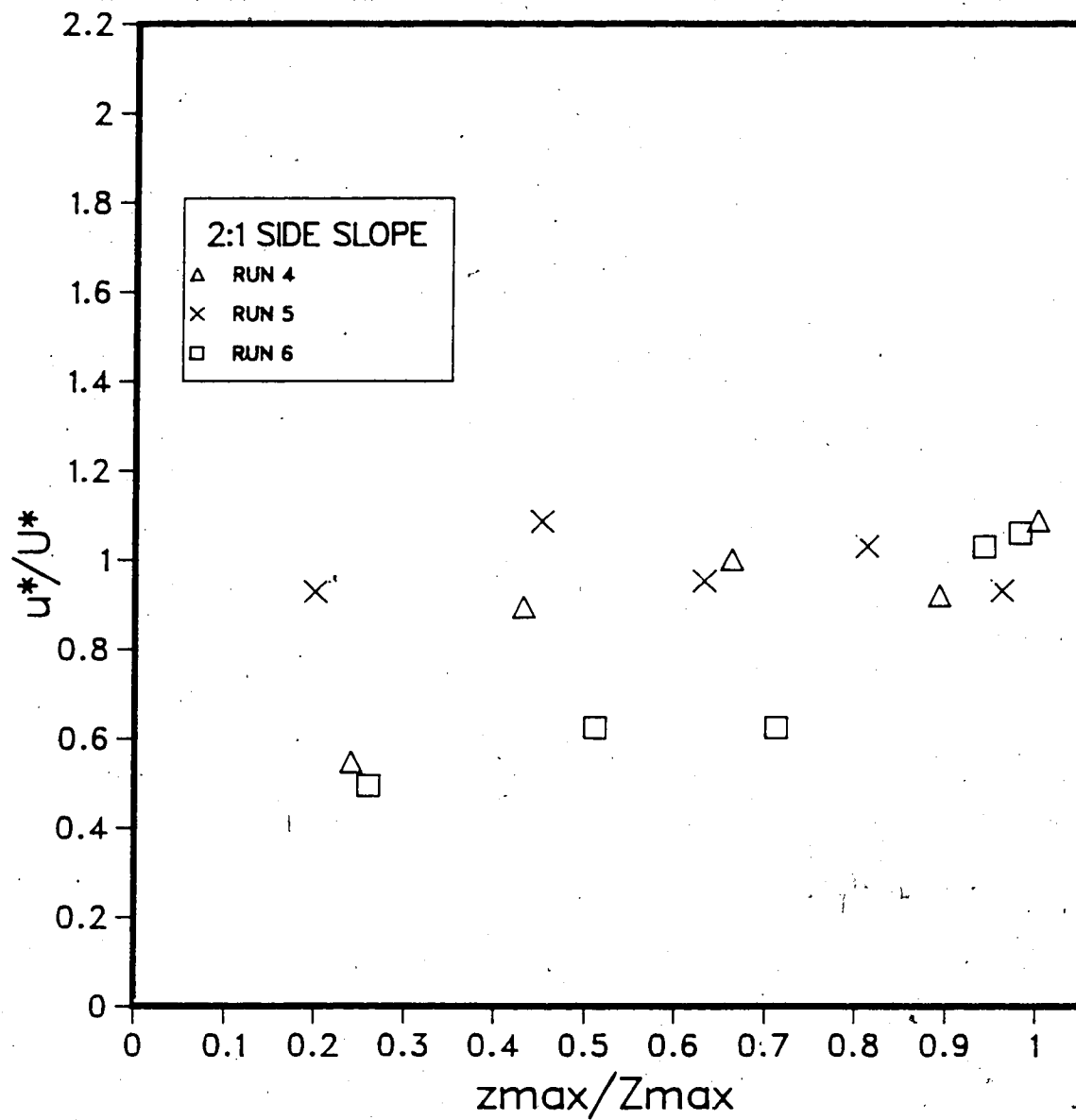Figure 44. Variation of Longitudinal Velocity up the 3 to 1 Slope (Run 1)
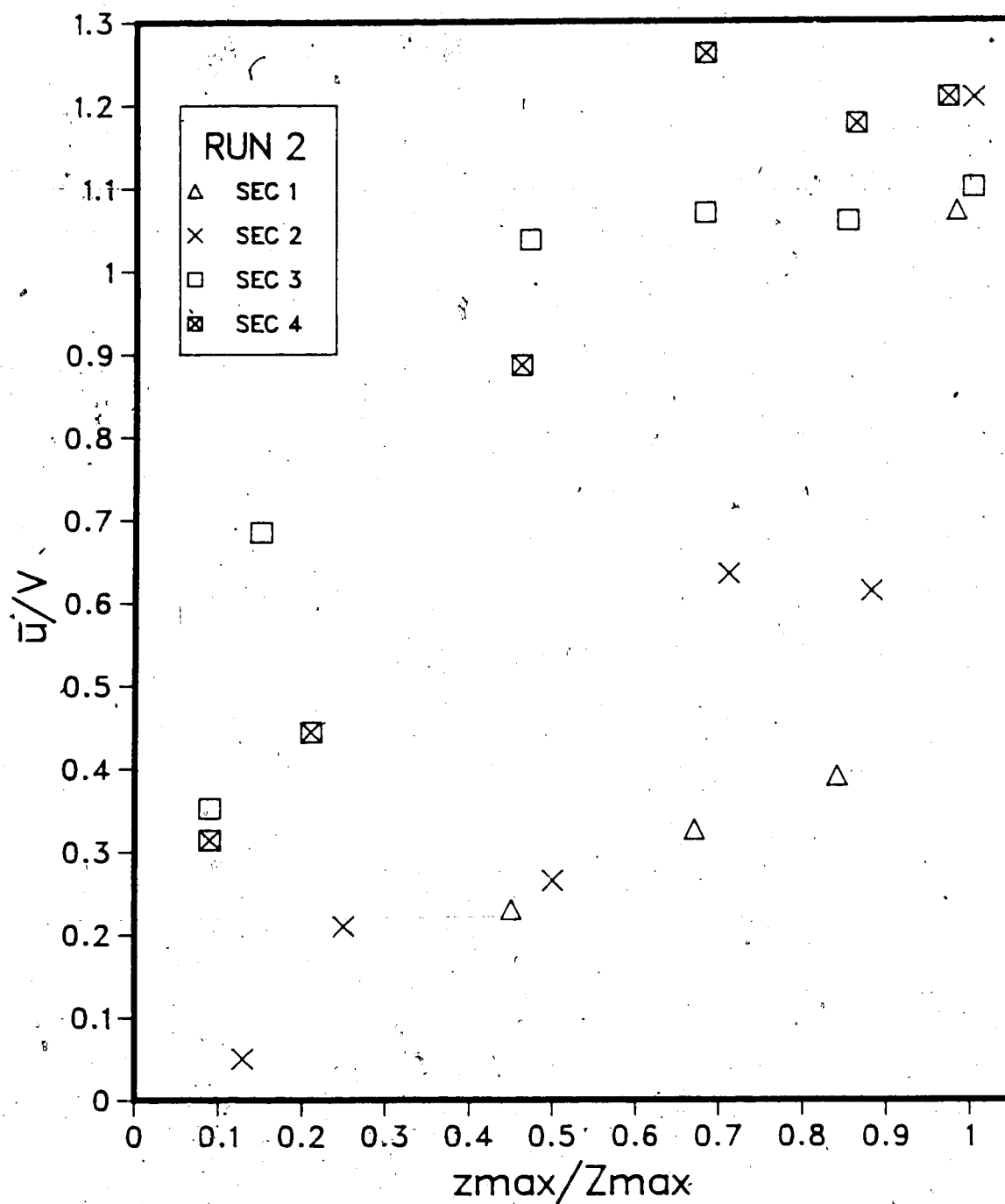
Figure 45. Variation of Longitudinal Velocity up the 3 to 1 Slope (Run 2)
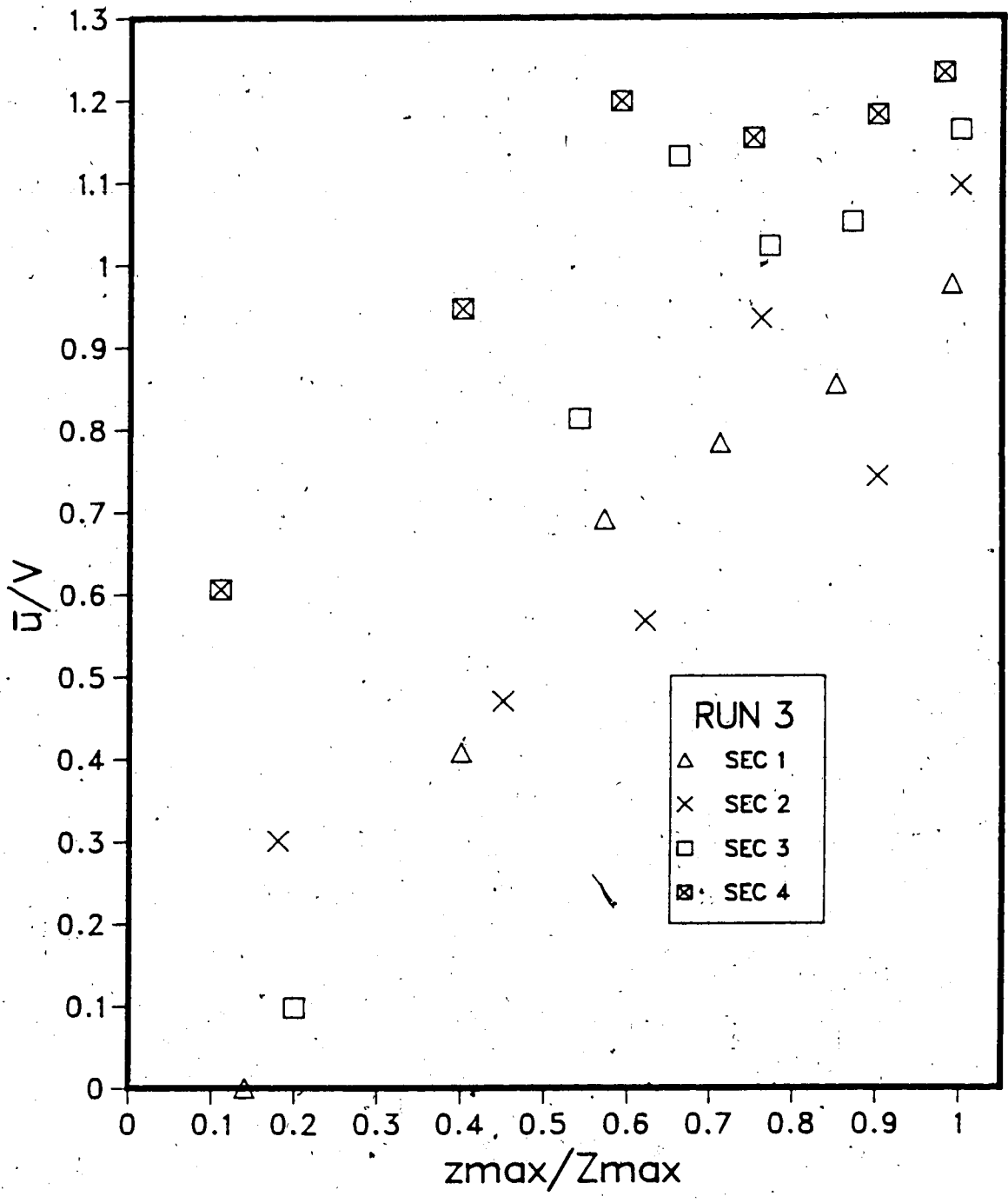
Figure 46. Variation of Longitudinal Velocity up the 3 to 1 Slope
(Run 3)
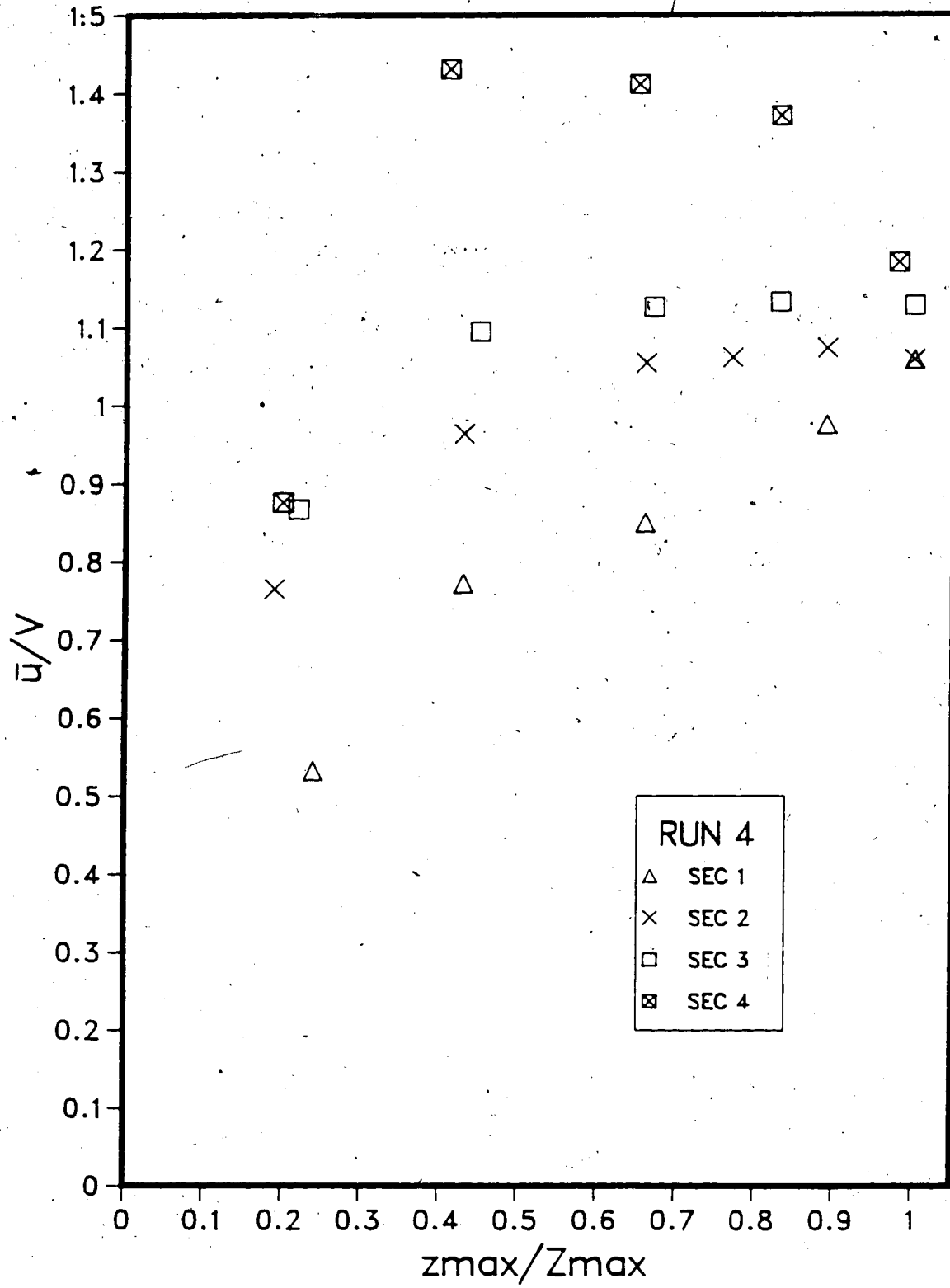
Figure 47. Variation of Longitudinal Velocity up the 2 to 1 Slope (Run 4)
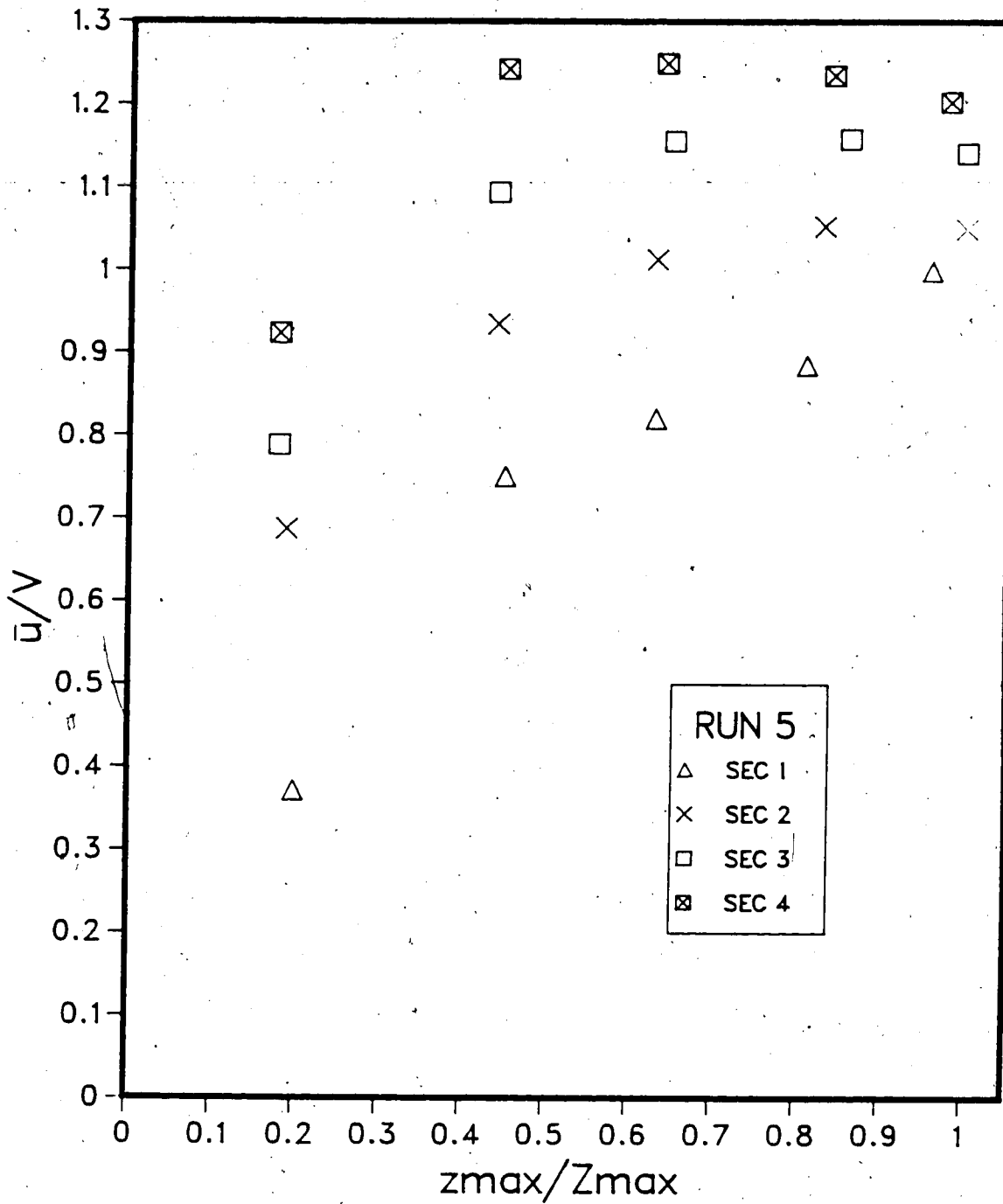
Figure 48. Variation of Longitudinal Velocity up the 2 to 1 Slope (Run 5)

Figure 49. Variation of Longitudinal Velocity up the 2 to 1 Slope (Run 6)

Figure 50. Variation of Longitudinal Shear Velocity
up the 3 to 1 Slope (Section 1)

Figure 51. Variation of Longitudinal Shear Velocity
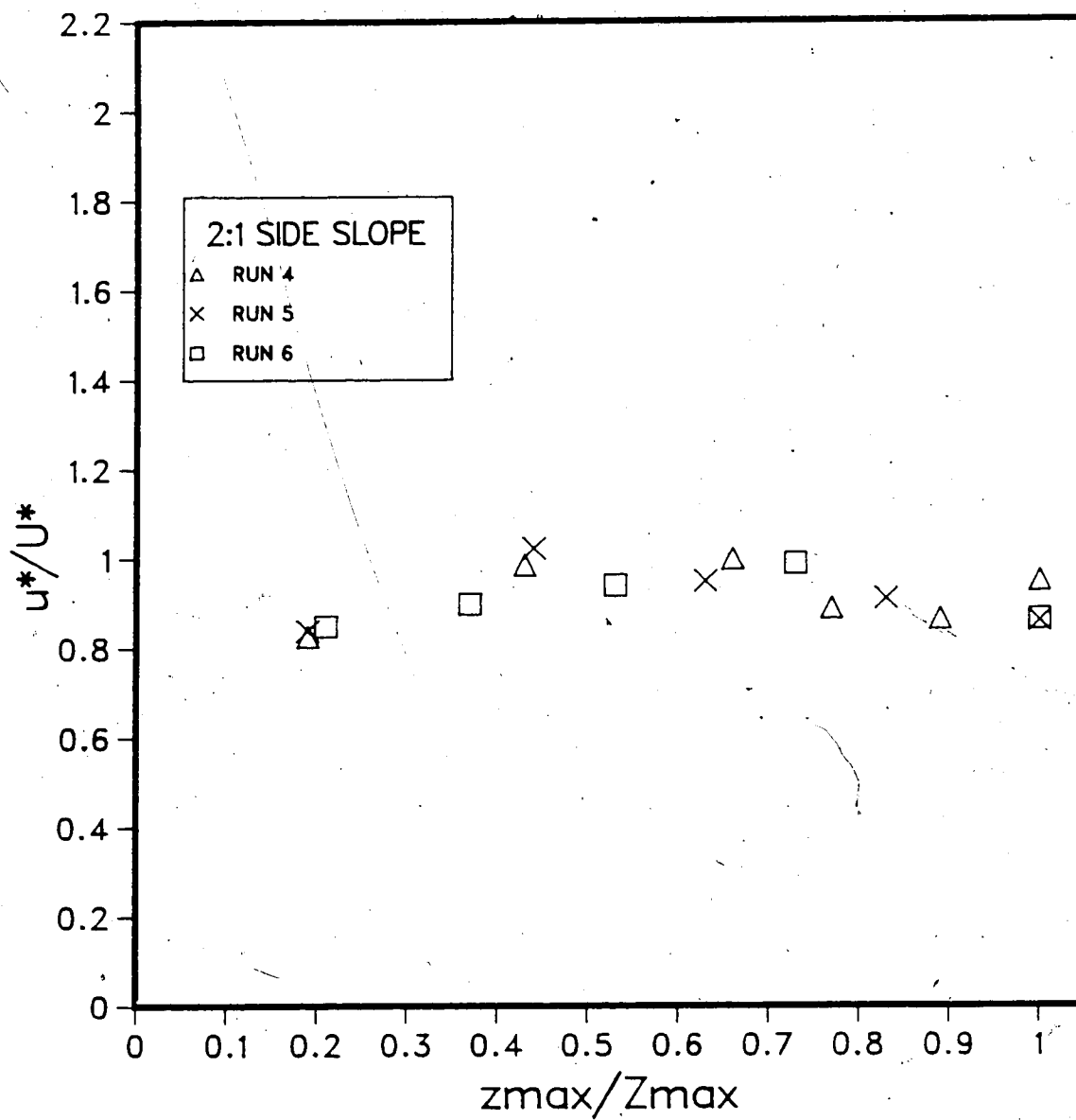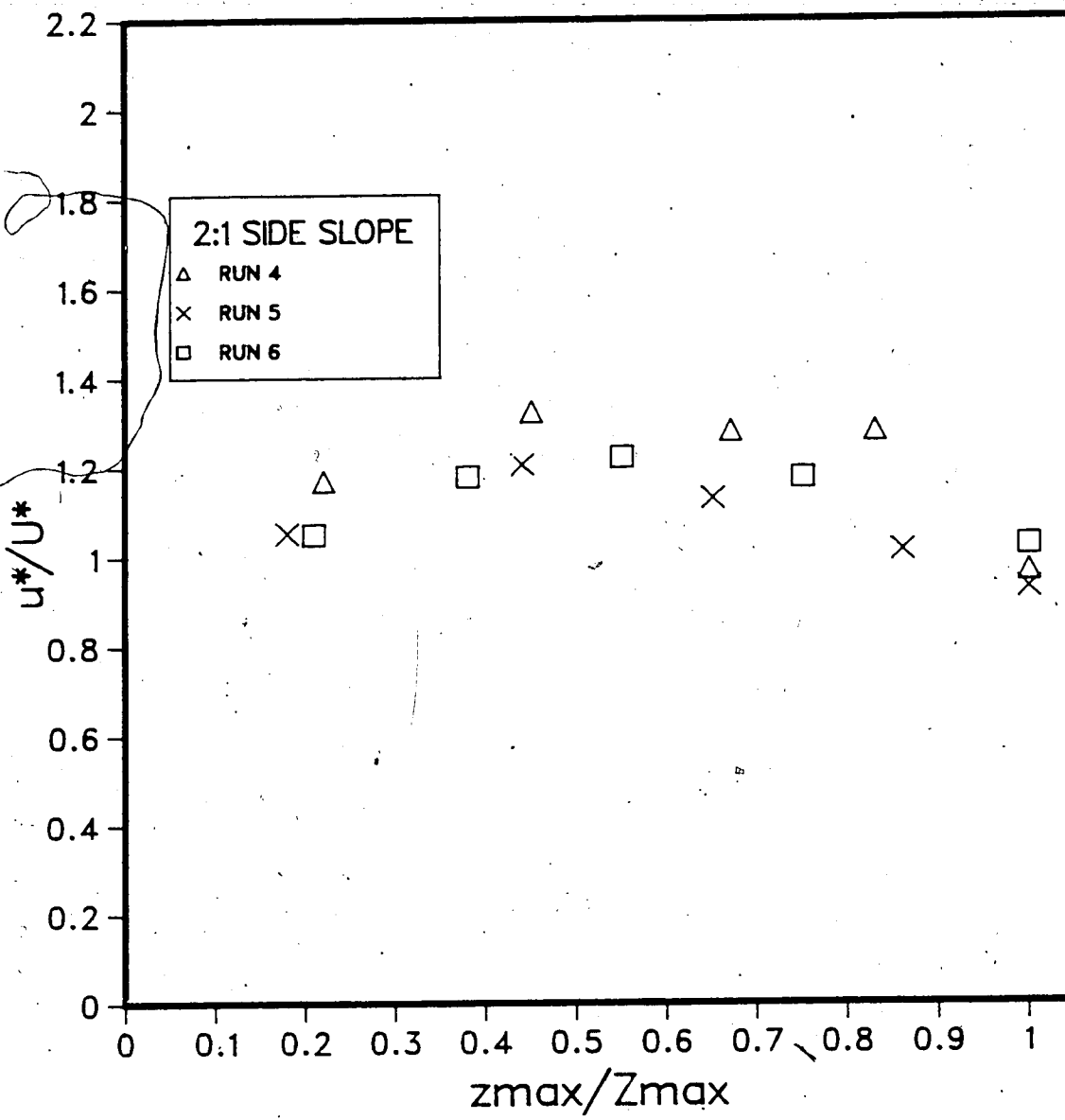   up the 3 to 1 Slope (Section 2)

Figure 52. Variation of Longitudinal Shear Velocity
up the 3 to 1 Slope (Section 3)

Figure 53. Variation of Longitudinal Shear Velocity
up the 3 to 1 Slope (Section 4)

Figure 54. Variation of Longitudinal Shear Velocity
up the 2 to 1 Slope (Section 1)

Figure 55. Variation of Longitudinal Shear Velocity
up the 2 to 1 Slope (Section 2)

Figure 56.   Variation of Longitudinal Shear Velocity
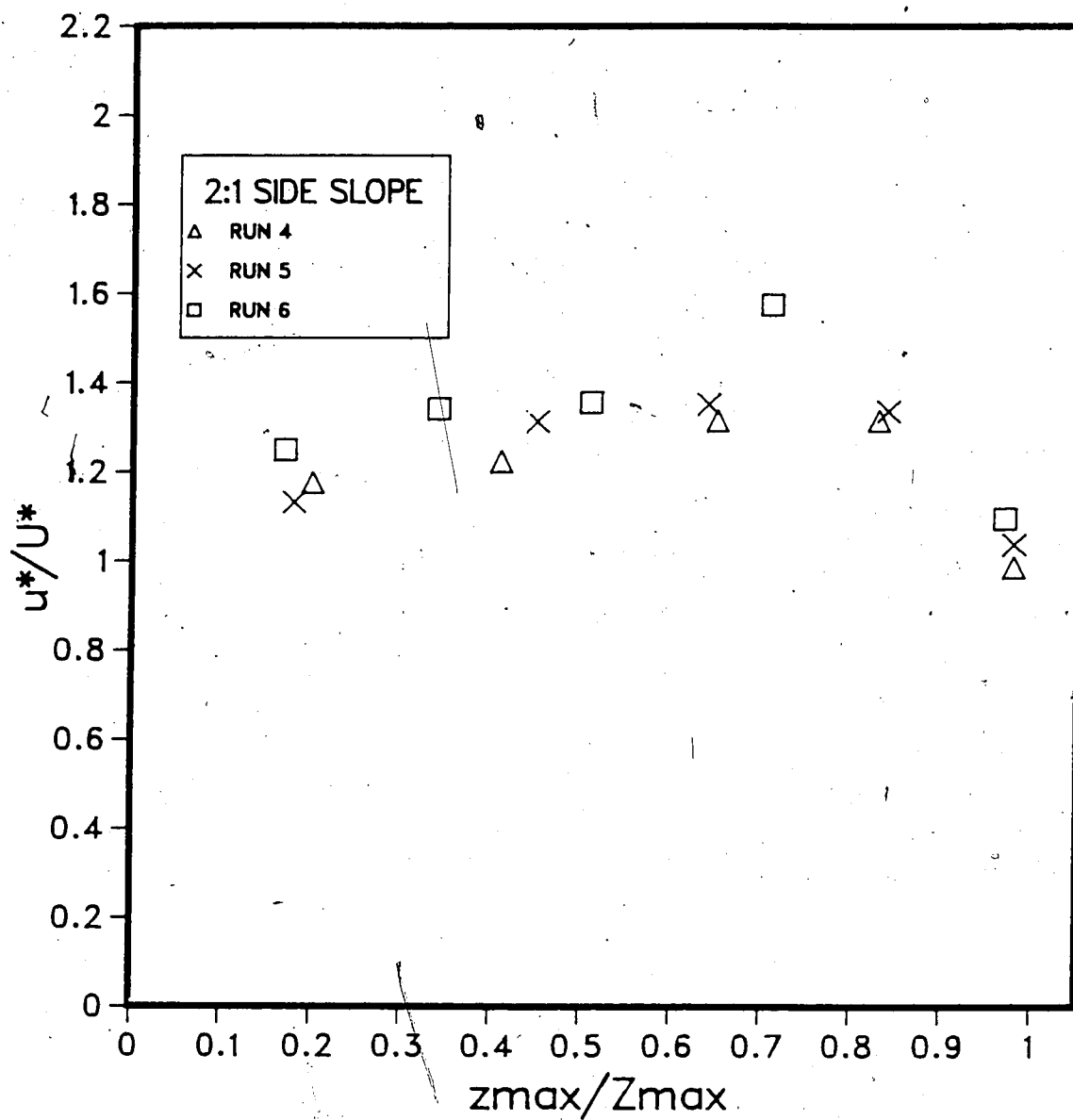   up the 2 to 1 Slope (Section 3)

Figure 57. Variation of Longitudinal Shear Velocity
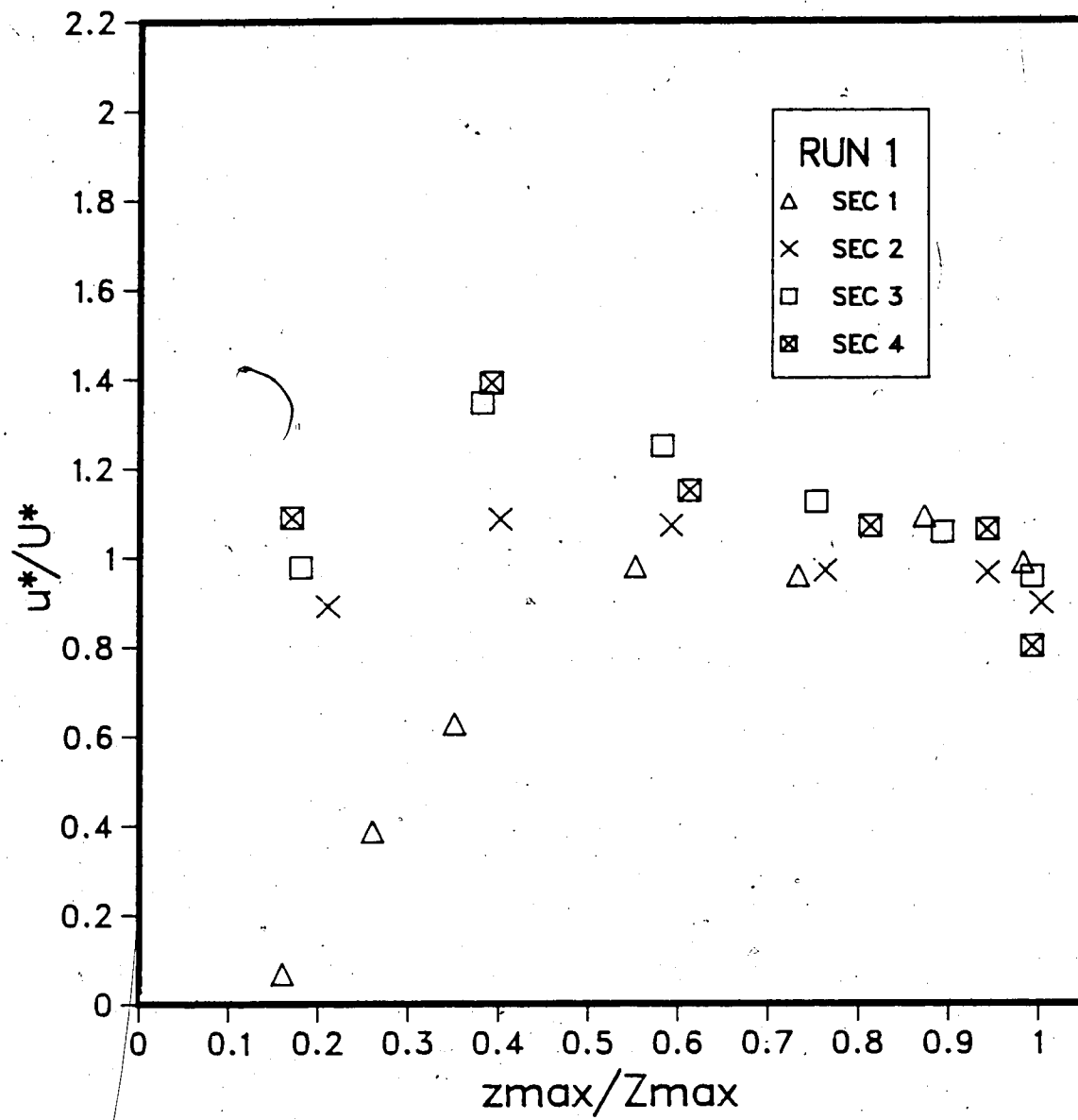   up the 2 to 1 Slope (Section 4)

Figure 58. Variation of Longitudinal Shear Velocity
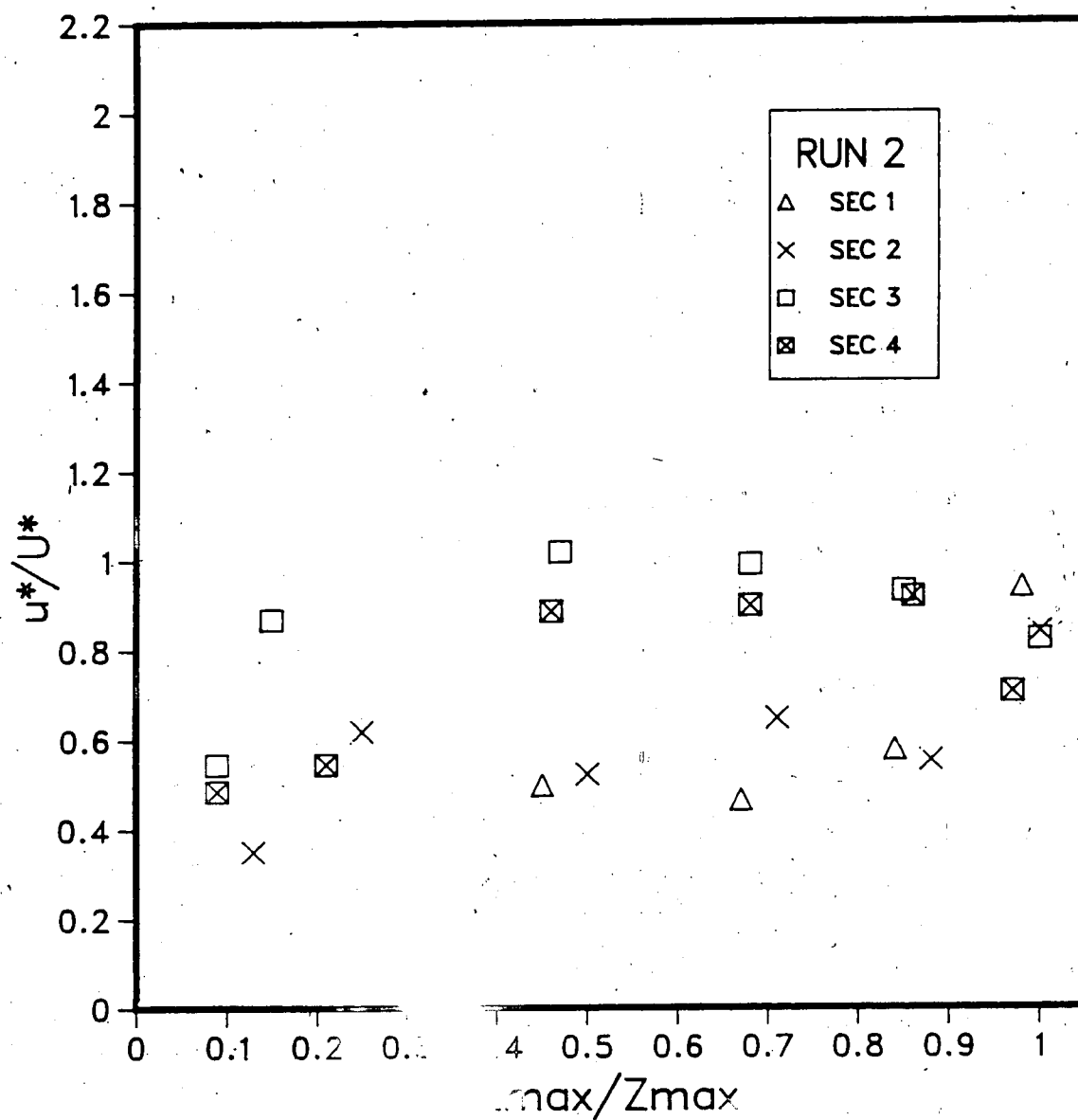up the 3 to 1 Slope (Run 1)

Figure 59. Variation of Longitudinal Shear Velocity
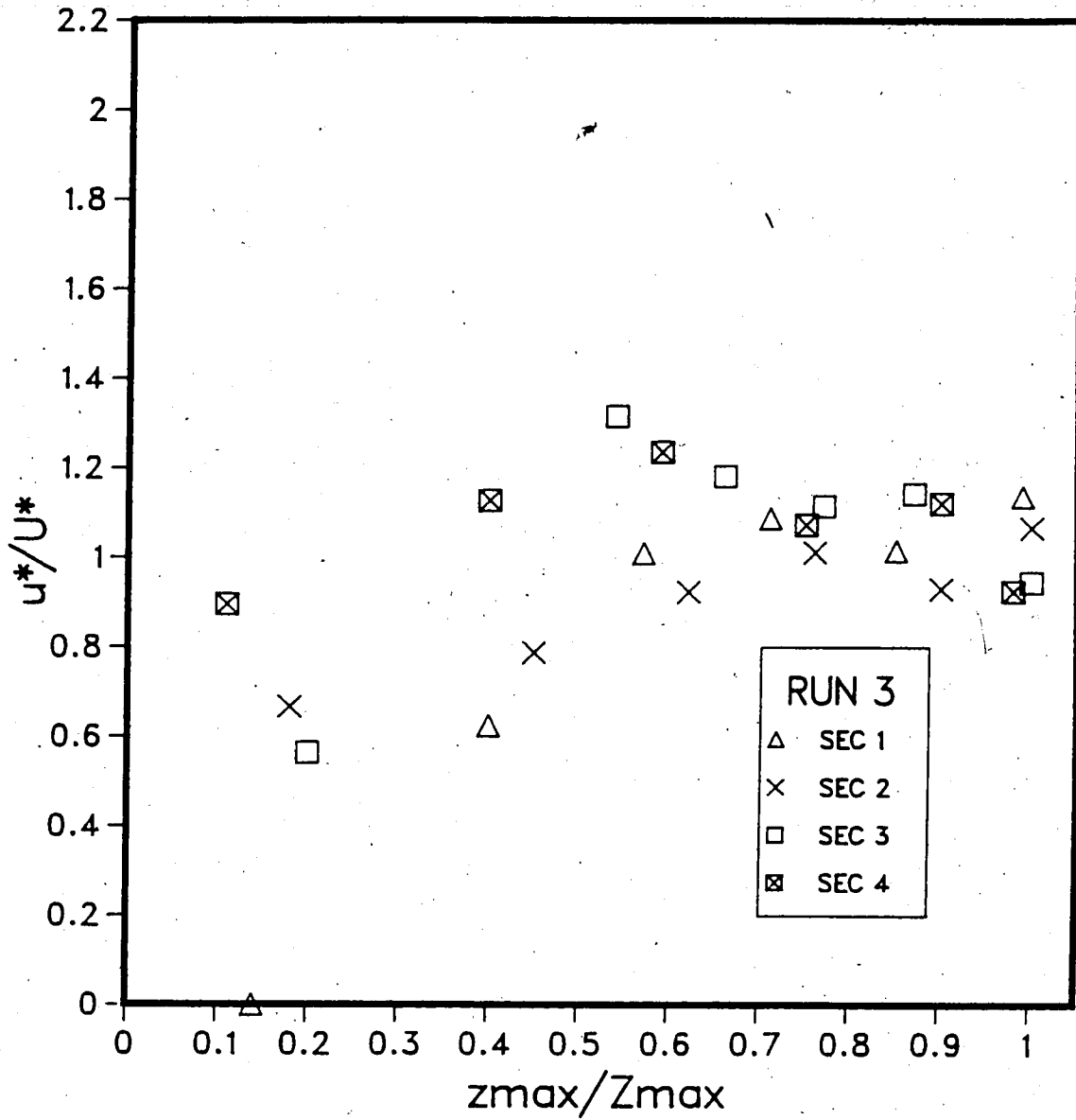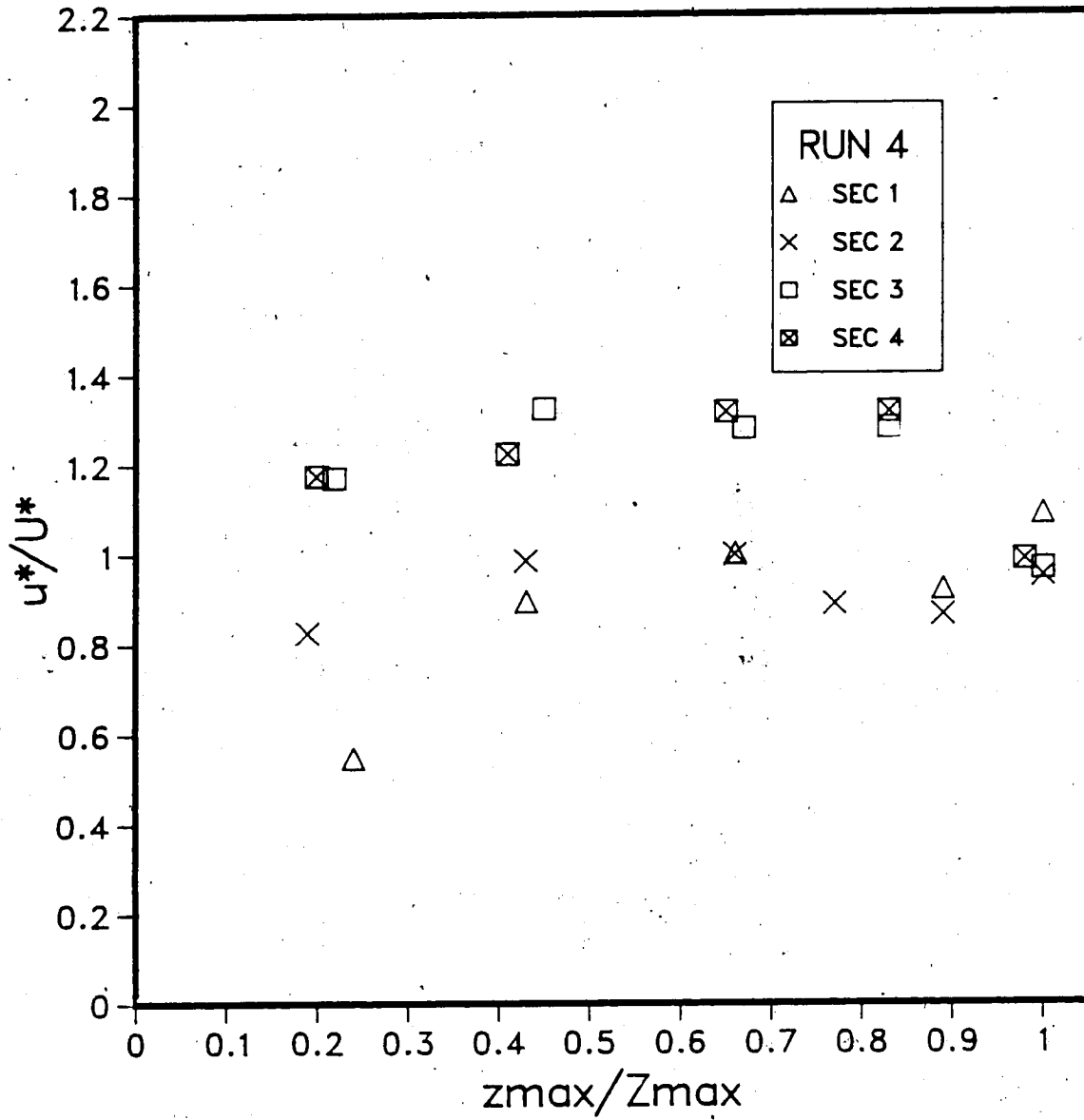up the 3 to 1 Slope (Run 2)

Figure 60. Variation of Longitudinal Shear Velocity
up the 3 to 1 Slope (Run 3)

Figure 61.   Variation of Longitudinal Shear Velocity
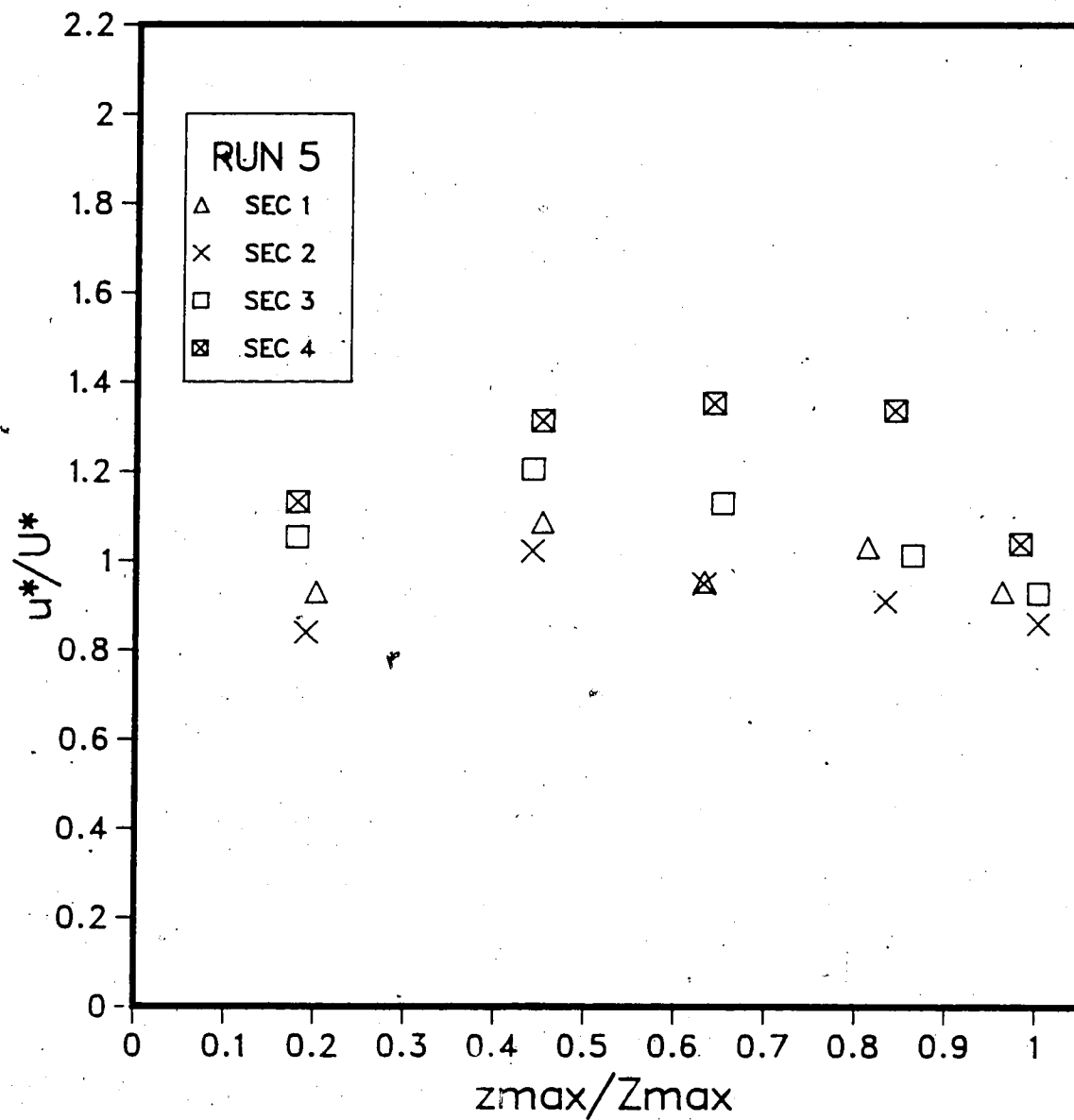   up the 2 to 1 Slope (Run 4)

Figure 62. Variation of Longitudinal Shear Velocity
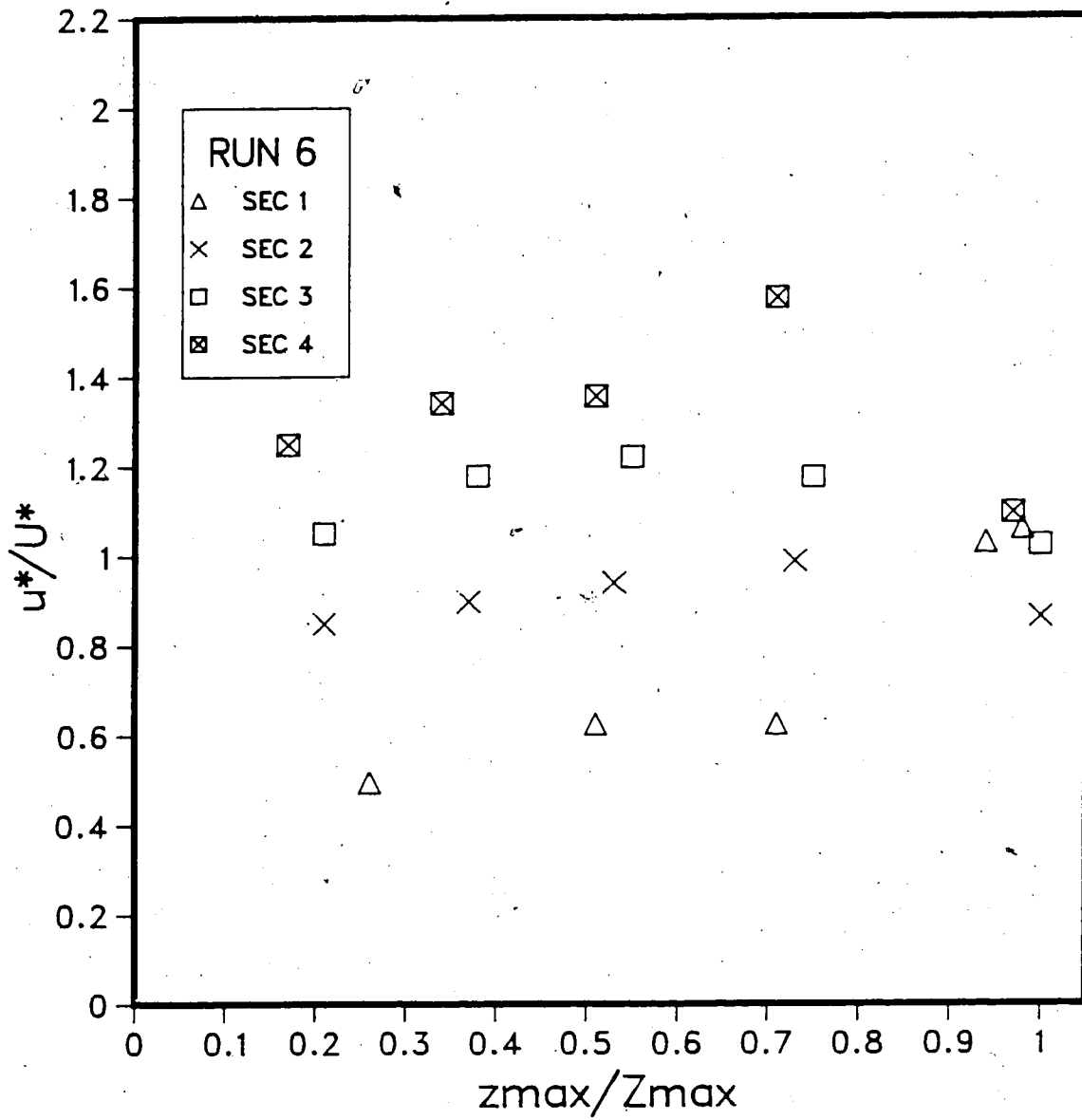up the 2 to 1 Slope (Run 5)

Figure 63. Variation of Longitudinal Shear Velocity
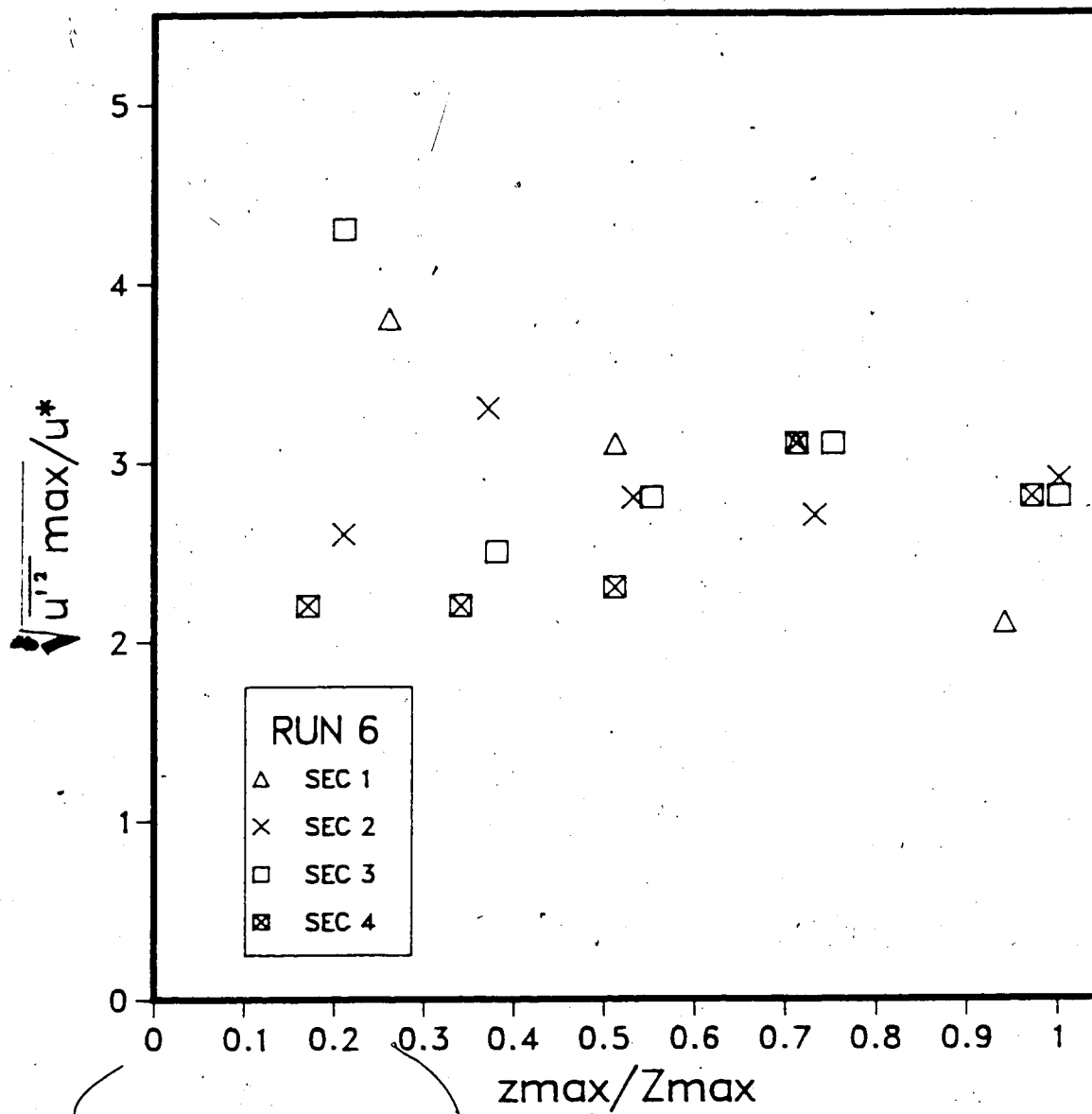up the 2 to 1 Slope (Run 6)

Figure 64. Variation of $\sqrt{u'^2_{max}}/u^*$
            up the 2 to 1 Slope (Run 6)

BIBLIOGRAPHY

Bathurst, J.C., C.R. Thorne, and R.D. Hey. 1979. Secondary Flow and Shear Stress at River Bends. Journal of the Hydraulics Division, ASCE 105(HY10); 1277-1295.

California Department of Transportation. 1970. Bank and Shore Protection in California Highway Practice. State of California Documents Section. 423 pp.

Choudhary, U.K. and S. Narasimhan. 1977., Flow in 180° Open Channel Rigid Boundary Bends. Technical note, Journal of the Hydraulics Division, ASCE 103(HY6): 651-657.

Chow, V.T., 1959 Open Channel Hydraulics. New York: McGraw-Hill. 680 pp.

Daugherty, R.L., and J.B. Franzini. 1977. Fluid Mechanics with Engineering Applications (seventh ed.). New York: McGraw-Hill. 564 pp.

Durst, F., A. Melling and J.H. Whitelaw. 1976. Principles and Practice of Laser Doppler Anaemometry. New York: Academic Press. 405 pp.

Engelund, F. 1974. Flow and Bed Topography in Channel Bends. Journal of the Hydraulics Division, ASCE 100 (HY11): 1631-1648.

Henderson, F.M. 1966. Open Channel Flow. New York: MacMillan. 522 pp.

Ippen, A.T., P. A. Drinker, W.R. Jobin, and O.F. Shemdin 1962. Stream Dynamics and Boundary Shear Distributions for Curved Trapezoidal Channels. Co-operative Research Report No. 47. Department of Civil Engineering, Massachusetts Institute of Technology. 81 pp.

Ippen, A.T. and P.A. Drinker. 1962. Boundary Shear Stresses in Curved Trapezoidal Channels. Journal of the Hydraulics Division, ASCE 88(HY5): 143-179.

Kellerhals, R., C.R. Neill and D.I. Bray. 1972. Hydraulic and Geomorphic Characteristics of Rivers in Alberta. River Engineering and Surface Hydrology Report 72-1. Edmonton Research Council of Alberta. 54 pp.

McCrea, G.H., 1983. Boundary Shear Stress and Velocity Distributions in 60 Degree Laboratory Channel bends. M.Sc. Thesis, University of New Brunswick. 200 pp.

Nash, J.F. and V.C. Patel. 1972. Three-dimensional Turbulent Boundary Layers. Atlanta. SBC Technical Books. 185 pp.

Nouh, M.A., and R.D. Townsend. 1979. Shear Stress Distribution in Stable Channel Bends. Journal of the Hydraulics Division, ASCE 105(HY10): 1233-1245.

Neill, C.R. (ed). 1973. Guide to Bridge Hydraulics. Roads and Transportation Association of Canada, University of Toronto Press. 191 pp.

Onishi, Y., S.C. Jain and J.F. Kennedy. 1976. Effects of Meandering in Alluvial Streams. Journal of the Hydraulics Division, ASCE 102(HY7): 899-917.

Rosovskii, I.L. 1961. Flow of Water in Bends of Open Channels. Jerusalem: Israel Program for Scientific Translation. 233 pp (Translated from Russian).

Schlichting, H., 1979. Boundary-Layer Theory (seventh ed.). New York: McGraw-Hill. 817 pp.

Steffler, P.M., N. Rajaratnam and A.W. Peterson. 1983. LDA Measurements of Mean Velocity and Turbulence Distribution in a Smooth Rectangular Open Channel. Water Resources Engineering Report WRE 83-4. Department of Civil Engineering, University of Alberta. 118 pp.

Steffler, P.M., 1984. Turbulent Flow in a Curved Rectangular Channel. Ph.D. Thesis, University of Alberta. 262 pp.

Varshney, D.V. and R.J. Garde. 1975. Shear Distribution in Bends in Rectangular Channels. Journal of the Hydraulics Division, ASCE 101(HY8): 1053-1066.

de Vriend, H.J. and H.J. Goldof. 1983. Main Flow Velocity in Short River Bends. Journal of Hydraulic Engineering, ASCE 109(7): 991-1011.

Yen, B.C. 1965. Characteristics of Subcritical Flow in a Meandering Channel. Institute for Hydraulic Research, University of Iowa. 76 pp.